AD 407 701

63-4-2

AFCRL-63-123

MICROWAVE INVESTIGATION OF ELECTRICALLY DRIVEN SHOCK WAVES IN GASES

by
J. GERARDO
C. D. HENDRICKS, JR.
L. GOLDSTEIN

MARCH 1963

Scientific Report No. 4
Contract AF19(604)-7473
Project 5634

Prepared for
AIR FORCE CAMBRIDGE RESEARCH LABORATORIES
OFFICE OF AEROSPACE RESEARCH
UNITED STATES AIR FORCE
BEDFORD, MASSACHUSETTS

GASEOUS ELECTRONICS LABORATORY
ELECTRICAL ENGINEERING DEPARTMENT
ENGINEERING EXPERIMENT STATION
UNIVERSITY OF ILLINOIS
URBANA, ILLINOIS

NOTICES

"Requests for additional copies by Agencies of the Department of Defense, their contractors, and other Government agencies should be directed to the:

DEFENSE DOCUMENTATION CENTER (DDC)
ARLINGTON HALL STATION
ARLINGTON 12, VIRGINIA

Department of Defense contractors must be established for ASTIA services or have their 'need-to-know' certified by the cognizant military agency of their project or contract."

"All other persons and organizations should apply to the:

U. S. DEPARTMENT OF COMMERCE
OFFICE OF TECHNICAL SERVICES
WASHINGTON 25, D. C."

power radiated by the shock wave plasma in the microwave frequency range. The microwave measurements were supplemented by observations of the visible light emitted from the shocked gas and by voltage induced signals on small metallic probes placed in the path of the propagating shock waves. The investigated shock waves were in the Mach 4 to Mach 14 velocity range and were produced in neon and argon gases at pressures from 0.1 to 5 mm Hg. The shock waves were initiated by passing an intense electric discharge current through a portion of the gas filling the shock tube. It is demonstrated that the background gas through which the shock waves subsequently passed was ionized to a non-negligible degree at the instant of the electrical discharge. It is shown that this preionization of the background gas is consistent with photoionization by photons of adequate energy from the discharge chamber of the shock tube. In particular it is shown that under the conditions of this experiment, the photoionization is consistent with ionization by X-rays from the electron bombarded anode in the discharge chamber. The

power radiated by the shock wave plasma in the microwave frequency range. The microwave measurements were supplemented by observations of the visible light emitted from the shocked gas and by voltage induced signals on small metallic probes placed in the path of the propagating shock waves. The investigated shock waves were in the Mach 4 to Mach 14 velocity range and were produced in neon and argon gases at pressures from 0.1 to 5 mm Hg. The shock waves were initiated by passing an intense electric discharge current through a portion of the gas filling the shock tube. It is demonstrated that the background gas through which the shock waves subsequently passed was ionized to a non-negligible degree at the instant of the electrical discharge. It is shown that this preionization of the background gas is consistent with photoionization by photons of adequate energy from the discharge chamber of the shock tube. In particular it is shown that under the conditions of this experiment, the photoionization is consistent with ionization by X-rays from the electron bombarded anode in the discharge chamber. The

power radiated by the shock wave plasma in the microwave frequency range. The microwave measurements were supplemented by observations of the visible light emitted from the shocked gas and by voltage induced signals on small metallic probes placed in the path of the propagating shock waves. The investigated shock waves were in the Mach 4 to Mach 14 velocity range and were produced in neon and argon gases at pressures from 0.1 to 5 mm Hg. The shock waves were initiated by passing an intense electric discharge current through a portion of the gas filling the shock tube. It is demonstrated that the background gas through which the shock waves subsequently passed was ionized to a non-negligible degree at the instant of the electrical discharge. It is shown that this preionization of the background gas is consistent with photoionization by photons of adequate energy from the discharge chamber of the shock tube. In particular it is shown that under the conditions of this experiment, the photoionization is consistent with ionization by X-rays from the electron bombarded anode in the discharge chamber. The

AF Cambridge Research Laboratories, Bedford, Mass. MICROWAVE INVESTIGATION OF ELECTRICALLY DRIVEN SHOCK WAVES IN GASES, by J. Gerardo, C. D. Hendricks, Jr., L. Goldstein, March 1963. 126 pp. AFCRL-63-123 Unclassified report

The application of microwave interaction with gaseous plasmas to the study of electrically driven shock waves in inert gases and gaseous plasmas is discussed. The microwave techniques used in this work include: (1) phase shift and resonant probe methods of measuring electron densities in the shock wave, (2) Doppler frequency shift of a microwave signal reflected by the shock wave plasma which enables one to measure the velocity of propagation of shock waves, and (3) radiometer measurements of the noise

UNCLASSIFIED
1. Title
2. Gerardo, J.
Hendricks, Jr., C. D.
Goldstein, L.

UNCLASSIFIED

AF Cambridge Research Laboratories, Bedford, Mass. MICROWAVE INVESTIGATION OF ELECTRICALLY DRIVEN SHOCK WAVES IN GASES, by J. Gerardo, C. D. Hendricks, Jr., L. Goldstein, March 1963. 126 pp. AFCRL-63-123 Unclassified report

The application of microwave interaction with gaseous plasmas to the study of electrically driven shock waves in inert gases and gaseous plasmas is discussed. The microwave techniques used in this work include: (1) phase shift and resonant probe methods of measuring electron densities in the shock wave, (2) Doppler frequency shift of a microwave signal reflected by the shock wave plasma which enables one to measure the velocity of propagation of shock waves, and (3) radiometer measurements of the noise

UNCLASSIFIED
1. Title
2. Gerardo, J.
Hendricks, Jr., C. D.
Goldstein, L.

UNCLASSIFIED

AF Cambridge Research Laboratories, Bedford, Mass. MICROWAVE INVESTIGATION OF ELECTRICALLY DRIVEN SHOCK WAVES IN GASES, by J. Gerardo, C. D. Hendricks, Jr., L. Goldstein, March 1963. 126 pp. AFCRL-63-123 Unclassified report

The application of microwave interaction with gaseous plasmas to the study of electrically driven shock waves in inert gases and gaseous plasmas is discussed. The microwave techniques used in this work include: (1) phase shift and resonant probe methods of measuring electron densities in the shock wave, (2) Doppler frequency shift of a microwave signal reflected by the shock wave plasma which enables one to measure the velocity of propagation of shock waves, and (3) radiometer measurements of the noise

UNCLASSIFIED
1. Title
2. Gerardo, J.
Hendricks, Jr., C. D.
Goldstein, L.

UNCLASSIFIED

AF Cambridge Research Laboratories, Bedford, Mass. MICROWAVE INVESTIGATION OF ELECTRICALLY DRIVEN SHOCK WAVES IN GASES, by J. Gerardo, C. D. Hendricks, Jr., L. Goldstein, March 1963. 126 pp. AFCRL-63-123 Unclassified report

The application of microwave interaction with gaseous plasmas to the study of electrically driven shock waves in inert gases and gaseous plasmas in discussed. The microwave techniques used in this work include: (1) phase shift and resonant probe methods of measuring electron densities in the shock wave, (2) Doppler frequency shift of a microwave signal reflected by the shock wave plasma which enables one to measure the velocity of propagation of shock waves, and (3) radiometer measurements of the noise

UNCLASSIFIED
1. Title
2. Gerardo, J.
Hendricks, Jr., C. D.
Goldstein, L.

UNCLASSIFIED

AFCRL-63-123

MICROWAVE INVESTIGATION OF ELECTRICALLY DRIVEN SHOCK WAVES IN GASES

by

J. Gerardo
C. D. Hendricks, Jr.
L. Goldstein

March 1963

Scientific Report No. 4
Contract AF19(604)-7473
Project 5634

Prepared for

AIR FORCE CAMBRIDGE RESEARCH LABORATORIES
OFFICE OF AEROSPACE RESEARCH
UNITED STATES AIR FORCE
BEDFORD, MASSSACHUSETTS

Electrical Engineering Research Laboratory
Engineering Experiment Station
University of Illinois
Urbana, Illinois

ABSTRACT

The application of microwave interaction with gaseous plasmas to the study of electrically driven shock waves in inert gases and gaseous plasmas is discussed. The microwave techniques used in this work include: (1) phase shift and resonant probe methods of measuring electron densities in the shock wave, (2) Doppler frequency shift of a microwave signal reflected by the shock wave plasma which enables one to measure the velocity of propagation of shock waves, and (3) radiometer measurements of the noise power radiated by the shock wave plasma in the microwave frequency range. The microwave measurements were supplemented by observations of the visible light emitted from the shocked gas and by voltage induced signals on small metallic probes placed in the path of the propagating shock waves. The investigated shock waves were in the Mach 4 to Mach 14 velocity range and were produced in neon and argon gases at pressures from 0.1 to 5 mm Hg. The shock waves were initiated by passing an intense electric discharge current through a portion of the gas filling the shock tube. It is demonstrated that the background gas through which the shock waves subsequently passed was ionized to a non-negligible degree at the instant of the electrical discharge. It is shown that this preionization of the background gas is consistent with photoionization by photons of adequate energy from the discharge chamber of the shock tube. In particular it is shown that under the conditions of this experiment, the photoionization is consistent with ionization by X-rays from the electron bombarded anode in the discharge chamber. The effect of the free electron constituent of the ionized background gas on the properties of shock waves as well as its direct effect on experimental observation techniques is discussed. In addition, the properties of the hot and highly ionized driver gas which expands from the discharge chamber and closely follows the shock wave down the expansion chamber is discussed. Particular emphasis is placed on the effect of the driver gas with regards to the establishment of an equilibrium state in the shocked gas.

CONTENTS

ILLUSTRATIONS

LIST OF SYMBOLS

V_s velocity of the shock wave

U_2 flow velocity of the shocked gas

e specific internal energy or charge of an electron (distinction is obvious)

ρ mass density

p gas pressure in mm Hg

h specific enthalpy

R gas constant

M Mach number with respect to neutral atoms at T = 290° K.

T temperature in degrees Kelvin

C_p specific heat at constant pressure

C_v specific heat at constant volume

γ ratio of C_p to C_v

n or n^o number density of neutral gas atoms

a velocity of sound or the wide dimension of rectangular waveguide (distinction obvious)

b narrow dimension of rectangular waveguide

k Boltzmann's constant

n_f number of degrees of freedom of the molecule

n^+ or n_i number density of singly ionized atoms

n^{++} number density of doubly ionized atoms

n_e number density of the free electrons

m or m_e mass of an electron

$\mathcal{M}$ mass of an atom

α degree of single ionization

δ degree of double ionization

X^o ionization energy of neutral atom

X^+ ionization energy of singly ionized atom

$\bar{E}_o$ excitation energy of a neutral atom

$\bar{E}_+$ excitation energy of a singly ionized atom

X_n^o excitation energy of the n^{th} state in the neutral atom

X_n^+ excitation energy of the n^{th} state in a singly ionized atom

g_n statistical weight of n^{th} state

T^o or T absolute temperature of neutral atoms

T_i or T^i absolute temperature of singly ionized atoms

T_e or T^e absolute temperature of electrons

f cyclicfrequency of electromagnetic waves

ω angular frequency of electromagnetic waves

V_p phase velocity of electromagnetic waves

V_R velocity of propagation of an EM reflecting body

ϵ_o permittivity of free space

ϵ_r relative permittivity

c velocity of light

λ_o wavelength of an EM wave in free space

ω_p plasma frequency

λ wavelength of X-ray radiation

μ linear absorption coefficient for photons in a gas at 1 mm Hg pressure

Z_{RAD} radiation impedance of an EM antenna

P_{RAD} power radiated by an antenna

ν_{em} electron-molecule collision frequency for momentum transfer

ν_{ei} electron-ion collision frequency for momentum transfer

ν effective collision frequency for momentum transfer (i.e. $\nu = \nu_{em} + \nu_{ei}$)

Re indicates the real part of a complex number or function

P_ω available noise power per unit frequency interval

A electromagnetic absorption coefficient of a medium

E electric field intensity of an EM wave

H magnetic field intensity of an EM wave

R_p power reflection coefficient for an EM wave incident on a medium

T_p power transmission coefficient for an EM wave incident on a medium

T radiation temperature or temperature of neutral gas atoms (distinction if obvious)

Γ magnitude of the reflection coefficient of an EM wave incident on a medium.

β phase constant of electromagnetic waves

1. INTRODUCTION

It is well known that a shock wave can be formed in a gas when a limited volume of it is selectively heated by an adequately intense electric discharge current passing through it.[1,2] The heated volume of gas is raised to a highly ionized high temperature state and subsequently expands into the unheated region. Thus the expanding gas in its highly ionized, high temperature state and also the shock wave and the phenomena associated with its propagation in the unheated region of gas can be investigated with respect to both the properties of the shock wave and the properties of the high temperature gas. It is generally appreciated that the structure of a shock wave originating in such electrical gas discharges may be in many ways different from that of a shock wave originating from other sources such as, for instance, those which are produced and driven by high pressure but low temperature nonionized gases.

In electric shock tubes the hot driver gas expands from the discharge chamber at nearly the velocity of the shock wave and its leading edge closely follows the shock front. In many cases the separation distance between the shock front and the driver gas is insufficient to allow the shocked gas to reach an equilibrium state before it passes through the driver gas interface. In this case it is obvious that the usual shock wave relations[3] will not apply. In addition, high energy radiation from the hot driver gas in an electric shock tube plays an important role in shock wave processes and greatly affects the structure of the shock wave. In an indirect manner the driver gas in electric shock tubes affects the structure of the shock wave by acting as either a heat sink or a heat source, whichever applies, for the entire volume of shock heated gas. This thermal contact between the driver gas and the shocked gas is much better in electric than in pressure driven shock tubes because the two volumes of gas are much closer together in the former and also (as will presently be discussed) due to the ever present preionized background gas in electric shock tubes.

It has previously been reported by several different investigators that in electric shock tubes with the usual types of electrode configurations[1,4] an intense disturbance propagates through the background gas, during the electric discharge, at a velocity equal to or nearly equal to the velocity of light in vacuo.[5,6] These high velocity disturbances are characterized by emission of light from the volume and by fairly high electron densities. It is generally believed that these disturbances in the background gas are a result of electron diffusion and/or ultra-violet radiation from the discharge chamber during the intense electric discharge. In some cases the walls of the shock tube expansion chamber are believed to play an important role in the total effect of the disturbance. It is shown below that in addition to, or in place of, the above mentioned mechanisms, the background gas in electric shock tubes with cylindrical type electrodes is most probably preionized at the time of the electric discharge by soft X-rays from the electron bombarded positive electrode. The degree of ionization in the volume prior to the passage of the shock wave is often sufficient to appreciably affect the structure of the shock wave. Of course, this depends on the discharge voltage, the material of the positive electrode, the type of background gas, and the distance from the discharge chamber.

In addition to the direct effect of the ionized constituents of the background gas on the shock wave structure, (including ionization rates, density profiles, luminosity profiles, etc.) many indirect effects are also apparent. As a result of this preionization the free electron constituent of the driver gas is in good thermal contact with the free electron constituent of the background gas via the free electron constituent of the shocked gas in the shock wave. The velocity of heat flow via the electron constituent of an ionized gas is known to be faster than or on the order of the velocity of normally produced shock waves.[7,8] Hence, as a result of the preionization, the energy loss processes in a shock wave may be much greater than expected. In addition, in some cases the ionized

driver gas may be sufficiently hot so that thermal energy may flow from the driver gas toward the shock front. Consequently this would greatly affect the equilibrium attaining processes occurring in the shocked gas. The ionized constituent of the background gas with its good thermal conduction properties may also account for precursor effects directly in front of the shock wave.[6,9]

It is immediately obvious that the interpretations of some experimental shock wave results obtained in electric shock tubes may be greatly in error if one does not consider the effect of the ionized constituent of the background gas on the sensing mechanisms. This is especially true in microwave investigations of shock waves in which case the phase velocity of an electromagnetic wave incident on the shock wave is dependent on the electron density in the background gas.[10] It is equally important to consider this constituent of the background gas when using other commonly used shock wave investigation techniques such as metallic probes in the path of the shock wave and optical methods of observation.

We discuss below the preionization of the background gas by the shock wave producing electric discharge, the influence of the preionization on shock wave propagation in such media, the properties of the hot and highly ionized driver gas as related to shock wave propagation, and the effect of the ionized constituent of the background gas on some commonly used shock wave investigation techniques. The discussion is limited to phenomena occurring in electrically driven shock tubes filled with monatomic gases. This case is relatively simple with respect to an investigation of shock phenomena in diatomic gases since dissociation and excitation of molecular rotational and vibrational degrees of freedom do not occur. Most of the experiments reported here were conducted in neon or argon gas in the pressure range from a few tenths of a millimeter of mercury to five millimeters of mercury. It is assumed that the results reported can be applied to any other monatomic gas although the rate of ionization by action of shock wave,[11,12] the rate of heat flow in the partially ionized gas,[8] and the

degree of preionization will be highly dependent for any given pressure on the monatomic gas used.

The shock waves which were investigated here ranged in velocity from Mach 4 to Mach 14. This range of shock velocities includes shock waves sufficiently intense to partially ionize an originally non-ionized background gas as well as shock waves which are too weak to produce any appreciable ionization.[13,14] The shock waves were simultaneously investigated by observing the visible light emitted from the shock heated gas, by observing the electric potential induced on small metallic probes extended into the path of the shock wave, by interaction of low power microwaves with the shock wave formed plasma cloud, and by measuring the noise power in the microwave frequency range radiated by the shocked plasma and associated driver plasma.

2. HISTORICAL SURVEY AND INTRODUCTORY MATERIAL

The nonlinear phenomenon of a shock wave in matter has been of interest to scientists for more than a century. Such notable scientists as Stokes, Earnshaw, Riemann, Rankine, Hugoniot, Lord Rayleigh and others wrote fundamental papers inaugurating this field of scientific endeavor. Among them they showed that sound waves in gases do not always propagate with a unique velocity relative to the gas but in some cases a discontinuity in velocity can occur and in this case the propagation is governed by nonlinear differential equations, and as a consequence the familiar laws of superposition, reflection, and refraction cease to be valid. The relationships which satisfy such nonlinear propagation can be obtained by forcing the three conservation laws of physics - mass, momentum and energy - to be satisfied across the propagating disturbance. If the additional condition is imposed that the disturbance must be an adiabatic reversible transition, then its propagation is governed by linear differential equations and its velocity of propagation is unique relative to the medium in which it is propagating. However, if it is assumed that the transition is irreversible and non-adiabatic then the velocity is not unique and is governed by nonlinear differential equations.[3] Irreversible processes are always present in physical situations and can be neglected only if the gradients of velocity and temperature are small, a condition which obviously is not realized in a shock wave.

A theory which includes the effects of the irreversible process in a shock wave would be mathematically complicated if it were not for the fact that actual phenomena show that irreversible processes occur in gases only in narrow zones where the gradients of velocity and temperature are very large while outside of these transition zones the processes obey the laws established for adiabatic reversible processes. Because of this it is accepted that a mathematically idealized model of a shock wave in a gas which reasonably approximated actual shock phenomena is an adiabatic and reversible flow except for a sudden jump

discontinuity with infinite gradients in some of the quantities. The three conservation laws of physics must be satisfied across this discontinuity and it can be shown that in the absence of viscosity and heat conduction this implies conservation of entropy in the continuous flow and a change of entropy across the discontinuity. The equations obtained in this manner are commonly referred to as the Rankine-Hugoniot equation and these equations predict reasonably well the change in state across a shock wave.

Following the initial work of the early investigators mentioned above, the development of shock wave theory and technology was left in the hands of a few men in applied research who were mainly interested in using shock waves as a tool for the investigation of relaxation phenomena in highly disturbed gases. Knowledge of shock wave phenomena advanced at a rather slow pace during this time and it was not until the advent of supersonic aircraft that a great deal of attention was directed toward shock waves and particularly toward shock waves in gases. The interest in shock waves experienced another rapid increase in the middle 1950's when it was proposed to use irreversible shock heating of a gas in order to produce a high temperature plasma with the implication that it might be possible to heat a gas in this manner to the extremely high temperature required for controlled fusion.

Prior to the early 1950's the only laboratory method available for the production of shock waves in gases was the pressure driven, diaphragm type shock tube. These tubes are constructed by separating an air tight chamber into two sections separated by a nonporous diaphragm. One of the sections is filled with a test gas at the desired pressure and the other is filled with a driver gas at a much higher pressure. If the diaphragm separating the two gases is ruptured, then the high pressure gas expands into the low pressure test gas. The velocity of the expanding column of gas is determined by the nature of the two gases and the pressure difference across the diaphragm. Under certain conditions the velocity

of expansion is supersonic with respect to the velocity of sound in the test gas and in this case a shock wave is formed in front of the expanding column of driver gas. With the most sophisticated shock tube techniques, such a combustion heating of the high pressure driver gas just prior to diaphragm rupture and installation of buffer gas sections, it is possible to obtain shock velocities up to about Mach 20 in this type tube.

The electrically driven shock tube which is capable of producing shock wave velocities in excess of Mach 100 was born quite by accident in 1951 by Fowler et al[1]. The original purpose of their work was to investigate the glow in an electrodeless discharge tube similar to that observed by Lord Rayleigh in 1943.[15] With a discharge tube similar to that used by Lord Rayleigh they observed that the plasma which shot out of the discharge section of the tube possessed a definite front and advanced at a definite velocity. The velocity of advance was measured and was found to be approximately equal to the velocity of sound in the hot expanding gas, hence supersonic with respect to the cold background gas. Velocities appreciably higher than those possible in the electrodeless tube were made possible by installing metal rod electrodes in two arms of a T-tube. When an electric discharge occurred between the two electrodes the heated gas expanded through the side arm of the T-tube much the same as in the electrodeless tube. With this type tube Fowler observed that the expanding front decelerated as it moved along the side arm, was reflected when it struck the far end of the tube, and it left in its wake a highly excited gas. From these observations they concluded that the phenomenon was not afterglow, as postulated by Lord Rayleigh, but instead the hot ionized expanding gas acted as a shock wave driver much as in a diaphragm shock tube.

Electric shock tube technology advanced quite rapidly after the initial work of Fowler et al. and by 1955 gas temperatures in excess of 30,000^{o}K could be obtained by shock heating. In the spring of 1955, in conjunction with the

Sherwood program, a group from the Naval Research Laboratories, proposed the use of electric shock tubes for the production of high temperature plasmas as is required for controlled fusion.[16] In spite of the fact that until this time the highest gas temperature available in the laboratory was produced by shock heating, the highest temperature attainable was considerably lower than that required for fusion, where millions of degrees is needed. However, at NRL and other laboratories, shock tube technology advanced rapidly and shortly after initiation of the program at NRL a modification proposed by Kolb made it possible to shock heat gases to temperature up to 500,000°K. Kolb's modification was incorporated into a standard T-tube and consisted merely of bringing one of the electrical leads to the discharge electrodes close to the wall of the discharge tubes.[16,17] Hence, a sudden electric discharge between the two electrodes results in a rapid heating of the gas and subsequent expansion of the heated gas into the side arm (expansion chamber). The magnetic field produced by the current in the electrode lead further accelerates this plasma and increases the shock velocity.

An electric shock tube which in principle is quite different than the T-tube was developed by Josephson[4] about this same time. It is also capable of producing shock velocities in excess of Mach 100. This tube is coaxial in design with a hollow ring electrode and a rod electrode so positioned to form a cone between the point of the rod and the inside of the ring electrode. A sudden electric discharge between the two electrodes heats the gas filling the chamber and this heated gas expands through the hollow electrode and down the expansion chamber. This type of shock wave driver is just as efficient, if not more efficient, than the T-type tube with magnetic back strap. The optimum cone angle formed by the two electrodes has been extensively investigated by Josephson,[4] and Hart[18] and others and was found to be dependent on the type of gas and the gas pressure.

One of the main difficulties with both the T-type and the coaxial type discharge tubes is contamination of the gas by erosion of the electrodes caused by the high current electric discharge. These impurities added to the gas by the discharge do not affect the shock wave as such because the shock is formed in front of the driver gas, but they do alter the properties of the driver gas which in turn affects the properties of the shock wave. Contamination of the gas can be eliminated in electrically driven shock tubes by inductively coupling the energy into the gas.[4] This can be accomplished in a variety of ways, as for example, by placing a one turn coil around a portion of the shock tube. A sudden increase in current through the coil indictively heats the contained gas which then expands down the expansion chamber and if sufficiently intense forms a shock wave. Discharges of this type are commonly referred to as a theta pinch discharge and can raise the temperature of the gas in the pinch to more than a million degrees.[16] The main disadvantage in using this type of discharge for the production of shock waves is its relative inefficiency.

Shock wave investigation techniques advanced during the last few years at a rate equally rapid as the advancement of shock wave production technology. Prior to 1950 most of the techniques available for the investigation of shock wave phenomena in gases were very unrefined. However, during the early and middle 1950's shock wave heating of gases to extremely high temperatures received an increased amount of interest and it became necessary to develop new and more refined techniques in order to investigate the properties of both the shock wave and the hot driver gas in much greater detail than was formerly possible. For the most part, the development of techniques for the investigation of a shock wave plasma is considerably more difficult than merely the extension of existing plasma investigation techniques to shock wave plasmas. The difficulty arises because the interested volume of gas in a shock wave moves at a very high velocity which requires all measurements of its plasma parameters to be completed in a

very short time (microseconds). In spite of obvious difficulties, many advances have been made in the field of shock wave investigation techniques during the last few years and the pace of development is rapidly increasing.

A complete review of all the techniques which have been or are being used to investigate shock wave phenomena in gases would be too extensive to conduct here. However, since a rather large portion of the work described below is devoted to the development of techniques for the investigation of shock wave phenomena it seems appropriate to mention some of the most widely used techniques. In general these techniques can be divided into two classes; those which detect radiation from the shock heated gas and those which depend on the interaction of externally produced radiation with the shock wave and/or its associated plasma. In the former class such devices as streak cameras,[1,19] high speed framing cameras,[20] photomultipliers,[11,13] and spectrographs[5,19,21] are commonly used to determine such shock wave phenomena as velocity of propagation, temperature, degree and rate of ionization, relaxation rates for the various degrees of freedom, gas pressure, density profiles and etc. In the latter class one finds interferometers,[22] static probes,[6,9,23,24] electron beams,[25,26,27] microwaves,[28,29,30,31] magnetic probes,[13,32] X-rays,[33,34] piezoelectric detectors,[35,36] vacuum ultraviolet,[37] and etc., very prominant for the measurement of such shock wave parameters as electron and atom density profiles, temperature, gas pressure, velocity of shock wave propagation, curvature and structure of the shock front, etc.

3. SHOCK RELATIONS AND PHENOMENA

The Rankine-Hugoniot "jump" relations across a shock wave in a gas are found by considering the propagation of a disturbed non-equilibrium volume of gas through a background gas filling a constant area duct. The equilibrium states on either side of the disturbed region of gas are related to each other via the three conservation laws of physics. If viscosity, radiation and heat conduction effects are neglected, the two equilibrium states are uniquely related independent of the individual processes which occur in the transition region.[3] The relationships between the two equilibrium states on opposite sides of the disturbed volume are, however, dependent on the equation of state in the disturbed gas and the velocity at which the disturbance propagates through the background gas.

Consider a disturbance propagating through a gas with a constant velocity V_s. The gas variables of state prior to the passage of the disturbance are denoted by subscript 1. The disturbance leaves in its wake a gas which, after equilibrium is once again attained, has a flow velocity U_2 in the direction of propagation of the disturbance and this volume of gas is described by state variables with subscript 2. In this case, the three conservation equations of physics in a coordinate system stationary on the propagating disturbance are given by Equations (1a, b, and c) respectively for mass, momentum and energy.

$$\rho_1 V_s = \rho_2 (V_s - U_2) \tag{1a}$$

$$\rho_1 V_s^2 - \rho_2 (V_s - U_2)^2 = p_2 - p_1 \tag{1b}$$

$$e_1\rho_1 V_s + \frac{1}{2}\rho_1 V_s^3 + p_1 V_s = e_2\rho_2 (V_s - U_2) + \rho_2 \frac{(V_s - U_2)^3}{2} + p_2 (V_s - U_2) \tag{1c}$$

In these equations, e is the specific internal energy (i.e., energy/unit mass), ρ is the mass density, and p is the gas pressure. Equation (1c) can be placed in a slightly simplified form by using Equation (1a) and the expression for specific enthalpy $h = e + p/\rho$. In this manner Equation (1c) can be replaced by Equation (1d)

$$\frac{1}{2}V_s^2 + h_1 = \frac{1}{2}(V_s - U_2)^2 + h_2 \tag{1d}$$

Equations (1) are the general relationships which must be satisfied across a normal shock wave. In order to determine the state variables jump relations across a shock wave it is usually necessary to solve these equations numerically. However, if the gas is considered to be thermally perfect, then explicite solutions for the jump relations can be obtained in terms of the Mach number ($M = V_s/\sqrt{\gamma RT_1}$). In this case Equations (2) are applicable as long as the gas is non-ionized and each gas atom is in its ground state.

$$p = \rho RT = nkT \tag{2a}$$

$$\gamma = C_p/C_v = \text{constant} \tag{2b}$$

$$a^2 = \gamma RT = \gamma p/\rho \tag{2c}$$

$$C_p - C_v = R \tag{2d}$$

$$h = C_p T = \frac{\gamma RT}{\gamma - 1} \tag{2e}$$

In these equations, a is the velocity of sound in the gas, k is Boltzmann's constant, T is the temperature of the gas in degrees Kelvin, n is the number of

atoms per unit volume, and C_p and C_v are the specific heat at constant pressure and constant volume respectively.

Equations (1) can now be solved algebraically with the help of Equations (2) in order to obtain the jump relations for pressure, density and temperature across a shock wave in a thermally perfect gas. These solutions are obtained in terms of the Mach number and the ratio of the specific heats. In this case the jump relations and the flow velocity of the shocked gas are given by Equations (3).

$$p_2/p_1 = \frac{2\gamma M^2 - (\gamma - 1)}{\gamma + 1} \tag{3a}$$

$$\rho_2/\rho_1 = \frac{(\gamma + 1)\, M^2}{(\gamma - 1)\, M^2 + 2} \tag{3b}$$

$$T_2/T_1 = \frac{[M^2(\gamma - 1) + 2][2\gamma M^2 - (\gamma - 1)]}{M^2(\gamma + 1)^2} \tag{3c}$$

$$U_2/a = \frac{2(M^2 - 1)}{M^2(\gamma + 1)} \tag{3d}$$

The ratio of the specific heats γ is obtained from the perfect gas relations and from statistical mechanics which leads to a simple expression for C_p in terms of the number of degrees of freedom n_f of the appropriate molecular model.

$$C_p = \frac{n_f + 2}{2} R \tag{4}$$

In the case of a smooth sphere or a point mass, n_f is equal to 3 and $C_p = 5/2\ R$. Since this model reasonably approximates a non-ionized monatomic gas, the jump

relations across a non-ionizing shock wave in a perfect non-ionized monatomic gas are given by Equations (3) with $\gamma = 5/3$. In this case, if excitation of the background gas by action of the shock wave is also neglected, then Equation (3) reduces to the following:

$$p_2/p_1 = \frac{5M^2 - 1}{4} \tag{5a}$$

$$\rho_2/\rho_1 = \frac{4M^2}{M^2 + 3} \tag{5b}$$

$$T_2/T_1 = \frac{(M^2 + 3)(5M^2 - 1)}{16M^2} \tag{5c}$$

$$U_2/a = \frac{3(M^2 - 1)}{4M} \tag{5d}$$

If the gas atoms either prior to or after the passage of the shock wave are excited or if the gas is partially ionized, then the jump relations 3 do not apply because Equations (2) must be modified in order to account for this phenomenon. In this case (accounting for single and double ionization only) the gas pressure is equal to the sum of the partial pressures,

$$p = kT(n^o + 2n^+ + 3n^{++}) = kT(n^o + n^+ + n^{++})(1 + \alpha + \delta) \tag{6}$$

where n^o, n^+, n^{++} are the densities of the neutral, singly, and doubly ionized particles respectively. The specific enthalpy $h = e + p/\rho$ must include the ionization and excitation energies, in addition to the usual translational energy. In this case the specific internal energy term e is given by

$$e = \frac{1}{\mathcal{M}} \left[\frac{3}{2}(1 + \alpha + 2\delta)\, kT + (1 - \alpha - \delta)\, \bar{E}_o + \alpha(X^o + \bar{E}_+) + \delta X^+\right] \tag{7}$$

and p/ρ is given by

$$p/\rho = (1 + \alpha + 2\delta)\, \frac{kT}{\mathcal{M}} \tag{8}$$

Hence the specific enthalpy of a partially ionized gas is given by

$$h = \frac{1}{\mathcal{M}} \left[\frac{5}{2}\, (1 + \alpha + 2\delta)\, kT + (1 - \alpha - \delta)\, \bar{E}_o + \alpha\, (X^o + \bar{E}_+) + \delta X^+\right] \tag{9}$$

where: $\mathcal{M}$ is the mass of an atom, $\alpha = n^+/(n^o + n^+ + n^{++})$ is the degree of single ionization, $\delta = n^{++}/(n^o + n^+ + n^{++})$ is the degree of double ionization, X^o and X^+ are the ionization energies of the neutral and single ionized atoms respectively and $\bar{E}_o$ and $\bar{E}_+$ are the excitation energies of the neutral atom and the single ionized atoms respectively.

The excitation energies $\bar{E}_o$ and $\bar{E}_+$ are given by the thermal averages with a suitable cutoff[38]

$$\bar{E}_o = \frac{\sum_n X_n^o\, g_n^o \exp(-X_n^o/kT)}{\sum_n g_n^o \exp\, (-\, X_n^o/kT)} \tag{10a}$$

$$\bar{E}_+ = \frac{\sum_n X_n^+\, g_n^+ \exp(-\, X_n^+/kT)}{\sum_n g_n^+ \exp(-\, X_n^+/kT)} \tag{10b}$$

where X_n^o and X_n^+ are the excitation energies of the nth state in the neutral and singly ionized atoms respectively and the g_n's are the statistical weights.

In order to solve for the jump relations across a shock wave when ionization is considered we need, in addition to the above equations, an expression relating the degree of single and double ionization to the gas temperature. This is, of course, given by Saha's equations

$$\frac{n^{+,++}\, n_e}{n^{o,+}} = \frac{2Z^{+,++}}{Z^{o,+}} \left(\frac{2\pi m_e kT}{h^2}\right)^{3/2} \exp -\left(\frac{X^{o,+}}{kT}\right) \tag{11}$$

where Z^o, Z^+ and Z^{++} are the partition functions for the respective states o, + and ++ are given by

$$Z^{o,+,++} = \sum_n g_n^{o,+,++} \exp(-X_n^{o,+,++}/kT) \tag{12}$$

It is now possible to solve Equations (1), with the aid of Equations (6) through (12), in order to determine the jump relations across either a shock wave in a partially ionized gas or an ionizing shock wave. However, in general only numerical solutions can be obtained and explicite solutions are possible only if certain simplifying assumptions are made. These equations have been solved numerically by various authors for the case of ionizing shock waves in initially cold, non-ionized, rare gases.[5, 13, 14, 39, 40] Some of these solutions are reproduced in Figures 1 and 2 for future reference.

The jump relations across a shock wave in a gas as given above indicate the difference in magnitude of the state variables in the two equilibrium volumes of gas on opposite sides of the shock wave. They do not indicate the rate of change or the profiles of these state variables in the shock wave. In order to calculate such profiles, as for example the electron density profile in the shock wave, it is necessary to consider the individual processes occurring in the shocked gas,

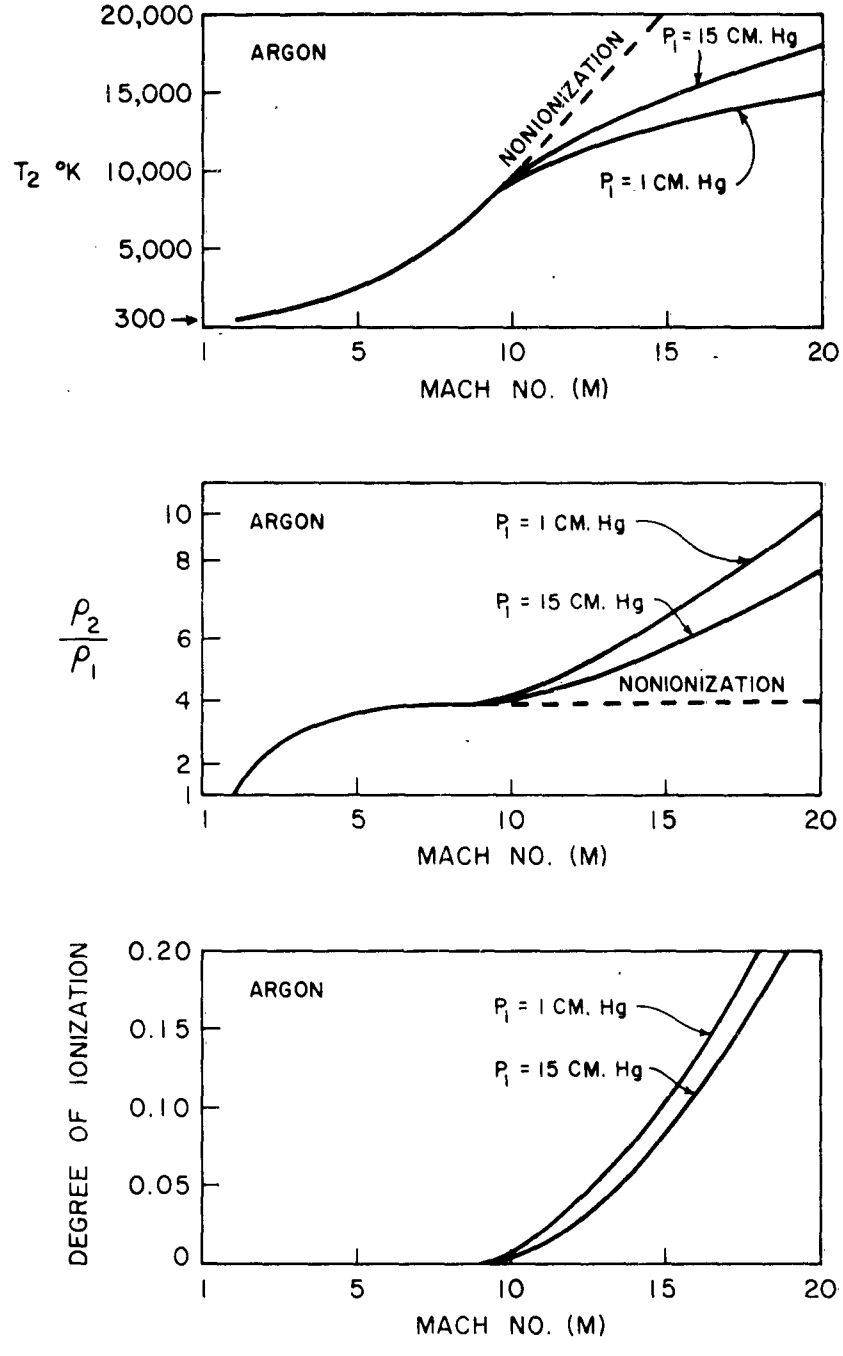

Figure 1. The temperature ratio T_2/T_1, density ratio ρ_2/ρ_1, and the degree of ionization as a function of Mach number for argon gas at 1 cm and 15 cm Hg pressure. $T_1 = 290^{\circ}$ K, $a_1 = 0$ (reprints from Resler et al.[13]).

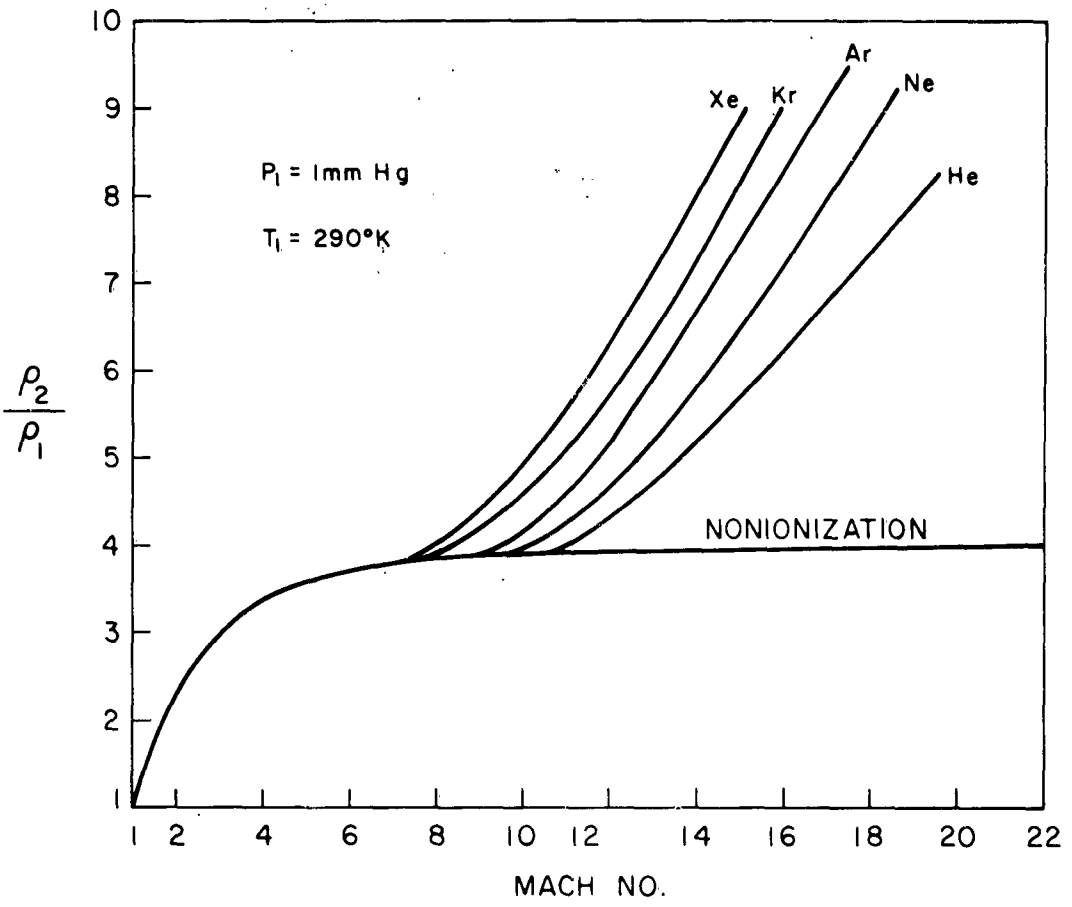

Figure 2. The density ratio ρ_2/ρ_1 as a function of Mach number for rare gases. $T_o = 296^o$ K, $P_o = 1$ mm Hg, and $\alpha_1 \approx 0$ (reprint from Niblett et al.[14]).

such as, collisional ionization processes and relaxation among the various degrees of freedom. Such computations are extremely complicated and can be pursued only after making certain drastic simplifying assumptions after which the validity of the computations are questionable. Even the basic method of attack is completely different than that used to find the jump relations across a shock wave. In that problem equilibrium prevailed which of course is not true in the shock wave. In spite of the inherent difficulties some work has been done in this area of endeavor and a limited amount of useful information has resulted. The most notable work along these lines is that by Petschek et al.[11] (1957) who computed the rate of ionization in shocked argon gas. A discussion of other work in this field of investigation for shock waves in both monatomic and polyatomic gases can be found in a review article by Losev et al.[41] (1961) concerning nonequilibrium phenomena in shock waves. The procedure used in these calculations is briefly discussed below. This same procedure will then be used to construct an approximate model for a shock wave in a slightly ionized background gas.

Consider the propagation of a shock wave in a non-ionized, room termperature, inert gas. The state of the shocked gas, after equilibrium is attained, is governed by the set of Equations (1) with appropriate expressions for pressure and enthalpy (Equations (6-12)). The set of conservation Equations (1) is equally valid across any two planes in the shock wave where equilibrium does not prevail but in this case Equations (10) through (12) do not apply. Hence, the set of Equations (1) can be used to determine the state variables profile in the shock wave if expressions for pressure and enthalpy are known or if reasonably approximate expressions for these variables can be obtained. This is difficult in the general case but approximate expressions for these variables can be obtained in the special case of low degree of ionization (i.e., $\alpha \ll 1$, $\delta \approx 0$). In this case, the approximate value of the pressure at any distance z behind the shock front, neglecting the charge particle partial pressures, is related to the gas particle

number density and the temperature by $p(z) \approx n(z)kT^{o}(z)$. Likewise, the specific enthalpy, neglecting low level excitation energies which in general is much less than translational energy, is approximately $h(z) = \frac{1}{m}\left[\frac{5}{2} kT^{o}(z) + a X^{o}\right]$.

In order to proceed further in the determination of state variable profiles it is convenient to follow a gas particle as it moves through the shock wave. At the shock front the translational degrees of freedom of the gas particles are suddenly altered. Translational equilibrium is attained among the shocked particles in a time on the order of a few mean times between collisions. The region in the shock wave where translational equilibrium is attained is known as the shock front. Behind the shock front the gas is in a non-equilibrium state. On the other hand, immediately behind the shock front a Maxwellian velocity distribution has already been attained in the shocked gas and a local gas temperature $T^{o}(z)$ can be introduced. All other relaxation processes in the shocked gas are much slower than that for translational equilibrium. Hence, immediately behind the shock front the entire shock energy is stored in translational energy of the shocked gas particles. As the heated particles proceed back from the shock front this energy is transferred into excitation and ionization energies. However, in the region immediately behind the shock front this transfer of shock energy has not proceeded appreciably and Equations (1) and (2) still apply. Hence, the jump relations 5 are approximately applicable across the shock front of ionizing shock waves as they are across the total shock wave if the shock wave is non-ionizing. This leads to an interesting observation which becomes apparent when Equations (1) are re-written in the following form

$$p_2 = p_1 + \rho_1 (1 - \rho_1/\rho_2) V_s^2 \tag{13a}$$

$$h_2 = h_1 + 1/2[1 - (\rho_1/\rho_2)^2]V_s^2 \tag{13b}$$

If p_2 and h_2 refer to the gas immediately behind the shock front, then $\rho_2/\rho_1 = 4M^2/(M^2 + 3)$ and this is valid regardless of whether or not the shock wave ionizes the gas. On the other hand, numerical solutions of Equations (1) and (6) through (12) show that the density ratio across ionizing shock waves never exceeds 8 even in the limit of infinite Mach numbers. Hence, it is obvious that in the special case of low degrees of shock ionization the density ratio cannot deviate appreciably from the value given by $\rho_2/\rho_1 = 4M^2/(M^2 + 3)$. In addition, since the shock velocity must be greater than Mach 8 for ionization to occur, then in the case of interest $\rho_2/\rho_1 \approx 4$. Therefore, for low degrees of shock ionization the density and the enthalpy are nearly constant throughout the shock wave and are approximately given by $\rho_2 = 4\rho_1$ and $h_2 = h_1 + \frac{15}{32} V_s^2$ respectively. Likewise, if excitation energies are neglected, then by considering the expressions for pressure and enthalpy in slightly ionized gases (i.e., $p = n^o kT^o$ and $h = \frac{1}{m}[\frac{5}{2} kT^o + \alpha X^o]$), it is obvious that in this case the temperature of the neutrals T^o and the neutral particle number density n^o are nearly independent of the distance behind the shock front.

Under the conditions and approximations imposed above the electron density profile in a shock wave can be approximately determined if the ionization rate of the gas at the appropriate temperature and density is known. Of course, the temperature and density of interest is the value given by usual shock relation 5. Calculations of this type have been made by Bond[12] and by Petschek et al.[11] Their results have been shown to reasonably approximate the conditions in a shock wave, hence indicating the validity of the above approximation.

The procedure used by Bond or that used by Petschek to determine the rate of ionization in shocked gases is too lengthy to discuss in detail in this paper. In essence, they showed that the ionization is predominately a two step process in which the shock energy is transferred from translational energy of the atoms to the free electrons in elastic collisons and after many energy gaining collisions the

kinetic energy of the electrons goes into ionization of the atoms as a result of inelastic electron-atom collisions. The fraction of the kinetic energy of an atom transferred to an electron in an elastic collision is equal to the ratio of the two masses. Hence, the number of energy gaining atom-electron elastic collisions required to raise the energy of an electron to the value necessary to ionize an atom or even to excite an atom in a collision is very large. In the case of argon gas with a thermal energy equal to about 1/10 the ionization energy ($T \approx 18,000^{\circ}K$), this requires approximately 10^6 energy gaining elastic collisions for each inelastic collision. It is obvious that in this case the rate of ionization is a rather slow process. The time required to reach equilibrium ionization has been determined both theoretically and experimentally. In the case of medium intensity shock waves ($M = 12$) in argon gas at a few mm Hg pressure, the time required for attainment of equilibrium is on the order of a few microseconds.

It is obvious that the shocked gas in its excited state will radiate energy in the visible and near ultraviolet spectrum. This radiation was neglected in the formation of our shock model and was considered to have a negligible effect on the properties of the shock wave. Although this assumption is probably valid under most conditions, a short discussion of this radiation is conducted below so that it can be used as a guide in the interpretation of experimental results presented in later sections of this paper. Only the visible radiated light is considered since this is the only part of the total spectrum which is transmitted through the glass walls of the expansion chamber to the photomultiplier detection cells.

The visible light radiated from the shocked gas is a combination of excitation and recombination light. The intensity of the recombination light in an ionized gas is directly proportional to the direct and indirect radiative recombination rate in the volume which in turn is directly proportional to the

square of the electron density (assuming $n_e = n_i$) and is also slightly dependent on the temperature of the electron gas. On the other hand, the excitation light is directly proportional to the number of excited atoms, hence is directly proportional to the electron density and is likewise dependent on the temperature of the electron gas. As was discussed above the temperature of the electron gas in a shock wave is governed by the termperature of the heavy constituents in the shocked gas. In addition, it was found that in the case of slight ionization ($\alpha \ll 1$) the temperature of the heavy constituents T^o is nearly constant throughout the shock wave ($T^o = T_i$ since particles of equal mass are in good thermal contact). Since the temperature of the electrons is governed by T^o although not equal to it, this implies that the temperature of the electron gas T_e is also nearly constant throughout the shock wave. Hence, to first order approximation the electron temperature is a constant throughout the shock wave and the temperature dependence of the excitation and recombination light in shocked inert gases can be neglected. Hence, the total radiation in the visible spectrum from the shocked gases is seen to monotonically increase with increasing electron density. Therefore, for shock waves in initially cold non-ionized inert gas the visible light intensity increases from zero intensity at the shock front and attains maximum intensity at the plane in the shock wave where equilibrium is established. The point of maximum light intensity in a shock wave has special significance in many shock wave experiments and is commonly referred to as the shock light front.

The problem of shock wave propagation in slightly ionized gases is important in many shock wave experiments and is especially important in electric shock tubes. This phenomenon is important in electric shock tubes because the background gas in the expansion chamber is preionized at the time of the shock producing electric discharge by photons of adequate energy from the discharge chamber. This process of photoionization is discussed in considerable detail in a later section. The purpose of the following discussion is to determine the effect of the preioniza-

tion on the properties of the shock wave and to obtain approximate jump relations across the shock wave with respect to both the neutral and the ionized constituents of the background gas.

It is apparent that the jump relations across a shock wave in a slightly ionized inert gas can be obtained by solving numerically the set of Equations (1) with appropriate expressions for pressure and enthalpy (Equations (6)-(12)). However, as is usually the case in numerical solutions, the physics of the phenomenon is lost in the computer. In addition, the numerical solution would only predict the state of the shocked gas after equilibrium is attained and would not indicate the jump relations with respect to the respective constituents of the background gas. Jump relations for each constituent can, however, be obtained directly across the shock front if certain simplyfying assumptions are made.

Consider a shock wave propagating through a slightly ionized inert gas. Let the degree of ionization of the gas prior to the passage of the shock wave be given by $\alpha_1 = n_1^+/(n_1^o + n_1^+)$. Assume that the ionized gas prior to the passage of the shock wave is in thermal equilibrium so that the temperature of the various constituents are equal ($T_1^o = T_1^e = T_1^i = T_1$). In addition, require the gas to be charge neutral ($n^+ = n_e = n_i$) both prior to and after the passage of the shock wave. In this case, the density, pressure, and specific internal energy of the ionized background gas is given by Equations (14a, b, and c) respectively.

$$\rho_1 = \mathcal{M}(n_1^o + n_1^+) = n_1' \mathcal{M} \tag{14a}$$

$$p_1 = kT_1(n_1' + n_1^+) \tag{14b}$$

$$e_1 = \frac{1}{n_1' \mathcal{M}} \left[\frac{3}{2} kT_1 \ (n_1' + n_1^+)\right] \tag{14c}$$

where $n_1' = n_1^o + n_1^+$. Contrary to the condition in front of the shock wave, the various constituents of the shocked gas immediately behind the shock front are not in thermodynamic equilibrium. If we consider a plane behind the shock front where each constituent has already attained a Maxwellian velocity distribution, we can speak of constituent temperatures which however are not necessarily equal to each other ($T_2^o \neq T_2^e \neq T_2^i$). These temperatures are not totally independent of each other but will relax to the same value after a sufficient number of energy exchanging collisions between unlike particles. Since the fraction of energy of a particle transferred to another particle in an elastic collision is equal to the ratio of the masses, the ions are always in good thermal contact with the atoms. Hence, immediately behind the shock front we have the following approximate thermodynamic relationship

$$T_2^o \approx T_2^i = KT_1 \tag{15}$$

where K is a proportionality constant possibly depending on the shock strength and the properties of the background gas. Contrary to this condition, the free electron gas is rather well thermally insulated from the atoms. Neglecting inelastic collisions, approximately $\mathcal{M}/m$ atom-electron or ion-electron collisions are required to attain thermodynamic equilibrium between the electrons and the heavy constituents. Depending on the degree of ionization and also on the temperature, this may occur in a time on the order of the time required to attain a Maxwellian velocity distribution in the heavy constituents, or possibly a much longer time. Hence, in order to keep the problem as general as possible we consider the plane behind the shock front where a Maxwellian velocity distribution is first attained in the heavy constituents and let the electron gas attain a temperature entirely independent of the heavy particles ($T_2^o = T_2^i \neq T_2^e$). The case of equal temperatures for each of the three gas constituents is an easy ex-

tension of the case considered.

The density, pressure, and specific internal energy of the shocked gas neglecting shock ionization and excitation, and for the case $T_2^{\,o} = T_2^{\,i} = KT_1 \neq T_2^{\,e}$ are given by Equations (16a, b, and c) respectively.

$$\rho_2 = \mathcal{M}(n_2^{\,o} + n_2^{\,+}) \tag{16a}$$

$$p_2 = k[(n_2^{\,o} + n_2^{\,+})\, KT_1 + n_2^{\,+}\, T_2^{\,e}] \tag{16b}$$

$$e_2 = \frac{1}{\mathcal{M}(n_2^{\,o} + n_2^{\,+})}\ \frac{3}{2}\, k[(n_2^{\,o} + n_2^{\,+})\, KT_1 + n_2^{\,+}\, T_2^{\,e}] \tag{16c}$$

Substitution of Equations (14) and (16) into Equations (1) leads to the following expressions which must be satisfied across the shock wave

$$\left\{\gamma M^2 \frac{n_1'}{n_2'}\left(1 - \frac{n_1'}{n_2'}\right) + \frac{n_1' + n_1^{+}}{n_2'} - K\right\} T_1 = \frac{n_2^{+}}{n_2'}\, T_2^{\,e} \tag{17a}$$

$$\left\{\frac{n_1' + n_1^{+}}{n_1'} + \frac{\gamma M^2}{5}\left[1 + \left(\frac{n_1'}{n_2'}\right)^2\right] - K\right\} T_1 = \frac{n_2^{+}}{n_2'}\, T_2^{\,e} \tag{17b}$$

where γ is the ratio of the specific heats in the non-ionized constituent, $n_1' = n_1^{\,o} + n_1^{\,+}$ and $n_2' = n_2^{\,o} + n_2^{\,+}$. Setting Equation (17a) equal to Equation (17b) and letting $\gamma = 5/3$ we find

$$n_2^{\,o} + n_2^{\,+} = \frac{4M^2(n_1^{\,o} + n_1^{\,+})}{M^2 + 3(1 + a_1)} \tag{18a}$$

or

$$n_2^+/n_1^+ = \frac{1}{a_1}\left\{\frac{4M^2}{M^2 + 3(1 + a_1)} - \frac{n_2^o}{n_1^o}\right\} + \frac{n_2^o}{n_1^o} \tag{18b}$$

where M is the Mach number with respect to the neutral constituent of the background gas.

The validity of Equation (18a) is independent of the degree of ionization of the background gas. If the background gas is not ionized, ($n_1^+ = n_2^+ = a_1 = 0$) then the compression ratio of the neutral constituent is given by

$$\frac{n_2^o}{n_1^o} = \frac{4M^2}{M^2 + 3} \tag{19}$$

which agrees with the previously calculated compression ratio given by Equation (5b).

If the background gas is fully ionized ($a_1 = 1$, $n_1^o = n_2^o = 0$), then the compression ratio of the charged constituents is

$$\frac{n_2^+}{n_1^+} = \frac{4M^2}{M^2 + 6} \tag{20}$$

Hence the compression ratio in the fully ionized case is nearly equal to the compression ratio in the non-ionized case and differs considerably only at low Mach number. Actually Equation (20) will apply only for $M \geq \sqrt{2}$. This restriction occurs because the shock velocity M is normalized with respect to the velocity of sound in a thermally perfect non-ionized gas, whereas the shock wave in this case is in a thermally perfect ionized gas for which (at $T_e = T_i$) the velocity of sound is $\sqrt{2}$ greater than the velocity of sound in a like, but non-ionized gas.

In a partially ionized gas ($0 < \alpha_1 < 1$) the compression ratios of the two constituents cannot be separated without considering the various relaxation processes in detail. However, in the case of slight degree of ionization ($\alpha \ll 1$) it is obvious that the compression ratio of the neutral constituent n_2^o/n_1^o will be, at most, only very slightly affected by the presence of the ionized constituents. Hence, in this case the compression ratio n_2^o/n_1^o is given approximately by Equation (19). Substitution of this expression into Equation (18b) with the additional approximation

$$\frac{1}{1 + \dfrac{3\,\alpha_1}{M^2 + 3}} = 1 - \frac{3\,\alpha_1}{M^2 + 3} \tag{21}$$

leads to Equation (22) for the compression ratio for the charged constituent in a slightly ionized inert gas

$$\frac{n_2^+}{n_1^+} = \frac{4M^2}{M^2 + 3}\left[1 - \frac{3}{M^2 + 3}\right] \tag{22}$$

As discussed above, this equation applies only if $M \geq \sqrt{2}$ because we have assumed in the derivation that the velocity of the shock wave is greater than the velocity of sound in the ionized constituent.

The above derivation shows that a shock wave in a slightly ionized gas compresses the charged constituents by a factor slightly less than the compression ratio of the neutral constituent. For shock velocities greater than about Mach 4 the two compression ratios are nearly equal but they differ considerably at low shock velocities. The near equality of the two compression ratios was experimentally verified by Takeda et al.,[42] although his results showed a much

smaller difference between the two ratios at low Mach numbers than that predicted by Equation (22). The reason for this discrepancy is most likely multifold. First of all, the velocity of propagation measured by Takeda is averaged over a distance of several centimeters, hence may be lower than the true shock wave velocity. On the other hand, it was assumed in the above calculation that the compression ratio in the neutral constituent is not altered by the ionized constituents. This is undoubtedly a very good approximation. However, since this compression ratio is divided by α in Equation (18b), a small variation in n_2^o/n_1^o due to the presence of the charged particles would have a large effect on the value of the compression ratio with respect to the charged particles. In addition, heat conduction was neglected in the above derivation. This is most probably a very good approximation in the absence of ionization. However, the effective velocity of heat flow via the free electron constituent of an ionized gas is under some conditions (depending on pressure, temperature, type of gas, etc.) supersonic.[7,8] Hence, this phenomenon may have a pronounced effect on the properties of shock waves, especially in the case of low velocity shock waves, and at least partially account for the small apparent discrepancy between the measured compression ratio and the value given by Equation (22).

The relatively high heat conductivity of a partially ionized gas and especially the velocity with which the heat energy propagates through an initially cold plasma medium has other far reaching implications in shock wave phenomena. These effects are especially pronounced in electric shock tubes as a result of the preionization of the background gas during the electric discharge and also due to the highly ionized driver gas which expands from the discharge section and closely follows the shock wave down the expansion chamber. Both of these phenomena are discussed in considerable detail in later sections of this paper and we consider here only the role of non-negligible heat conductivity on shock wave formation in electric shock tubes.

Consider an electrically driven shock wave propagating through a partially ionized background gas. The shock wave will compress the free electron constituent of the background gas according to Equation (22) and will also heat it. The initial temperature attained by the shocked free electron constituent of the background gas will be almost entirely independent of the temperature attained by the neutrals. However, these two temperatures will relax to the same value in a time on the order of m/m times the mean time between atom-electron collisions. In the absence of heat conduction these two temperatures will then remain nearly equal, with the temperature of the atoms slightly higher than that of the electrons. If the shock wave is sufficiently intense, kinetic energy is continuously transferred from the atomic gas to the electron gas and then back to the atoms in elastic collisions, until equilibrium is attained. This phenomenon was discussed above and is rather well understood. However, if the effect of heat conduction is considered, then it is obvious that it may play an important role in both the process of shock wave ionization and energy loss from the shock wave. In order for this effect to be important, the effective velocity of heat flow must be greater than the velocity of the shock wave. This condition is satisfied in some gases if they are ionized to a sufficiently high degree and if the heat source is sufficiently hot.[7,8] If this condition is satisifed, then heat energy can flow via the electron gas from the ionized shocked gas to the colder ionized gas in front of the shock wave, thereby quickly cooling the shocked gas. This same cooling process can also occur behind the shock wave, in which case shock energy is transferred via the electron gas from the ionized shocked gas to the ionized driver gas. Conversely, if the ionized driver gas is hotter than the shocked gas, then heat energy may flow from the driver gas to the shocked gas. Since heat energy can, under some conditions, flow either into or out of either end of the column of shocked gas, it is apparent that as a result of heat conduction the electron temperature in the shocked gas may be either higher or lower

than the temperature of the heavy constituents in the shocked gas. In addition, instead of the electron temperature being nearly constant throughout the shock wave, as in the case of negligible heat conduction, it may vary considerably. Both of these effects would affect the ionization rate and the visible radiation from the shocked gas. This phenomenon will be more fully discussed in a later section of this paper and some experimental evidence of the effect will be presented.

In addition to the cooling of the shocked gas as a result of heat conduction, it is possible that some precursor effects in front of shock waves are a direct result of this phenomenon. Several investigators have observed propagating precursor disturbances which propagate with a velocity nearly equal to the velocity of the shock wave.[6,9] To our knowledge, a mechanism for their production has not been found. It appears possible that percursors may be a result of heat flow from the shock wave to the gas in front of the shock wave. However, sufficient data is not available in order to determine whether or not this is the actual production mechanism. Precursors of this type were not observed in this work. This is most probably due to the use of insufficiently sensitive detection techniques.

4. DOPPLER SHIFT MEASUREMENTS OF SHOCK WAVE VELOCITY

When a shock wave travels through a background gas at a sufficiently high velocity it ionizes it. The degree of this ionization is, of course, dependent on a number of conditions. The mechanism of shock ionization is discussed in the previous section. In connection with Figures 1 and 2 it is seen that in the case of shock waves moving in room temperature inert gases the shock wave will ionize the gas to a significant degree only if the shock wave velocity is greater than about Mach 8 (slightly gas dependent). Above this threshold velocity the degree of shock ionization is a rapidly increasing function of shock wave velocity. If a shock wave in neon gas at 2mm Hg pressure has a velocity greater than about 2 Mach numbers above the threshold velocity for ionization, then the equilibrium degree of ionization is already sufficient to appreciably interfere with the propagation of 3 cm wavelength electromagnetic waves (i.e., $n_e > 10^{11}$ /cm^3). The phenomenon of EM wave interaction in the shock ionized gas can be applied to the determination of shock wave velocity and is also useful in the investigation of the electrical properties of the produced plasma. In this section we consider the measurement of shock wave velocities by Doppler frequency shift of an EM wave reflected by the shock wave plasma.

Doppler frequency shift of an electromagnetic (EM) wave of known frequency reflected by the plasma associated with a shock wave has previously been used by other investigators to measure the velocity of shock waves.[28,29] In these works the investigators assumed that the velocity of the EM reflecting plasma cloud was equal to the velocity of the shock front, that the EM reflection coefficient of the plasma cloud was time independent, and that the phase velocity of the incident EM wave immediately before reflection was equal to its phase velocity in vacuo. The first two of these assumptions are approximately realized in practice if the shock wave is sufficiently intense (> Mach 10), but the latter assumption is usually not realized in electric shock tubes at relatively short times after

the end of the shock producing electric discharge. This is due to the preionization of the background gas at the time of the discharge. In this section EM reflection by a propagating plasma cloud characterized by a time independent EM reflection coefficient and propagating through a background plasma of known electron density is considered. Although the properties of such reflections are well known, some elaboration will prove useful in discussions conducted in later sections of this paper.

We consider an EM reflecting body characterized by a time independent EM reflection coefficient propagating in the z direction through a plasma medium of known electron density. The electron density of the background plasma is assumed to be spatially independent in the x and y directions but relatively slow spatial variations are permitted in the z direction. In addition, it is assumed that the electron density at each point in space is time independent. For an incident EM wave of frequency f_o the frequency of the reflected wave f_R is determined by summing the time required for a wave train to pass through adjacent regions of the background medium of infinitesimal thickness dz. A wave train of any convenient length can be used in this calculation but for convenience a wave train one wavelength long is considered. Under these conditions the period of the reflected wave $\tau_R = 1/f_R$ is given by

$$\tau_R = \tau_o - 2\int_{z'}^{z_o} \frac{dz}{V_p(z)} \tag{23}$$

where $\tau_o = 1/f_o$ is the period of the incident wave, $V_p(z)$ is the phase velocity of the incident at position z, z_o is the position of the reflecting surface at the time when the leading edge of the sensing wave train first reaches it, and z' is the position of the reflecting surface when the trailing edge of the sensing wave train reaches the reflecting surface. In general z' is not known

but is related to the velocity of the reflecting surface (V_R) and the phase velocity of the incident wave by the following equation.

$$\int_{z''}^{z'} \frac{dz}{V_p(z)} = \frac{z_o - z'}{V_R} \tag{24}$$

where z'' is related to the physical length of the sensing wave train when it first reaches the reflecting surface. Its functional dependence in terms of the period of the incident wave is given by Equation (25).

$$\int_{z''}^{z_o} \frac{dz}{V_p(z)} = \tau_o \tag{25}$$

If the EM reflecting surface is propagating along the longitudinal direction of a metal rectangular waveguide and if all modes of the incident EM wave are cut off except the $TE_{1,0}$ mode, then the phase velocity of the incident EM wave is given by Equation (26).

$$V_p = \frac{c}{\sqrt{\epsilon_r - (\lambda_o/2a)^2}} \tag{26}$$

where c is the velocity of light in vacuo, ϵ_r is the relative dielectric constant of the medium filling the waveguide, a is the wide dimension of the rectangular waveguide, and $\lambda_o = c/f_o$. If the waveguide is filled with a plasma of known electron density $n_e(z)$, then the relative complex dielectric constant at angular fre-

quency $\omega_o = 2\pi f_o$ is given by

$$\epsilon_r(z) = 1 - \frac{(\omega_p(z)/\omega_o)^2}{1 + j\,\nu/\omega_o} \tag{27}$$

where $\omega_p(z) = (n_e(z)\, e^2/\epsilon_o m)^{1/2}$ is the plasma frequency, e and m are the electron charge and mass, and ν is the effective electron-molecule collision frequency for momentum transfer. Substitution of this value of ϵ_r into Equation (26) with the additional assumption that $\nu \ll \omega$ one obtains (it will be shown in a later section of this paper that this assumption is valid in the experiments conducted in this work)

$$V_p(z) = \frac{c}{\sqrt{1 - (\omega_p(z)/\omega_o)^2 - (\lambda_o/2a)^2}} \tag{28}$$

Equations (23)-(25) with the aid of Equation (28) expresses the Doppler frequency shift of an EM wave reflected by a surface propagating through a plasma medium in a rectangular waveguide. Of course for this equation to apply the phase velocity of the incident EM wave prior to reflection must be real valued (i.e., $[(\omega_p/\omega_o)^2 + (\lambda_o/2a)^2] < 1$). In the special case where the electron density in the background medium filling the waveguide is independent of z the above equations reduce to Equation (29).

$$\Delta f = \left| f_R - f_o \right| = \frac{2V_R}{\lambda_o} \sqrt{1 - (\omega_p/\omega_o)^2 - (\lambda_o/2a)^2} \tag{29}$$

This simplified equation relating the Doppler shift to the reflector velocity is approximately valid if the phase velocity $V_p(z)$ is nearly constant throughout the region traversed by the reflecting surface during the time required to measure the frequency of the reflected wave.

It will presently be seen that Equation (29) is approximately applicable in the case of electrically driven shock waves only if the time of observation is sufficiently later than the time of the shock producing electric discharge. This equation will usually not apply at short times after the electric discharge due to rapid spatial and time variations in the background electron density. Many of the experiments discussed below are concerned with either the direct or indirect application of Equation (29) to the study of phenomena occurring in electrically driven shock tubes.

5. THE SHOCK TUBE

The investigated shock waves were produced by sending a pulse of high current through a low pressure gas in a cylindrical discharge chamber similar to the chamber used by Josephson.[4] The particular configuration used in the majority of this work is illustrated in Figure 3. It consisted of a molydenum rod electrode (1/4 inch diameter) and a 0.85 inch inside diameter stainless steel ring electrode. The sleeve of the ring electrode was insulated from both the rod electrode and the electric discharge heated gas by a short length of Vycor glass tubing. Pyrex glass insulating walls were used in some early discharge chamber models. While Pyrex glass is advantageous in many respects, especially since it can be formed into any desired shape without introducing excessive strain, it was found that Pyrex would not withstand the intense heat produced in the volume by the electric discharge. However, Vycor glas has far superior thermal and mechanical properties and appeared to be negligibly damaged even after several thousand shock wave producing electric discharges.

Shock wave producing electric discharges were made by discharging a 14.5 μf, 20 kv low inductance capacitor through the gas filled discharge chamber. The energy storage capacitor was electrically connected to the two electrodes of the discharge chamber by means of a short length of double braid coaxial cable. The electric discharge was initiated at the desired time by a trigger pulse to a GL-7703 ignitron in series with the discharge chamber and the capacitor. A second GL-7703 ignitron, placed directly across the terminals of the energy storage capacitor was used as a crowbar circuit. A schematic representation of the circuitry involved is illustrated in Figure 4. The sequence of events is as follows. The energy storage capacitor with the positive terminal grounded was first charged to the desired potential. At the desired time the main ignitron was triggered. This trigger pulse was obtained by discharging a 2 μf capacitor, charged to 3 kilovolts, through the primary of an air core 2 : 1 step-up trans-

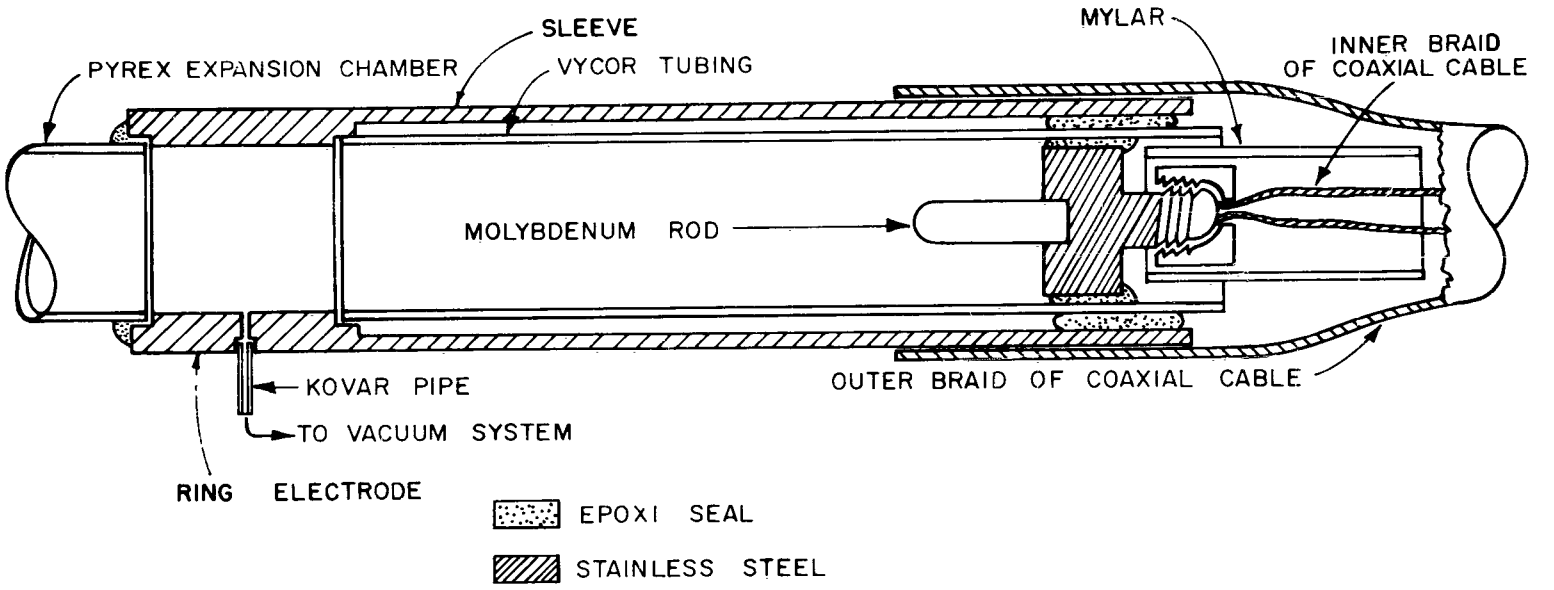

Figure 3. Cross-sectional view of the discharge chamber.

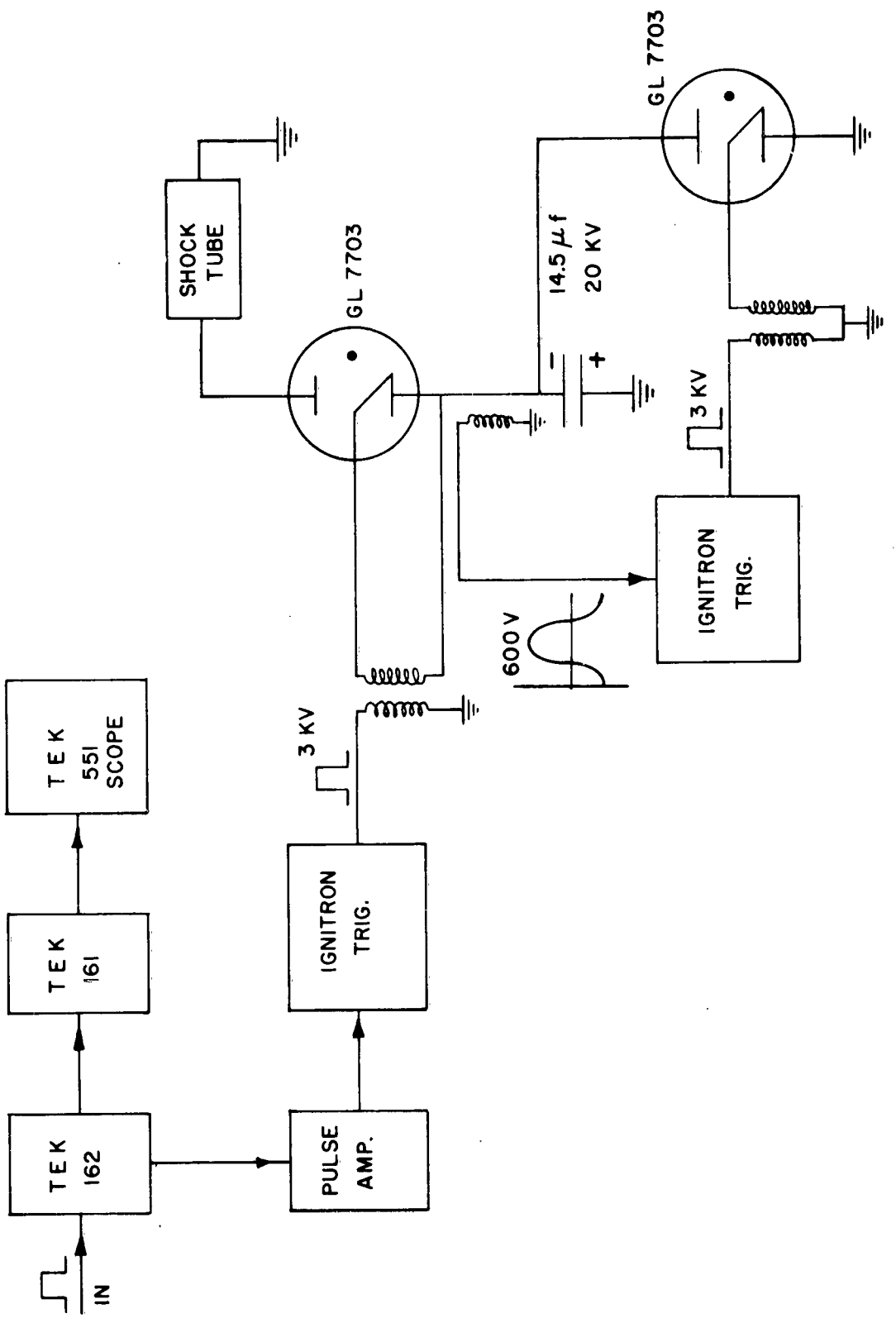

Figure 4. Block diagram of the electrical system used to trigger the shock wave producing electric discharge. The electrical system used to crowbar the oscillating electric discharge is also shown.

former whose secondary voltage is applied to the ignitor. With the discharge chamber filled with a gas at a few mm Hg pressure the current reached its maximum value in about 4 microseconds. Without the crowbar circuit in operation the discharge current would then continue to oscillate at approximately a 62 kilocycle rate. The number of cycles of oscillation before the discharge current fell to a negligible value was, of course, dependent on the discharge voltage and the type and pressure of the gas filling the discharge chamber. The oscillating discharge current is disadvantageous in many respects and especially because successive shock waves are formed during each half cycle. The successive shock waves travel in a gas already heated by previous shock waves, hence over take the shock wave formed by the first half cycle of discharge current and reinforce it. This reinforcement tends to complicate experimental observations of shock wave phenomena and also complicates the phenomena itself. The successive shock waves were eliminated by placing a second ignitron directly across the capacitor and igniting it a fraction of a microsecond after the voltage across the energy storage capacitor went through zero from negative to positive. The pulse applied to the ignitor of the crowbar ignitron was obtained in a manner similar to that applied to the main ignitron. The timing for this trigger pulse was conveniently obtained by a search coil placed close to the center lug of the energy storage capacitor. The magnitude of the voltage across the search coil was, of course, dependent on the magnitude of the discharge current. In the case of a 12 kv discharge, the search coil voltage had a maximum amplitude of about 600 volts. A diode across the input of the trigger circuit to ground prevented the first quarter cycle of the search coil signal from saturating the circuitry in the trigger circuit. This trigger circuit was constructed so that it would fire when the sinusoidal input signal reached a voltage equal to about 6 volts positive. With the crowbar circuit in operation the peak value of the first negative swing of the discharge current was reduced to less than 10 $^{o}/_{o}$

of its peak value without the crowbar ignitron. After this time the current through the discharge chamber continued to oscillate for about 35 microseconds but at a reduced amplitude. With the crowbar circuit in operation no evidence of formation of more than one shock during any one discharge was found.

An essential feature of shock wave production by electric discharge is the necessity of heating the gas in the discharge chamber in a very short time. This requires a fast rising discharge current and consequently it requires small stray inductances in the discharge circuitry. The stray inductance was minimized by the coaxial geometry design of the discharge circuitry. The construction of the ignitron housing is illustrated in Figure 5. The main ignitron is mounted directly on the center lug of the energy storage capacitor. A cylindrical housing around this ignitron is used as the return path for the discharge current. Double braid coaxial cable with the inner conductor connected to the plate of the main ignitron and the outer conductor connected to the cylindrical housing of the main ignitron, guides the discharge current from the capacitor to the coaxial discharge chamber. Mylar in sheet form is wrapped around the ignitron and its mounting in order to electrically insulate it from the cylindrical housing. The plate of the crowbar ignitron is electrically connected to the center lug of the capacitor with a 1/8 inch thick copper plate.

The shock tube expansion chamber used in the majority of the experiments discussed below is illustrated in Figure 6. The open end of the discharge chamber was epoxy sealed to a piece of Pyrex glass tubing. The inside diameter of this tubing was 0.8 inches which is also the inside diameter of the hollow ring electrode. A slow transition from the circular to rectangular cross section (0.4 inches by 0.9 inches dimensions) funnelled the shock waves to the inside dimensions of x-band waveguide (i.e., WR-90). An x-band waveguide cover flange (i.e., UG-39/U) with an o-ring groove was epoxy sealed to the far end of the rectangular cross section glass wall expansion chamber. This permitted easy in-

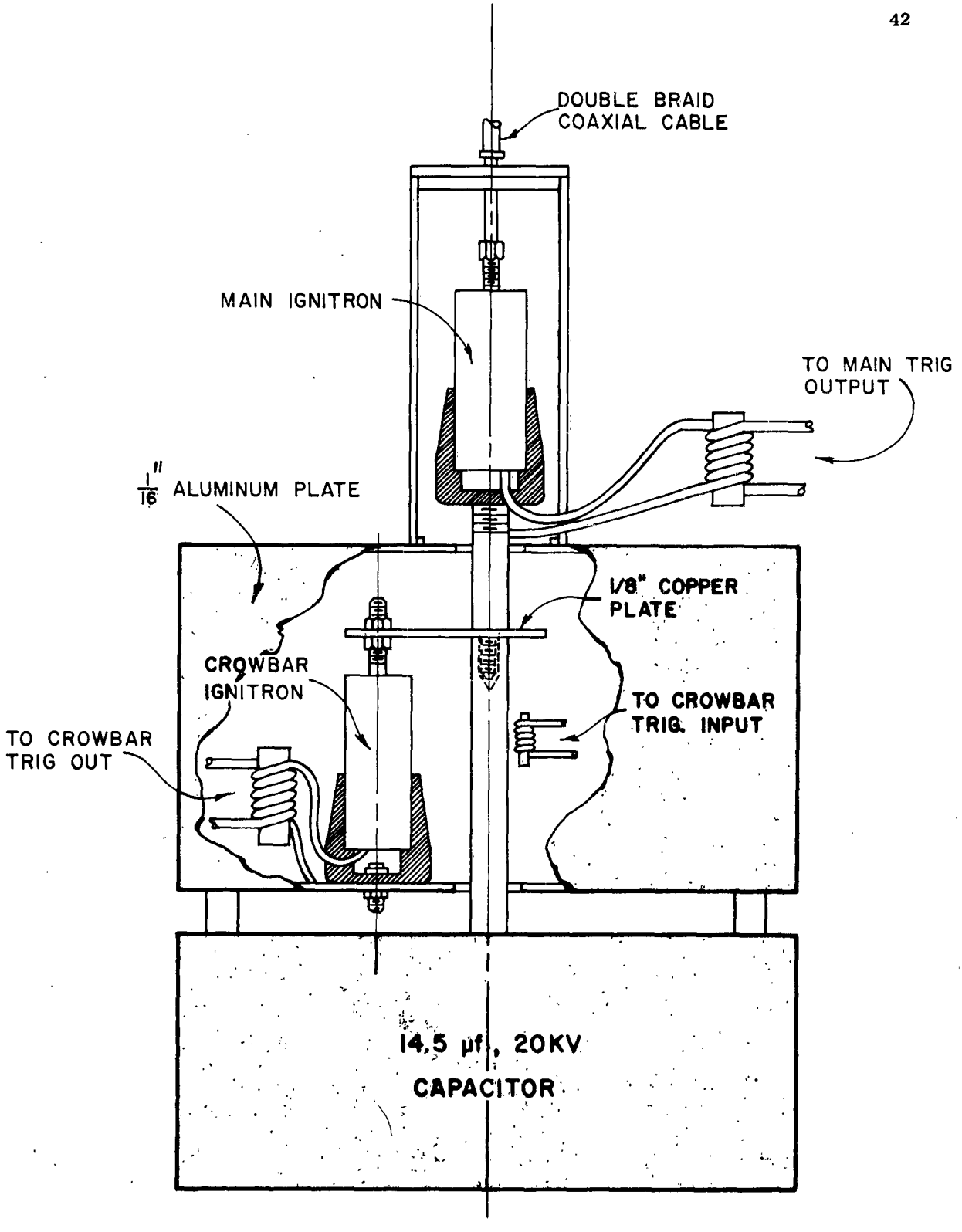

Figure 5. Illustrates the mounting of the two ignitrons which were used to trigger and crowbar the shock wave producing electric discharge.

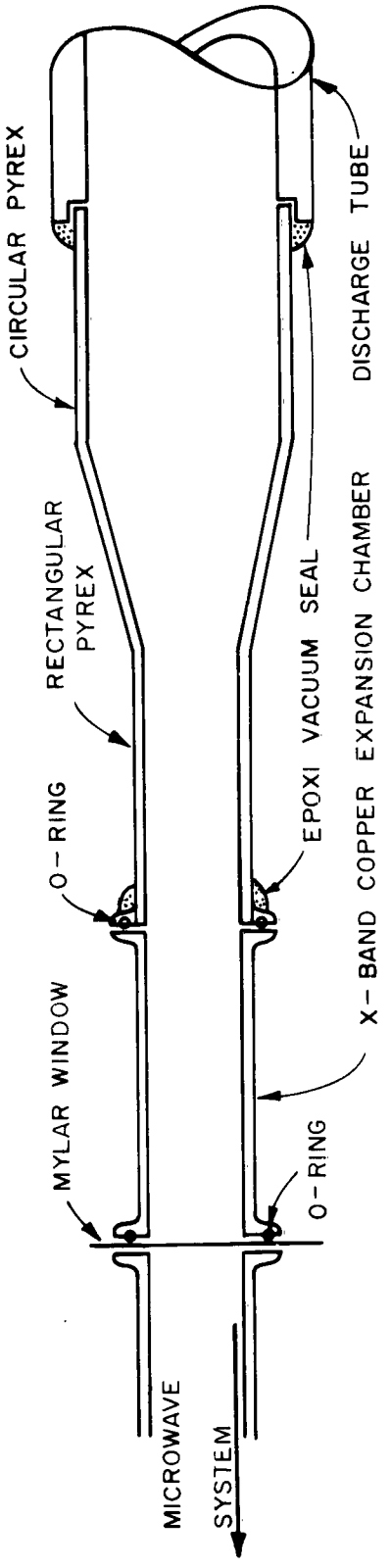

Figure 6. Cross-sectional view of the shock tube expansion chamber.

stallation of various metal wall expansion chambers. Most of the experiments discussed below were conducted in the metal wall section of the expansion chamber. Several different designs were used as expansion chamber observation sections and each is fully described below. Each of these observation sections was constructed with a length of stock x-band waveguide as the expansion chamber walls. The downstream end of the metal expansion chamber was connected to an x-band microwave source and detection system. An eight mil mylar window with an o-ring was used at this connection as a vacuum seal.

The vacuum pumping system and gas supply was connected to the shock tube through a 3/16 inch diameter hole in the ring electrode of the discharge chamber. The entire shock tube was evacuated to less than 10^{-6} mm Hg and then filled with the desired gas at the desired pressure before each discharge. Most of the experiments discussed below were conducted in a background gas of either neon or argon at a few mm Hg pressure. These gases were obtained from Linde Corporation in one liter glass flasks. In some experiments air was used as the background gas. This was obtained at the desired pressure by slightly opening a stop-cock which was open to the room and letting Illinois air leak into the system. The vacuum pumping system was an all glass system utilizing greased (Apiezon type N vacuum grease) stop-cocks, a three stage water cooled oil diffusion pump, and a mechanical fore pump. Gas pressure measurements were made by an RCA 1949 ionization gauge, an RCA 1946 thermocouple gauge, and an Octoil-S oil manometer.

Figures 7 and 8 illustrate the two expansion chamber observation sections which were used in the majority of the experimental work discussed below. Each of these was constructed from a length of copper wall x-band waveguide. They were fitted with special o-ring grooved cover flanges so that vacuum interconnection of sections could be made with relative ease. The chamber illustrated in Figure 7 includes four ports of observation each separated by five centimeters. At each observation port a 62 mil diameter hole was drilled in the center of one

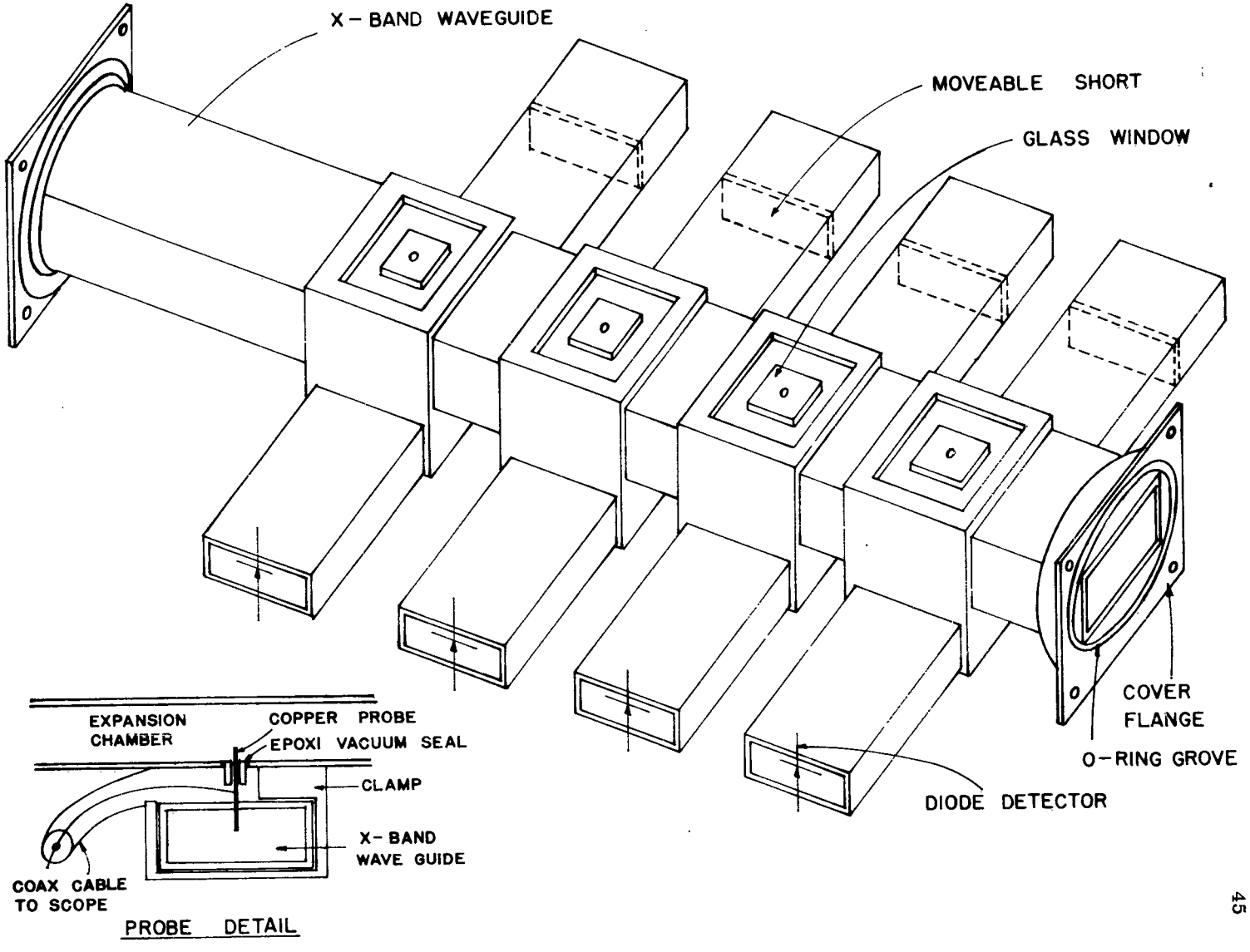

Figure 7. A metal wall test section expansion chamber.

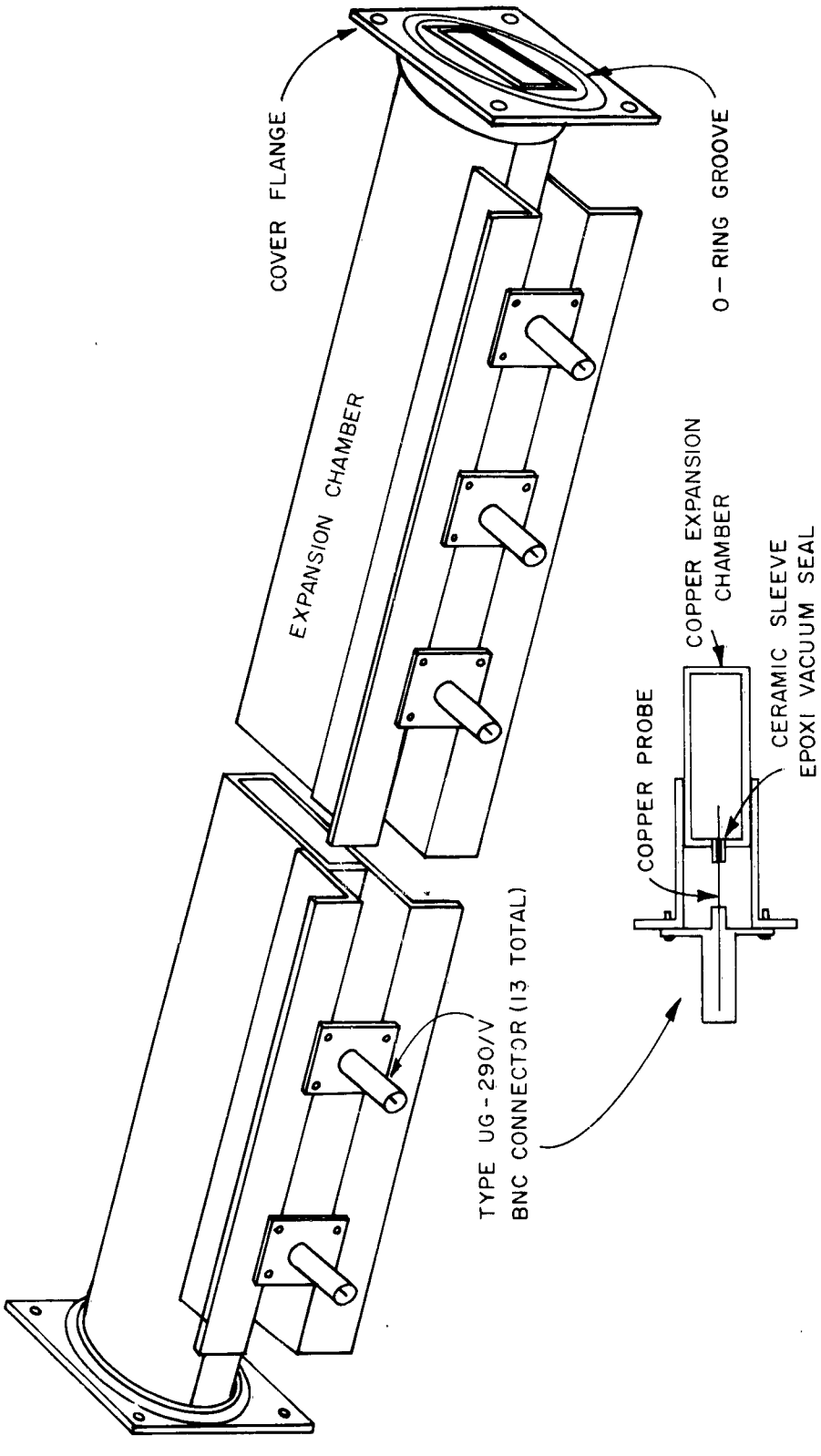

Figure 8. A metal wall test section expansion chamber.

of the broad walls of the waveguide and was covered with a thin piece of glass plate. The glass cover was vacuum sealed to the metal wall with epoxy cement. A quartz fiber light pipe, placed against the glass cover and directly in front of the hole, guided light radiated by the shocked gas to photomultipliers. Directly opposite each light port, in the center of the other broad wall of the metal wall expansion chamber, a small metal probe penetrated through the wall and extended into the chamber. Each of these metal probes was a 10 mil copper wire and each extended 1/16 inch into the interior of the expansion chamber. Each probe was electrically insulated from the metal wall by a ceramic sleeve and was vacuum sealed with epoxy cement. Outside the expansion chamber, a short length of coaxial cable was connected to each of the metal probes. Each of the coaxial cables was terminated in a 2.2k ohm resistor and the voltage across this resistor was monitored as the shock wave passed over the respective probe.

The small metal probes were also used as microwave antennas. A microwave signal was propagated down the expansion chamber while a shock wave advanced along the chamber in the opposite direction. The plasma column associated with the shock wave partially reflected the incident microwaves. The reflection coefficient of the incident EM waves was, of course, dependent on the frequency of the waves and the electron density profile in the shock wave. The resulting EM waves in the waveguide at the position of each of the metal probes was sampled by the respective probe and partially coupled into that probe's respective detection waveguide. The length of the detection waveguides, between the coupling probe and the detector mount, was sufficient to prevent the low frequency signal on the probe due to charge distribution in the expansion chamber from reaching the microwave detector. The magnitude of the EM signal coupled from the expansion chamber into a detection waveguide was obviously dependent on the position of and the reflection coefficient of the propagating plasma column reflector. Prior to the passage of the shock front over the probe, the

magnitude of the coupled EM wave varied in time according to Equation (29). During the passage of the shock wave over the probe the amplitude variation of the coupled EM wave depended on the electron density profile of the propagating plasma reflector. This method was used to investigate the structure of shock waves and is more fully described in a later section.

In a second application of the expansion chamber shown in Figure 7, the microwave source was located in one of the secondary (detection) waveguides and the probes were used to couple a portion of this EM energy into the expansion chamber. When so used the measurements were based on the fact that the impedance of the probe as seen by the microwave signal in the secondary waveguide was dependent on the radiation impedance of that portion of the probe in the expansion chamber. Consequently, the impedance of the probe measured in the secondary waveguide varied sharply as the shock wave plasma passed over the probe.

The expansion chamber illustrated in Figure 8 is similar to the one illustrated in Figure 7, except the probes penetrated through the narrow wall of the expansion chamber and provision was not made to observe the light radiated by the shocked gas or to measure the EM energy spatial distribution in the waveguide.

6. CONCERNING THE PREIONIZATION OF BACKGROUND GAS

The apparatus used to investigate the ionization process in the background gas during the shock wave producing electric discharge is illustrated in Figure 9. The expansion chamber is similar to the glass wall portion of the chamber illustrated in Figure 6, but in this case the metal section was removed in order to eliminate the possibility of a direct electric discharge through the background gas. The electron density in the expansion chamber and between the two waveguide horns was measured by the now well-known electromagnetic propagation technique. The 30.8 Gc microwave apparatus could be positioned at any point along the 25 cm long glass wall expansion chamber either in or downstream from the external transverse magnetic field. The intensity of this magnetic field was variable from 0 to 3.5 kilogauss and was used to curtail the diffusion of charged particles across the field lines down the chamber. The specific application of the magnetic field will be further discussed when appropriate.

The microwave propagation technique of measuring electron density in plasmas is well known and will not be discussed here in detail.[10] Electron densities less than $9.5 \times 10^{12}/cm^3$ but greater than $10^{12}/cm^3$ could be determined with the indicated 30.8 Gc waves by measuring the EM transmission coefficient of the waves incident on the plasma filling the expansion chamber.[43] It was assumed in this measurement that the traversed plasma was effectively an infinite slab of plasma of known thickness. This assumption is justified since all measurements were conducted in the rectangular cross section expansion chamber, the width of which was much larger than the width of the EM beam. The error in the experimentally measured values of electron density throughout the indicted density range is believed to be less than $10^{o}/o$. The measurable range of electron density as well as the accuracy could both be increased by using more sophisticated EM measuring techniques but this was found to be unnecessary.

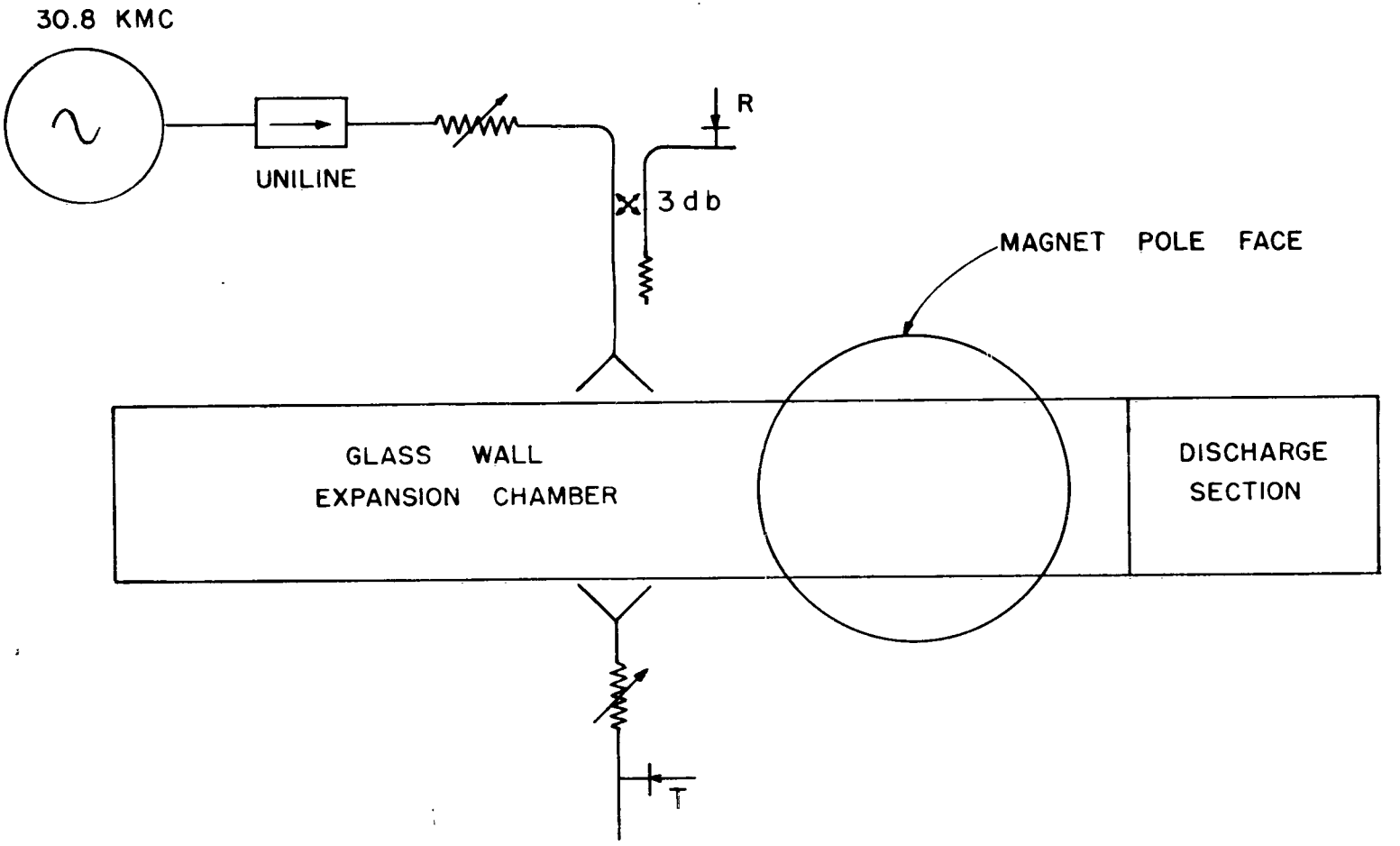

Figure 9. Block diagram of the experimental apparatus used to investigate the electrical properties of the background gas.

Figure 10 illustrates the variation in amplitude of the transmitted 30.8 Gc EM wave during and after a typical shock wave producing electric discharge. Upward deflection represents increased transmission and the level of the trace following the passage of the shock wave at t = 22 μ seconds represents zero level transmission. In the case illustrated, the discharge voltage was 12 k volts, in neon gas, at 4 mm Hg pressure and the probing microwave system was located 15 cm downstream from the open end of the discharge chamber. The initiation of the electric discharge was delayed 2 μ seconds with respect to the start of the scope sweep. The amplitude of the transmitted EM wave is seen to exhibit a decrease shortly after initiation of the electric discharge and reach a temporary minimum at t = 6 μ seconds which is also the time of maximum discharge current. The amplitude of this wave subsequently increased and returned to nearly total transmission until the shock wave passed the point of observation at t = 22 μ seconds. From experimental calibration curves it is found that at the time of maximum discharge current, the voltage transmission coefficient of the 30.8 Gc EM wave was $T_p^{\frac{1}{2}} = 0.28$ from which it is determined that $n_e = 9 \times 10^{12}/cm^3$.

The degree of preionization of the background gas during the time of the shock wave producing electric discharge was highly dependent on the type and pressure of the background gas, the discharge voltage, and the distance from the discharge chamber. The time at which the degree of preionization attained its maximum value was coincident (within the accuracy of the measurement $\sim 10^{-7}$ sec.) with the time of maximum discharge current and did not vary along the 25 cm long expansion chamber. The phenomenon was investigated in both neon and argon gases in the pressure range from 0.1 to 5 mm Hg. The information obtained in these experiments is fully described below.

Several mechanisms for the preionization of the background gas at the time of the shock wave producing electric discharge have been postulated by other authors but to our knowledge no definite conclusions have been drawn.[5,6] The

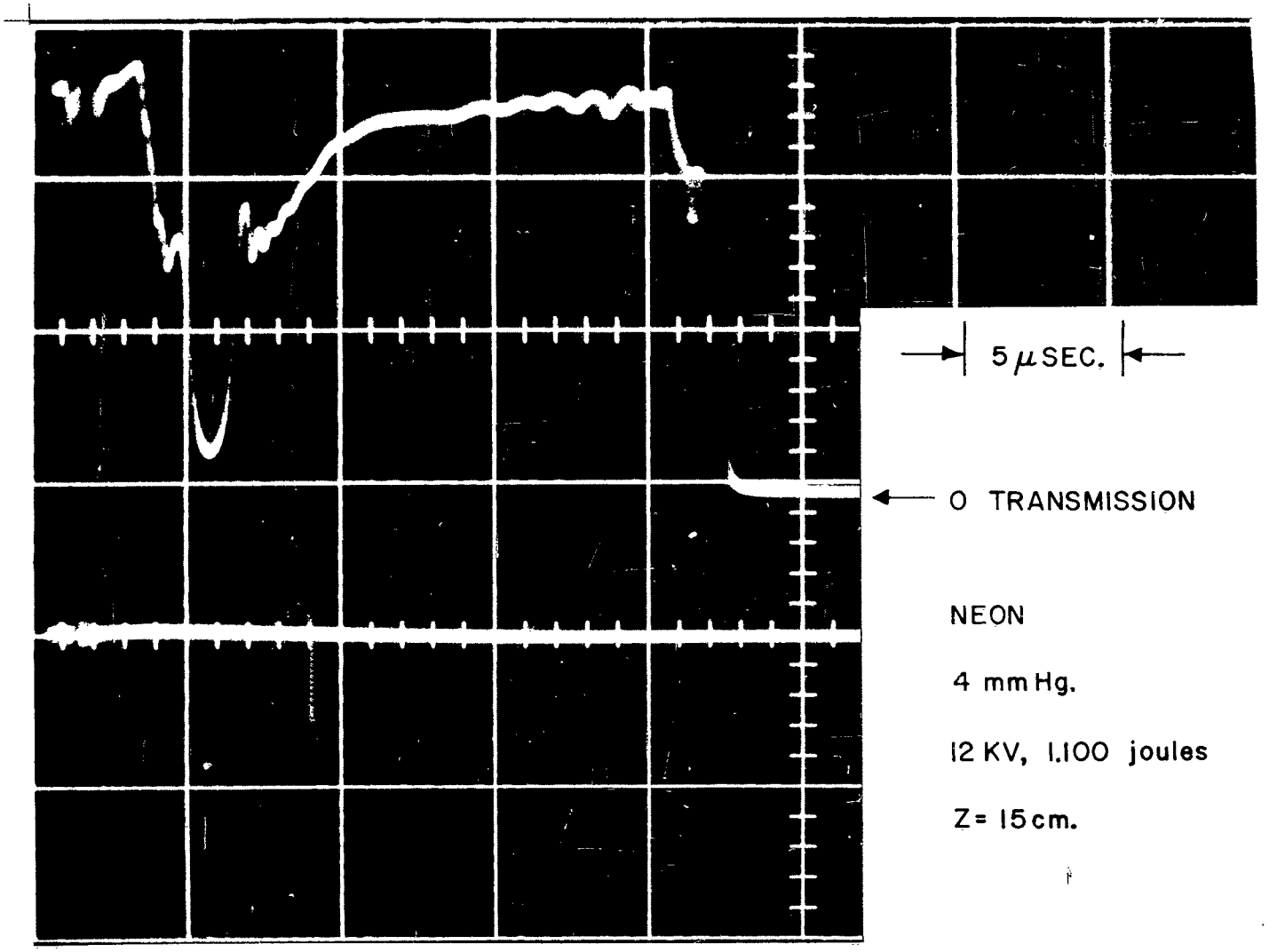

Figure 10. Represents the amplitude of the transmitted 30.8 Gc EM waves across the glass wall expansion chamber at a distance 15 cm from the discharge chamber during and after a shock wave producing electric discharge.

purpose of the following discussion is to show that under some circumstances this preionization may be predominately due to photoionization by soft X-rays (λ on the order of a few angstroms) emitted from the discharge chamber during the electric discharge. A spectometer for this range of wavelengths was not available for this investigation so consequently the results are not conclusive. However, it is shown that in the shock tube used in this investigation the electron density spatial decay resulting from the preionization is consistent with ionization by K radiation from the electron bombarded, stainless steel anode. Other mechanisms such as diffusion of energetic electrons from the discharge heated gas and short range, high energy ultraviolet radiation may also be important under some circumstances. However, as is discussed below, at points further from the discharge chamber greater than a few tube diameters and with the gas conditions considered here our results indicate that the preionization is most probably predominately due to soft X-rays.

Consider a photon stream originating in the discharge chamber and flowing through the expansion chamber. Let z be the distance along the chamber measured from the open end of the discharge chamber and let $I(z,\lambda)d\lambda$ represent the total number of photons in the wavelength range $\lambda + d\lambda$ flowing through an expansion chamber of arbitrary cross section at z cm from the discharge chamber. In this case, the flow density $I(z,\lambda)\ d\lambda$ can be expressed in terms of the geometry of the shock tube and the type and pressure of the background gas. This expression is given by Equation (30).

$$I(z,\lambda)\ d\lambda = \Omega(z)\ I(o,\lambda)\ e^{-\mu pz}\ d\lambda \qquad (30)$$

where $\mu(\lambda)$ is the linear absorption coefficient for photons of wavelength λ in the respective background gas, p is the gas pressure in mm Hg, and $\Omega(z)$ is a geometrical factor which accounts for loss of photons from the photon stream defined

by the bounding walls.

The total number of photons lost from the stream in length dz is given by Equation (31)

$$-\frac{\partial}{\partial z}\left[I(z,\lambda)d\lambda\right]dz = I(o,\lambda)\, e^{-\mu p z}\, d\lambda \left[\mu p \Omega - \frac{\partial \Omega}{\partial z}\right] dz \qquad (31)$$

The first term on the right hand side of this equation accounts for loss of photons from the stream by absorption in the volume and the second term accounts for loss of photons from the stream by striking the bounding walls (assuming that all photons which strike the walls are captured).

An exact analytical expression for $\Omega(z)$ cannot be obtained for all z because we have no way of knowing exactly where the photons originate or their initial flow direction. However, at distances sufficiently far downstream it is obvious that the photon stream can be projected back to an apparent point source located somewhere in or behind the discharge chamber. Therefore at values of z greater than a few shock tube diameters $\Omega(z)$ is given by a constant K times the solid angle subtended by the expansion chamber from the apparent point source arbitrarily located at z = -c. In the case of a rectangular cross section expansion chamber a x b on a side this is given approximately by Equation (32)

$$\Omega(z) \approx \frac{K\, ab}{(z+c)^2} \quad \text{if} \quad z \gg \left[(b/2)^2 + (a/2)^2\right]^{1/2} \qquad (32)$$

In order to determine the total number of free electrons at any value of z which results from the incident photon stream, we must consider all secondary electrons. This must include the effect of the energetic photoelectrons as well as the effect of fluorescence and re-emission from the photon excited and secondary electron excited atoms and ions. These two effects are accounted for by the factors α and γ in Equation (33) which expresses the total number of electrons

in the volume abdz evaluated at z due to the incident ionizing photon stream.

$$n_e(z) = abK\int_0^{\ell} \frac{d\tilde{z}}{(\tilde{z}+c)^2} \int_0^{\infty} I_{(o,\lambda)} \left[\mu p^{\alpha}(z-\tilde{z},\lambda,gas) + \frac{2}{\tilde{z}+c}\,\gamma(z-\tilde{z},\lambda,gas)\right] e^{-\mu p\tilde{z}} d\lambda \quad (33)$$

In particular, the factor $\alpha(z-\tilde{z},\lambda,gas)$ represents the average number of secondary electrons produced in the volume abdz at z due to a primary photon of wavelength λ being absorbed in the volume abdz at $\tilde{z}$. Likewise, the factor $\gamma(z-\tilde{z},\lambda,gas)$ represents the average number of secondary electrons produced in the volume abdz at z due to a primary photon of wavelength λ striking the bounding walls in the length dz at $\tilde{z}$.

Atoms excited by absorption of primary radiation and atoms excited by collisions with photoelectrons resulting from this absorption will subsequently emit fluorescent radiation with ionizing capabilities. The effective energy spending range of both the photoelectrons and the fluorescent radiation will, under some conditions, be relatively long. In addition, successive fluorescence and successive re-emission will tend to make their effective energy spending range for ionization even longer. For purposes of illustration let us consider how energy is transferred from a primary photon to the gas when it is absorbed by a gas atom in the interior of a gas filled rectangular cross section expansion chamber a by b on a side. The absorbed photon will eject one or more electrons (accounting for Auger electrons) from the atom, possibly from an inner energy shell, leaving it in a highly excited and ionized state. The energy of the photoelectrons will be spent in inelastic collisions in the background gas and secondary electron emission from the containing walls. The effective energy spending range of the energetic photoelectrons is dependent on the gas conditions, the energy of the electrons, and the geometry of the expansion chamber. Under some conditions this energy spending range is relatively long and in this case the factor $(z - \tilde{z})$ in the term $\alpha(z-\tilde{z},\lambda,gas)$ is appreciable and must be considered in the

evaluation of the integral. However, the energetic electrons can be forced to spend the majority of their energy locally by placing the expansion chamber on a sufficiently intense transverse magnetic field which curtails diffusion of electrons across the magnetic field lines and down the chamber. It was experimentally found that within the accuracy of this experiment and under the investigated experimental conditions, a transverse magnetic field of 3.5 kilogauss had no observable effect on the resulting electron density either in or at any point downstream from the magnetic field. In view of this, even in the absence of the external magnetic field, the photo and secondary electrons spend the larger fraction of their energy locally. Hence, to first order approximation the term $\tilde{z}$ in $a(z-\tilde{z},\lambda,\text{gas})$ can be set equal to z.

The excited ion resulting from the absorption of the primary photon will subsequently emit fluorescent radiation with ionizing capabilities. The effect of this fluorescence and especially successive fluorescence and successive re-emission is very difficult to consider. However, by a phenomenological argument it can be shown that this effect will be small and localized in the vicinity of the primary absorption if the cross sectional dimensions of the expansion chamber is sufficiently small. This can be shown in the following manner. Consider a small section of the expansion chamber Δ z cm long and determine how much of the energy initially stored in the excited atoms contained in this volume will propagate down the expansion chamber, possibly by successive fluorescence and re-emission, and how much of this initial energy will flow to the bounding walls and be absorbed there. Since the fluorescent and re-emission radiation has no preferred direction, the fraction of energy transferred down the expansion chamber as compared to the total energy which leaves the volume under consideration, is equal to the ratio of the cross sectional area of the chamber to the total surface area of this volume. In the case of an expansion chamber 2.28 cm by 1.27 cm (used in this experiment) it is found that if we consider the fluorescent

energy initially in a section 1 cm long, then of this energy which leaves the volume only 45 $^{o}/o$ is transferred either upstream or downstream while 55 $^{o}/o$ is absorbed in the walls of the expansion chamber possibly producing photoelectrons in the process. Hence, it is obvious that under the conditions of this experiment, the ionizing effect of fluorescence and re-emission is localized in the vicinity of the primary photon absorption and these phenomena cannot play an important role in the ionization process. This of course is necessarily true only at distances from the discharge chamber greater than a few tube diameters.

From the above discussion it is seen that under the conditions of this experiment a primary ionizing photon absorbed in the background gas spends the majority of its ionization energy locally. Hence to first approximation the variable $\tilde{z}$ in Equation (33) can be set equal to z.

Experiments in both neon and argon gases at a few mm Hg pressure showed that the electron density spatial decay at sufficiently large values of z was dominated by the exponential factor. Typical spatial decay curves in the case of neon gas are illustrated in Figure 11. Each experimental point on this plot represents the electron density measured by the EM propagation technique with the 30.8 Gc apparatus located at distance z from the open end of the expansion chamber. The scatter of experimental points above and below the drawn lines is due to error in experimental measurement of electron density and also is partially due to slight variations in degree of ionization for successive discharges. The fact that the electron density decayed exponentially along the expansion chamber with a rate of spatial decay highly dependent on the pressure of the background gas indicates that the ionization was dominated by absorption of photons in the volume rather than in the containing walls. At small values of z ($z < 10$ cm) the decay rate was erratic as experimental conditions were varied (pressure, discharge voltage, etc) which most probably indicates the effect of short range radiation and subsequent fluorescence and/or electron diffusion from

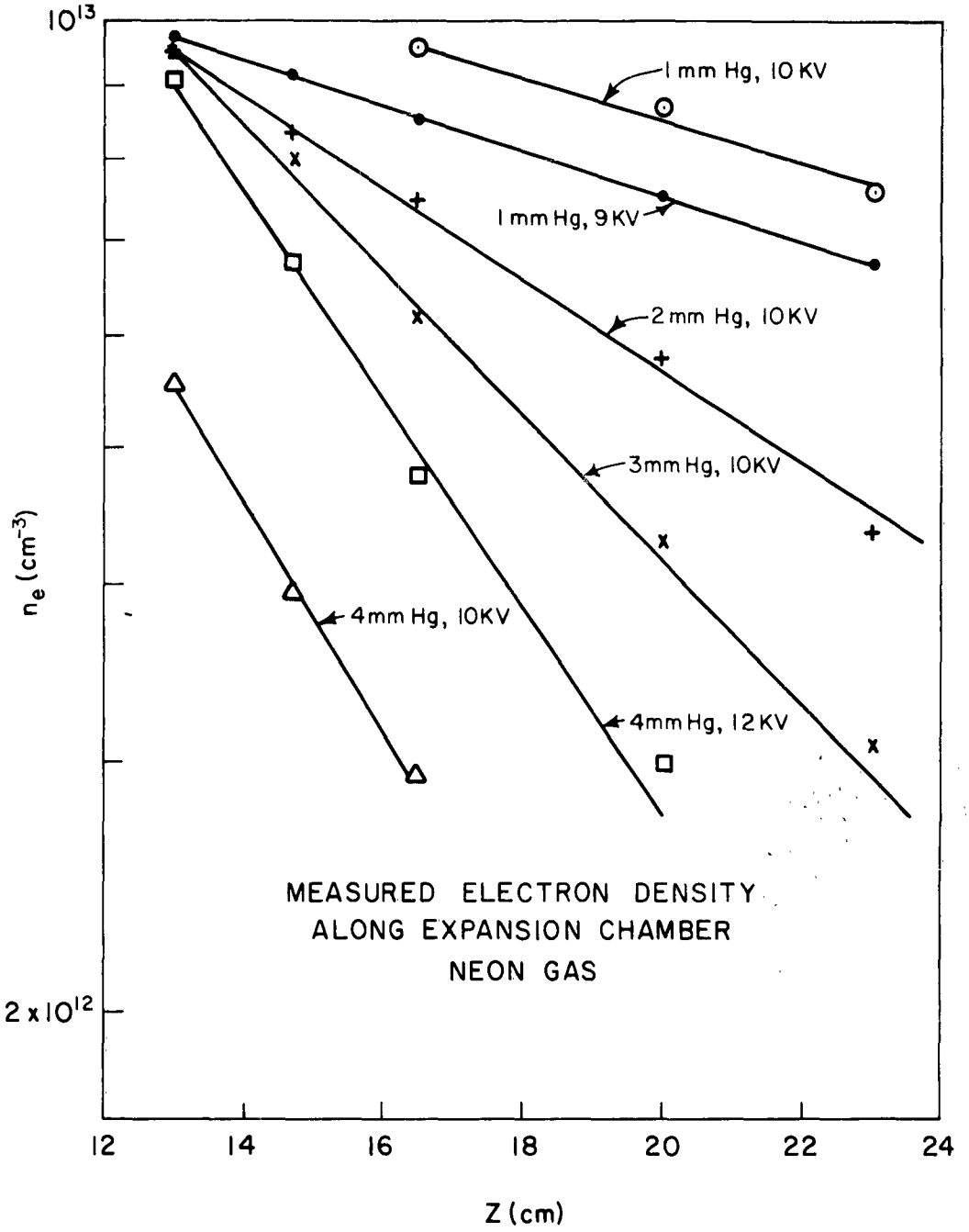

Figure 11. The experimentally measured electron density at the time of maximum discharge current as a function of distance from the discharge chamber for neon gas at various pressures.

the discharge chamber and/or the effect of absorption of primary radiation by the containing walls. However, at distances from the discharge chamber greater than about 10 cm the measured electron density spatial decay rate was always exponential over a fairly large range of experimental conditions as is indicated in Figure 11. The decay rate determined from these curves when compared to known decay rates ($e^{-\mu pz}$) in the gases used, predicted an ionizing photon beam in the wavelength range 1 to 4 Å. Since this was true in both neon and argon gases over a fairly large range of pressures, it was postulated that the ionizing photon beam was very probably characteristic radiation or at least its frequency spectrum was rather narrow. In this special case the integral Equation (33) reduces approximately to Equation (34).

$$n_e(z) = \frac{K}{(z + c)^2} I_o \left[a\mu p + \gamma \frac{2}{z + c}\right] e^{-\mu pz} \qquad (34)$$

where in the shock tube used in this experiment and for $z > 10$ cm the first term of the right hand side completely dominates the second term.

An effective linear absorption coefficient of the ionizing photon stream was determined by comparing the measured electron density spatial decay rate to the decay rate predicted by Equation (34). The effective wavelength of the ionizing portion of the photon beam was then determined by comparing the measured value of μ to known linear absorption coefficients in the gases used. The known values of μ in neon and argon were obtained from the Handbook of Chemistry and Physics, 40th edition, and for convenience are plotted in Figure 12 for the wavelength range 10^{-1} to 10^{2} Å.

The effective wavelength of the photon stream was determined in both neon and argon gases at several different gas pressures and several different discharge voltages. In every case it was found that if the discharge voltage was greater than about 8 kv, then the effective wavelength was approximately 1.75 Å.

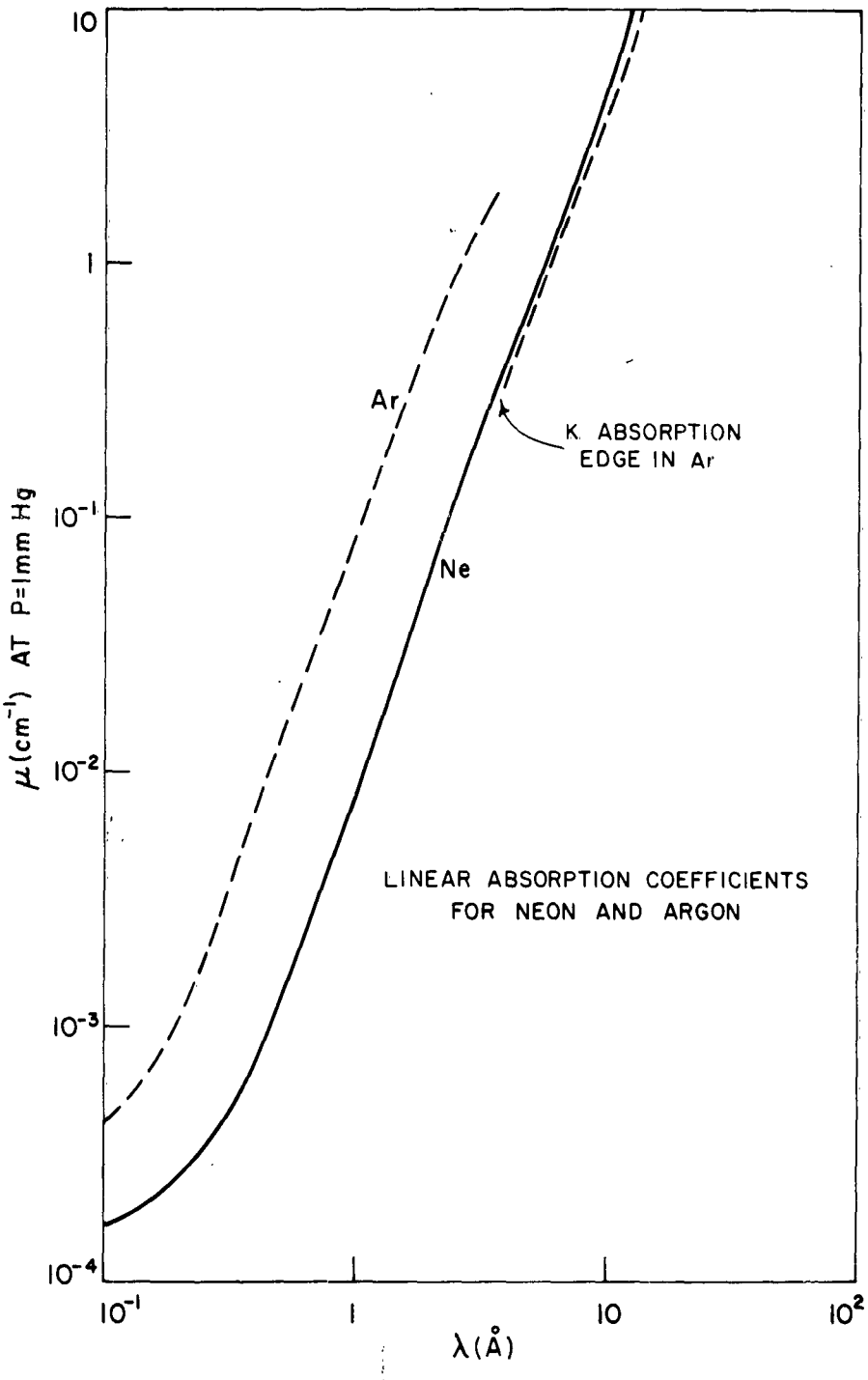

Figure 12. Linear absorption coefficient for photons in the wavelength range 10^{-1} to 10^{2} angstroms in neon and argon gas at 1 mm Hg pressure. (from the Handbook of Chemistry and Physics, 40th edition).

Since the K absorption edge of iron is 1.7394 Å, the radiation which predominated in the photoionization of the background gas was most probably K radiation from the electron bombarded, stainless steel anode.

In agreement with other investigators, the final degree of preionization was found to be slightly dependent on the material of the containing walls. This is in agreement with photoionization of the gas by absorption in the volume. That is, even though absorption of primary photons is predominately absorption in the volume rather than absorption in the containing walls, the wall will play a major role in the ionization process. For example, in neon gas at 1 mm Hg pressure the mean free path for an elastic collision between a 7 kev electron (approximate energy of an electron resulting from the absorption of K radiation from stainless steel) and a neon atom is approximately 2 cm. Therefore if the cross sectional dimensions of the expansion chamber are smaller than 2 cm, then a 7 kev primary photoelectron will on the average make less than one energy losing collision in the gas before it strikes the containing walls, possibly producing one or more secondary electrons. In addition, the highly excited ions and atoms which result from photon absorption and electron-molecule collisions, will subsequently fluoresce. A large percentage of this fluorescent radiation will be absorbed in the walls with a possible large yield of photoelectrons.

In spite of the strong indication that the preionization was due mainly to K radiation from the anode, this inference is not conclusive. In addition, if K radiation predominates in the preionization as is inferred above, then this ionization mechanism will not exist when the discharge voltage is below the threshold value needed for K radiation. For a stainless steel anode, the threshold voltage for K radiation is approximately 7.1 k volts. It was found in this experiment that if the discharge voltage was less than about 8 k volts, then the degree of preionization at relatively large values of z ($z > 10$ cm) was several orders of magnitude less than the degree of ionization indicated in

Figure 11 for slightly higher discharge voltages. At smaller values of z the degree of ionization did not seem to experience this rapid decline as the discharge voltage was decreased below 8 k volts. These observations reinforced the inference that the preionization was predominantly due to K radiation from the anode at z greater than a few tube diameters and was predominantely due to other phenomena (short range radiation, diffusion, wall effects, etc.) at smaller values of z.

A limited number of observations in a shock tube with a T-type discharge chamber showed that the background gas in this tube was also preionized at the time of the shock wave producing electric discharge. However, contrary to the case of the cylindrical geometry discharge chamber, the preionization was not consistent with ionization by soft X-rays and the degree of ionization at any particular value of z varied irregularly as the experimental conditions were changed. In addition, for nearly identical experimental conditions the degree of preionization in the T-type tube was generally much smaller than in the cylindrical type tube.

7. DOPPLER SHIFT RESULTS AND SHOCK WAVE STRUCTURE

In Chapter 4 we developed the relations which relate the velocity of an EM reflecting body propagating through a rectangular cross section waveguide filled with plasma to the Doppler frequency shift of the EM wave reflected by it. The microwave apparatus which was used in conjunction with the x-band metal wall expansion chamber to measure the Doppler frequency shift of an EM wave reflected by the plasma associated with a shock wave is illustrated in Figure 13. The measurement was made by observing the variations in amplitude of the EM signal detected by the probe in the slotted line as the shock wave passed through the expansion chamber. A typical recording of this is shown in Figure 14. The slotted line detected EM signal was displayed on a dual beam oscilloscope on which the upper trace was delayed until the shock wave entered the metal section of the expansion chamber and the lower trace was delayed with respect to the upper trace by 90 microseconds. Each trace was swept at a 10 microseconds per division rate and the incident EM wave was pulsed off for a short time as is indicated by the pulse on the lower trace.

The slotted line detected EM signal illustrated in Figure 14 can be interpreted in a variety of ways. Perhaps the most descriptive interpretation is that it displays the motion of the standing wave in the waveguide which is continually in motion due to the motion of the load (shock plasma) seen by the incident EM waves. Regardless of the interpretation, the frequency of this signal is equal to the magnitude of the shift in frequency due to Doppler effect and each full cycle of the detected signal corresponds to a one half guide wavelength displacement of the EM reflecting body. Of course, in this sense one half wavelength refers to the actual guide wavelength in the plasma filled waveguide immediately in front of the EM reflecting body which is equal to $z'' - z_o$ as defined by Equations (23)-(25).

From the pulsed off portion of Figure 14 it is obvious that the EM reflection coefficient of the shock wave associated plasma is relatively high. In the par-

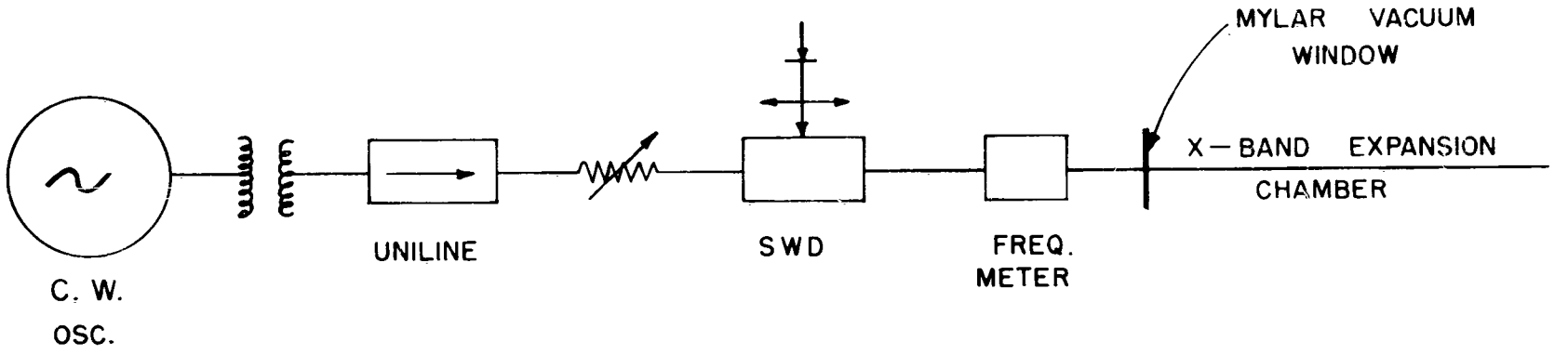

Figure 13. Block diagram of a microwave system used in connection with the x-band metal expansion chamber to measure the Doppler frequency shift of an EM wave reflected by the shock wave and its associated plasma.

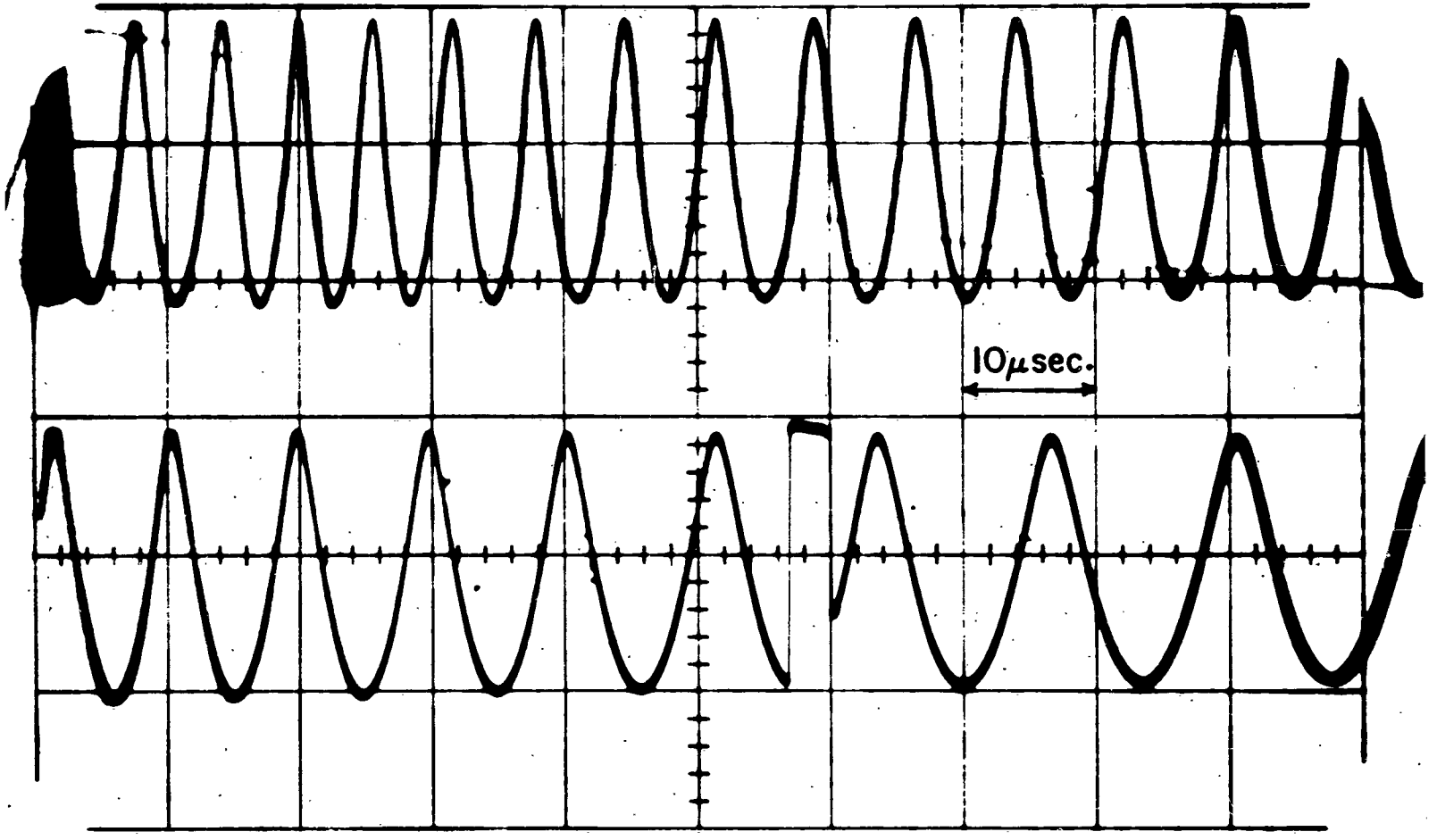

Figure 14. Represents the time variation of the EM wave in the x-band waveguide (slotted line detected) during the passage of a shock wave through the gas in the x-band expansion chamber. The lower trace was delayed with respect to the upper trace by 90 microseconds. The incident cw wave was pulsed off at 5.7 divisions from the left of the lower trace for 3 microseconds. Neon gas, p_1 = 2 mm Hg, f_o = 8.5 Gc, 10 μ sec/division sweep speed.

ticular shock tube used in this experiment, when filled with neon gas at 2 mm Hg pressure, the power reflection coefficient of 8.5 Gc EM waves varied from about 0.88 at Mach 14 to about 0.55 at Mach 2. It is obvious that at least for the lower shock wave velocities in this velocity range this measurement is relative to the ionized driver gas rather than to the shocked gas. This is evident from Figure 2 because shock waves less intense than Mach 10 will not appreciably shock ionize the background neon gas, hence will not cause a significant reflection of the incident EM waves. Therefore if the velocity of the shock wave is lower than about Mach 10, the incident EM wave is dominantly reflected by the ionized driver gas and the magnitude of the Doppler shift is relative to the velocity of the driver gas rather than the shock wave. This effect is illustrated in Figure 15. The upper trace is a record of the amplitude of the EM signal coupled from the expansion chamber into one of the secondary waveguides as illustrated in Figure 7. The lower trace represents the voltage induced on the same probe that acted as the EM coupling antenna. The shock front reached the probe at time t_1 and at this time it was traveling at a velocity approximately equal to Mach 6. At times prior to the passage of shock front over the coupling probe ($t < t_1$) the coupled EM signal is similar to the slotted line detected EM signal (see Figure 14) and can be interpreted in a like manner. The time at which the shock front reached the probe is characterized by a sudden increase in probe voltage and a rapid decrease in the magnitude of the coupled EM energy. The latter indicates that either the EM coupling coefficient of the probe suddenly decreased or that the value of the radio frequency electric field decreased rapidly in the vicinity of the shock front. In either case the decrease in amplitude of the coupled EM wave could only be caused by a sudden change in the dielectric constant of the medium surrounding the portion of the probe located in the expansion chamber. However, since the change in amplitude can be attributed to either a change in electric field intensity or a change in the coupling coefficient of the probe

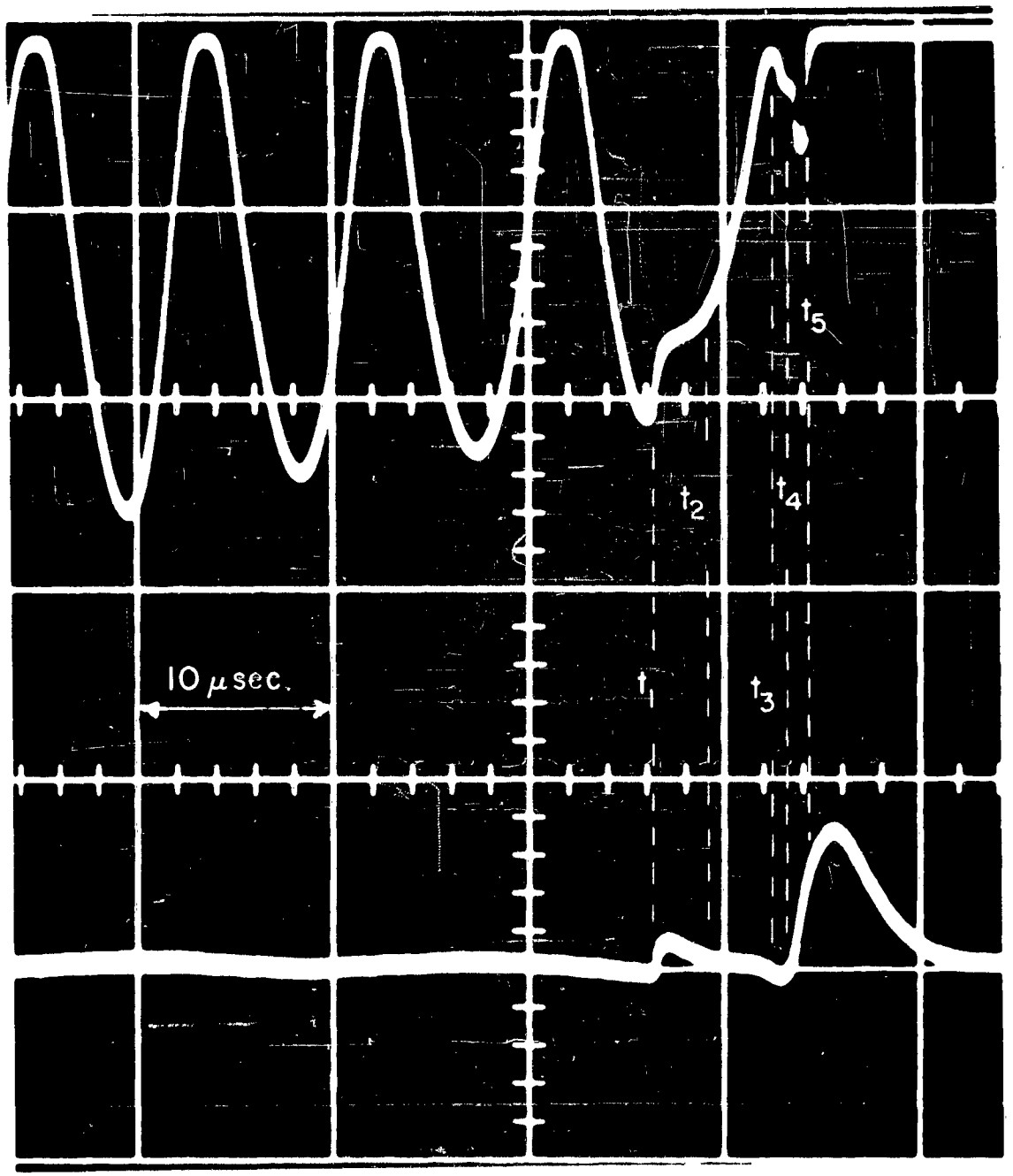

Figure 15. Upper trace represents the amplitude of the EM wave coupled from the expansion chamber into one of the detection waveguides by its respective coupling probe (see Figure 7). The lower trace represents the voltage induced on this same probe. Neon gas, p_1 = 2 mm Hg, f_o = 8.5 Gc, 10 μ sec/division sweep speed, and M = 6.

or both, it is difficult to relate this measured change to the actual change of electron density in the medium surrounding the probe. On the other hand, we are assured that the rate of increase of electron density at the shock front was such that in a few tenths of a microsecond it reached a value sufficiently high to appreciably affect the 8.5Gc EM wave incident on the shock wave. Since the shock wave was insufficiently intense to appreciably ionize the background gas, it is obvious that the electron gas that cuased the disturbance at t_1 was the shock compressed free electron constituent of the background gas (see Equation (22)). This was experimentally verified by increasing the degree of ionization of the background gas by external means in which case it was found that the effect on the coupled EM signal at time t_1 was greater.

After the shock front passed the probe the shock compressed electron gas is evidenced by the time varying slope of the coupled EM wave. That is, assume that the shock wave is not decelerating and also assume that the EM reflection coefficient of the shock wave plasma cloud is constant in time. Both of these assumptions are approximately realized over sufficiently short times. In this case the coupled EM wave will be a constant amplitude, constant frequency sinusoid as long as the coupling coefficient of the probe and the phase velocity of the EM wave in the region of the probe are constant. Hence a sudden change in slope from the expected sinusoidal value can be caused only by a time varying EM coupling coefficient or a space varying phase velocity. Such a change is experimentally observed in the time interval $t_1 - t_3$ and is especially pronounced in the interval $t_1 - t_2$. The slow relaxation of this signal after t_1 back to its expected sinusoidal variation indicates that the electron density decreases as one proceeds from the shock front toward the driver gas. This, of course, is due to recombination and diffusion of the shock compressed gas to the containing walls as well as diffusion toward the driver gas interface.

As the driver gas interface is approached from the front the electron density increases very rapidly as is evidenced by the rapid variations in the amplitude of the coupled EM wave in the time interval $t_3 - t_5$. It is difficult to determine the exact position of the interface but we are assured that it passed the probe in this time interval. It is also evident that the incident EM signal did not penetrate into the hot driver gas beyond the position corresponding to t_5.

In the particular case illustrated in Figure 15 the velocity of the shock wave as it passed the probe was approximately Mach 6. At both higher and lower shock velocities the response was very similar to that shown in Figure 15 and differed from it only in degree. For example, in the case of a Mach 10 shock wave the response was similar except the shock front was closer to the driver gas interface and the penetration of the EM waves (3 cm) into the ionized driver gas was usually less than the resolution capabilities of the EM coupling probe. The depth of EM wave penetration into the driver gas is less at higher shock velocities because the driver gas is more highly ionized at the higher velocities due to the higher discharge voltage which is necessarily required to produce the higher velocity shock wave. Also, at higher shock velocities (> Mach 8) the shock wave transfers energy to the background gas at a rate sufficiently rapid to produce a significant degree of ionization and the free electrons produced in this manner supplement the electron constituent of the driver gas causing an increase in the space rate of change of electron density at the ionization front. In some cases, depending on the degree of ionization of the background gas and the shock wave velocity, the shock compressed electron cloud formed immediately behind the shock front was sufficiently dense to prevent penetration of the EM waves through it.

The delay time between the passage of the shock front and the subsequent passage of the driver gas interface was measured as a function of shock wave

velocity by simultaneously observing the voltage induced on eight of the probes in the expansion chamber illustrated in Figure 8. A typical recording of this is shown in Figures 16a and 16b. The letters S_n and L_n on these recordings indicate the passage of the shock front and the ionization front respectively over probe number n. The probes are numbered consecutively beginning with the probe closest to the discharge chamber. The data obtained in this manner is plotted in Figure 17 for shock velocities in the range from Mach 3 to Mach 12 in neon gas at 2 mm Hg pressure. As delay time we took the time separation between L_n and S_n which corresponds to the time $t_4 - t_1$ as shown on Figure 15. In the case of non-ionizing shock waves ($<$ Mach 8) this time delay corresponds to the time delay between the shock front and the driver gas interface, hence determines the maximum time available to measure the properties of the shocked gas. If the shock is sufficiently intense to appreciably ionize the background gas ($>$ Mach 8), then the measured delay time is that between the shock front and the ionization front which might be slightly less than the time delay between the shock front and the driver interface. However, due to the short time available for the shocked gas to ionize before it passes through the driver gas interface it is highly unlikely that an ionization front will form in front of the interface.

The delay time shown in Figure 17 is for shock waves in neon gas at 2 mm Hg pressure. However, it was found that this delay was nearly independent of gas pressure throughout the pressure range from 1 to 5 mm Hg and was also nearly the same in both argon gas and air. Since the rate of ionization in the shocked gas should depend on both gas pressure and the type of gas,[11,12] this also indicates that throughout the shock velocity range investigated, ionization equilibrium in the shocked gas was not attained in the short time available before it passed through the driver gas interface. The delay time is most probably dependent on the geometry of the shock tube but this was not investigated.

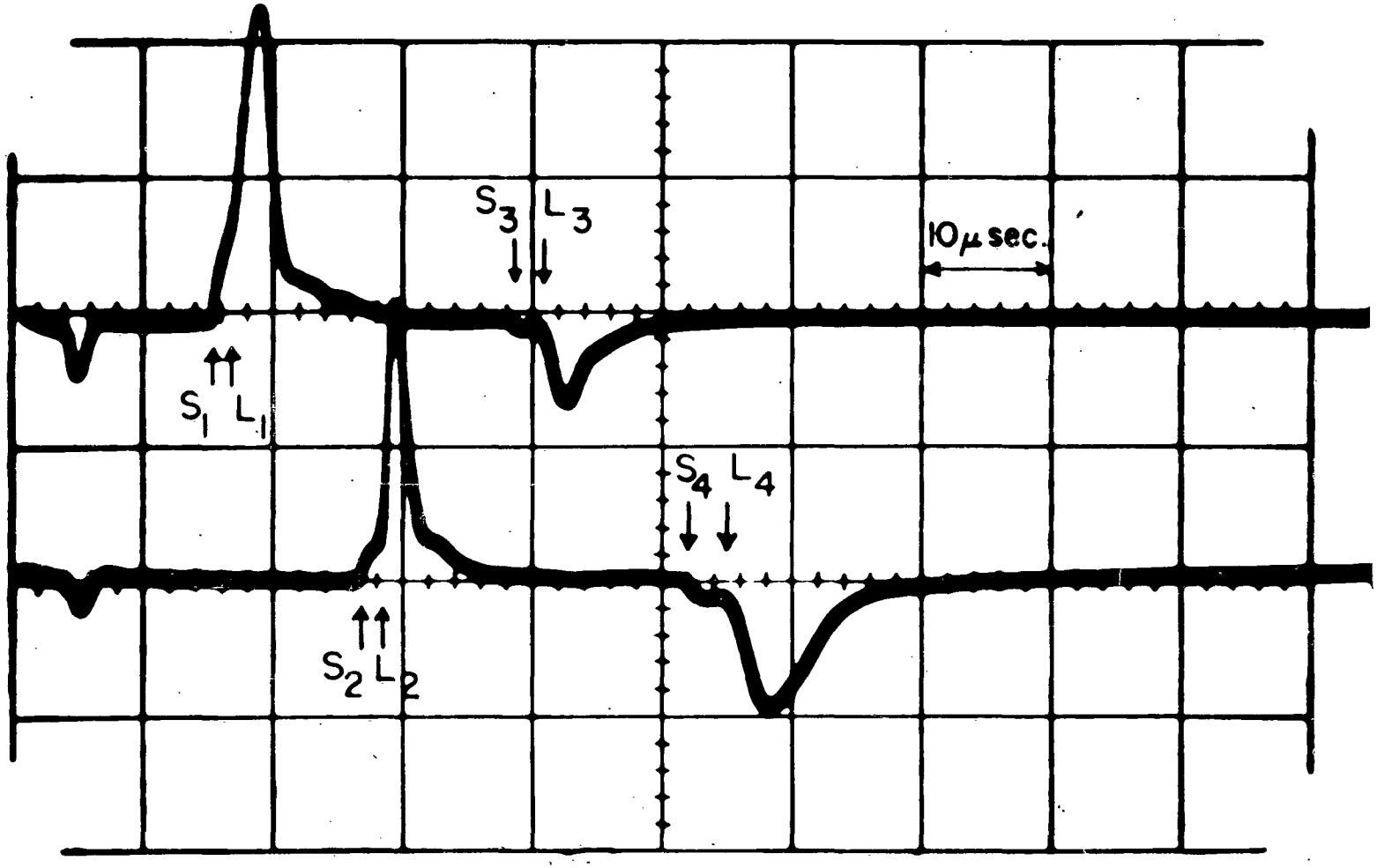

Figure 16a. Represents the amplitude of the voltage induced on four of the metal probes as illustrated in Figure 8. Each trace represents the voltage induced on one of the probes and the negative of the voltage induced on a second probe 10 cm further downstream. The portion of the signal attributed to probe n is identified by subscript n. Neon gas, p_1 = 2 mm Hg.

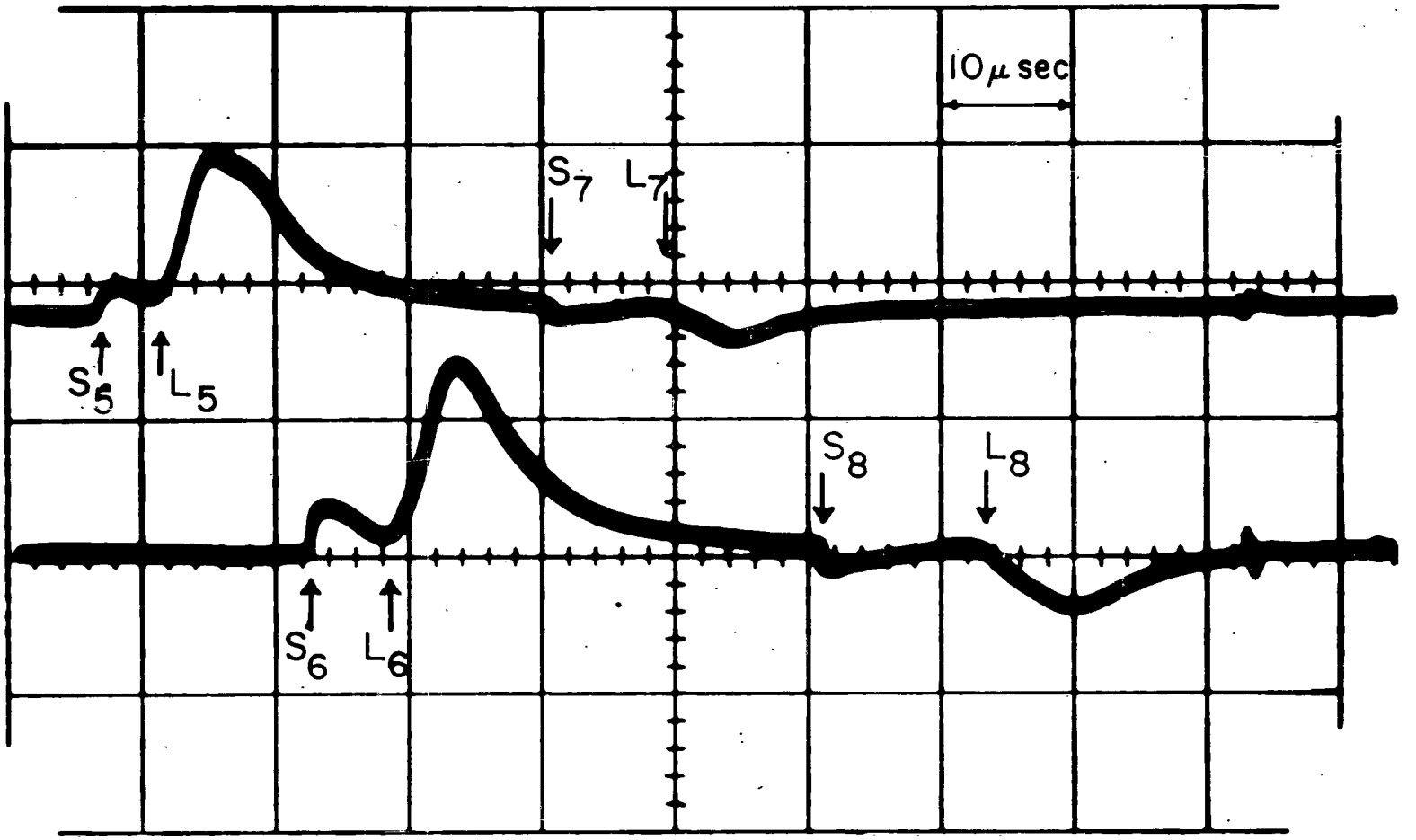

Figure 16b. Same as 16a except scope sweep delayed in time by 60 microseconds.

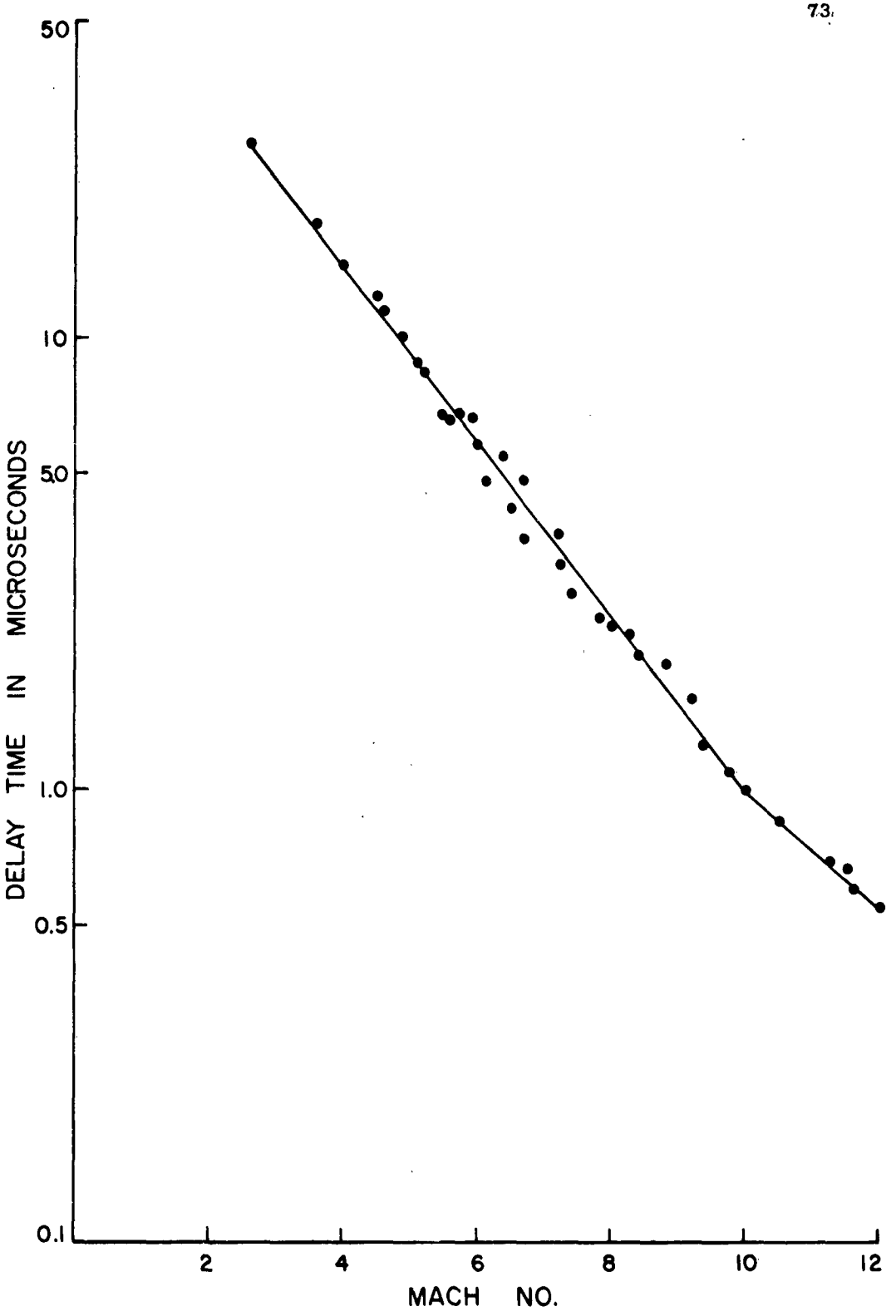

Figure 17. Time elapsed between the passage of the shock front and the passage of the driver gas interface in neon gas at 2 mm Hg pressure as a function of Mach number.

The measured delay time as plotted in Figure 17 is also very closely related to the delay time between the passage of the shock front and the time at which maximum light is emitted from the shocked gas. This is illustrated in Figure 18 where the top trace is the light emitted from the shock associated plasma at light port 3 (see Figure 7) and the bottom trace represents the voltage induced on probe 3 and the negative of that induced on probe 4. In the case illustrated, the velocity of the shock wave as determined by the time it took to pass between the two probes was approximately Mach 10. In every case, for both faster and slower shock waves, it was found that maximum light emission corresponded very closely to maximum induced voltage on the metal probe. Hence, with the help of Figure 15 it is seen that maximum light emission occurs at nearly the time represented by t_5. Since t_5 is very nearly equal to t_4 for shock velocities greater than about Mach 4, then in this case the delay time plotted in Figure 17 is also very nearly equal to the time delay between passage of the shock front and the subsequent passage of the light front. It must be reiterated however, that these delay times may be highly dependent on the geometry of the shock tube.

In Chapter 4 the velocity of an EM reflector was related to the Doppler frequency shift and the electron density of the medium through which it is moving. The effect of the background electron gas on the magnitude of the frequency shift is illustrated in Figure 19. The data plotted in this figure was obtained by observing the voltage induced on eight of the probes in the expansion chamber illustrated in Figure 8 and also simultaneously measuring the Doppler frequency shift. The velocity by Doppler measurement is the apparent velocity of the shock associated plasma cloud which one obtains if Equation (29) is used to relate the shock velocity to the magnitude of the frequency shift with the additional assumption that the plasma frequency in the background gas is much less than the frequency of the incident EM wave. It is seen that in the particular

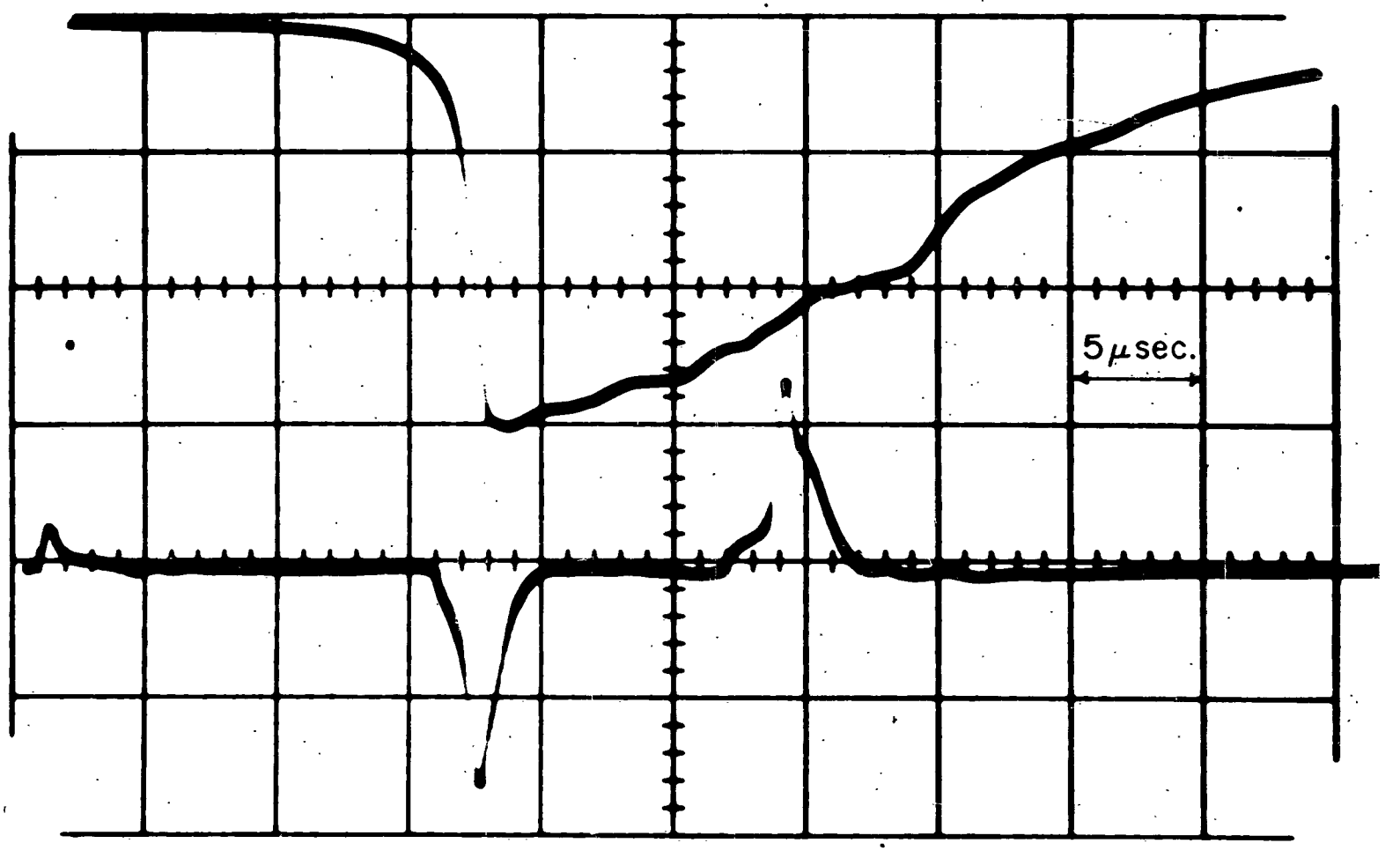

Figure 18. The upper trace represents the output of a photomultiplier located at light port number 3 of the test section illustrated in Figure 7. The lower trace represents the negative of the voltage induced on probe 3 added to the voltage induced on probe 4. Neon gas, p_1 = 2 mm Hg, M = 10.

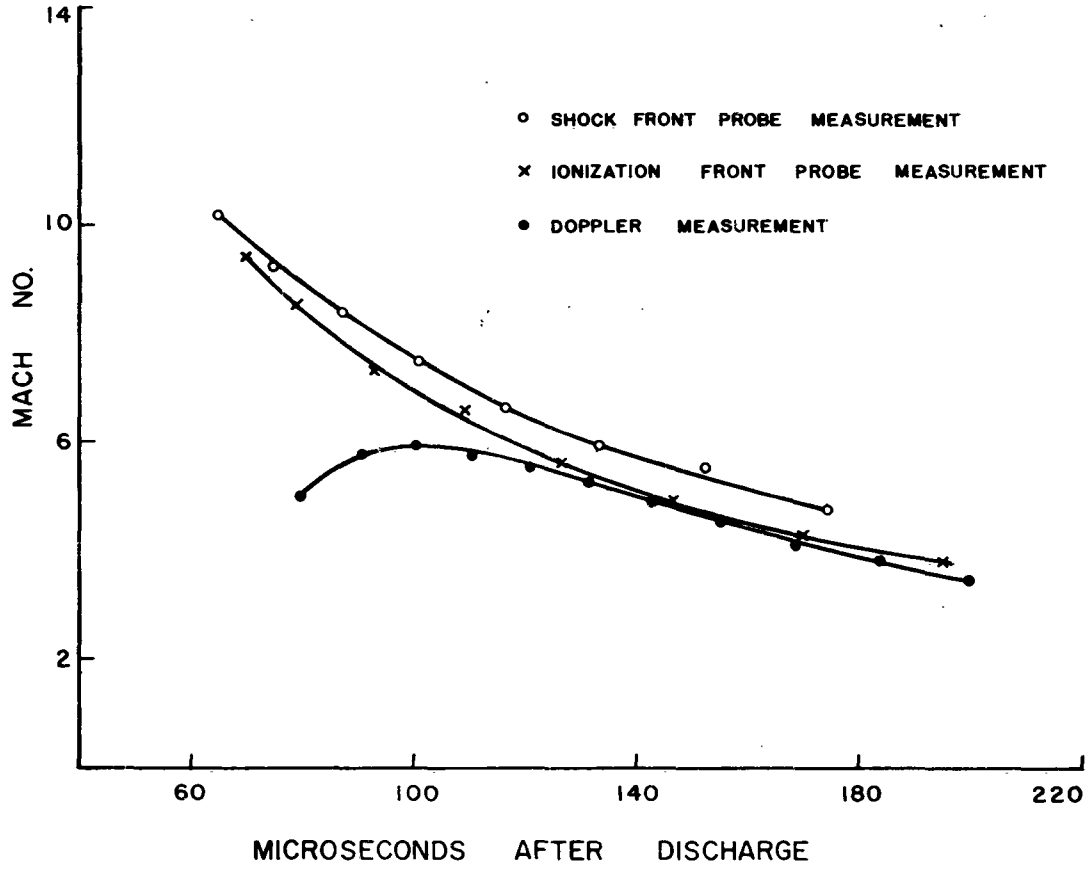

Figure 19. Experimentally determined shock wave velocity as a function of time after the initiation of the electric discharge. Shows the error in Doppler shift measurements of shock wave velocity as a result of pre-ionization of the background gas during the shock wave producing electric discharge. Neon gas, p_1 = 2 mm Hg, f_o = 8.5 Gc.

case illustrated in Figure 19 the two methods of measuring the shock velocity did not even reasonably agree until more than 130 microseconds after the initiation of the electric discharge which produced the shock wave. Hence, the electron density of the background gas immediately in front of the shock wave was greater than $10^{10}/cm^3$ throughout the first 130 microseconds of observation. In addition, the fact that the Doppler shift was not observed during the first 80 microseconds of travel indicates that throughout this time the background electron gas was sufficiently dense to completely cutoff the incident EM waves and prevent them from reaching the shock associated plasma cloud ($[\omega_p/\omega]^2 > [1 - (\lambda_o/2a)^2]$).

The technique of measuring the velocity of a shock wave ionization front by both EM waves (Doppler frequency shift) and a second independent method can be used to make a fairly accurate measurement of the background electron density. If the assumption is made that the background electron density is constant along the total length of the expansion chamber or if the change in electron density per guide wavelength is small, then the Doppler frequency shift for a reflector propagating with a velocity V_R through a background electron gas described by ω_p is given by Equation (29). The electron density in the background gas is found by substituting the Doppler frequency shift and the velocity of the shock wave obtained by a method independent of the Doppler frequency shift into this equation. This technique was used to measure the electron density spatial decay along the expansion chamber as a supplement to the electron density measurements discussed in Chapter 6. However, this technique has the disadvantage in that the electron density at various points along the chamber is not measured at the exact same time. On the other hand, this technique of measuring the electrical properties of gaseous plasmas by microwave interaction with the investigated plasma in conjunction with reflection of the transmitted microwaves by an ionized shock wave may find application in general plasma diagnostics.

In addition to the above technique for measuring the background electron density, an EM phase shift technique employing a shock wave reflection of the sensing EM waves was also used. This technique is very similar to the usual phase shift method of measuring electron densities[10] and as is discussed below, it is in some respects advantageous in general plasma diagnostics. Consider the difference in phase between two EM signals coupled from the expansion chamber into two of the detection waveguides illustrated in Figure 7. Let the coupling probe closest to the discharge chamber be located at z_1 and the other one at z_2. The phase difference $\Delta\phi$ between the two detected EM waves is given by Equation (35)

$$\Delta \phi = \int_{z_1}^{z_2} \frac{\omega}{V_p(z)} \, dz \tag{35}$$

where the phase velocity V_p is given by Equation (26) in terms of the electron density in the gas filling the waveguide. In the special case where the phase velocity of the sensing microwaves is independent of z, the electron density is easily determined by comparing the phase difference with the waveguide empty $\Delta \phi_o$ to the phase difference with the waveguide filled with plasma $\Delta \phi$. This relationship is given by Equation (36)

$$(\omega_p/\omega)^2 = [1 - (\lambda_o/2a)^2][1 - (\Delta \phi/\Delta \phi_o)^2] \tag{36}$$

The phase difference without plasma ($\Delta \phi_o$) can be either measured experimentally or can be calculated with the aid of Equations (28) and (35). The phase difference with a plasma filling the waveguide can be measured in a variety of well known ways. In this work, the two EM signals coupled into the two detection

waveguides were each displayed on one of the traces of a dual beam oscilloscope. With a shock wave traversing the waveguide between the discharge chamber and the first probe each of the detected signals were similar to the signal displayed in Figure 15 prior to t_1. The difference in phase $\Delta \phi$ between these two coupled signals at any particular time was easily obtained from a photograph of the displayed signals.

The above described method of measuring the electron density in the background gas was used to measure the degree of preionization resulting from the shock producing electric discharge. It was also used to measure the electron density of the background gas just prior to the passage of the shock wave. This particular method of measuring electron density in a gas may find application in general plasma diagnostics. Its most important features are: (1) the phase shift across the volume of plasma between the two coupling probes can be displayed directly on an oscilloscope, (2) the measurement is instantaneous, (3) the end boundaries of the plasma have no effect on the magnitude of the phase shift because these are also included in $\Delta \phi_o$ (hence cancel), and (4) the simplicity of the microwave apparatus required for the measurement.

8. SHOCK WAVES IN INDEPENDENTLY PRODUCED GASEOUS PLASMAS

Phenomena connected with shock waves in a background gas in which the degree of ionization was enhanced by external means, above the value resulting from the shock producing electric discharge are discussed in this section. A considerable amount of work in this area of endeavor was previously conducted by Takeda et al.[42] The work presented below is not intended to supplement the work of Takeda but rather was conducted and is discussed here in order to obtain a better understanding of the results discussed in the previous sections of this paper. It was desired to use the same investigation techniques in this work as were used in the work discussed in Chapter 7 in order that comparisons could be made between the two cases (i.e., with and without enhanced preionization). The usual high current pulse discharge method of producing a background gaseous plasma is not applicable in the metal wall expansion chamber used in this work.[10] Hence, a high power radio frequency wave was used to ionize the background gas in the metal wall expansion chamber. This type of gas breakdown proved to be quite satisfactory but, as is usually the case in radio frequency gas breakdown, it is difficult to isolate the high power radio frequency breakdown pulse from the sensing microwave apparatus and prevent it from saturating the sensing wave detectors. Because of this isolation difficulty, the microwave techniques discussed in Chapter 7 had to be modified in order to use them to investigate shock wave phenomena in gaseous plasmas produced by high power radio frequency waves.

The background gas was preionized by means of a short duration, high peak power, narrowly pulsed (1.2 μsec.) radio frequency wave. A subsequent electrical discharge in the discharge section of the shock tube produced a shock wave which then traversed the region of partially ionized gas. Provision was also made so that the high power radio wave could be pulsed on after the shock wave first entered the metal x-band expansion chamber. In this manner the effect of an intense pulsed radio wave incident on the shocked gas was also investigated. In

both cases the shock wave and the associated phenomena were simultaneously investigated by low power level EM sensing waves and by observation of the visible light emitted from the shocked gas. The expansion chamber test section illustrated in Figure 7 was used in this investigation. A schematic of the microwave instrumentation which was used in connection with this test section is shown in Figure 20.

The electrical properties of the medium filling the main waveguide (i.e., expansion chamber) were investigated on the basis that the impedance of the coupling probe as measured in the secondary waveguide is dependent on the dielectric constant of the medium surrounding that portion of the probe which is located in the main waveguide. In particular, knowledge of the power transmitted passed the probe (P_T) and the power reflected by the probe (P_R) is sufficient to determine the power coupled by the probe from the secondary waveguide into the expansion chamber. This in turn is related to the radiation impedance of that portion of the probe located in the expansion chamber.

Detailed analysis shows that the radiation impedance is dependent on the size of the probe, the geometry of the surrounding metal walls, and the dielectric constant of the medium surrounding the probe. In general, an analytic expression which describes the radiation impedance of an antenna in a metal waveguide cannot be obtained in closed form. However, if the physical size of the antenna in the waveguide is small compared to the dimensions of the waveguide then, at least in a qualitative sense, the radiation impedance of the antenna should depend on the medium in which it is immersed in a manner similar to that of a dipole immersed in an identical but boundless medium. In order for this analogy to hold it is necessary that the radiation impedance not be dependent on alterations of the properties of the medium at distances from the antenna greater than the distance from the antenna to the nearest metal wall. If this were not true, then the metal walls of the waveguide would play a prominant role in the

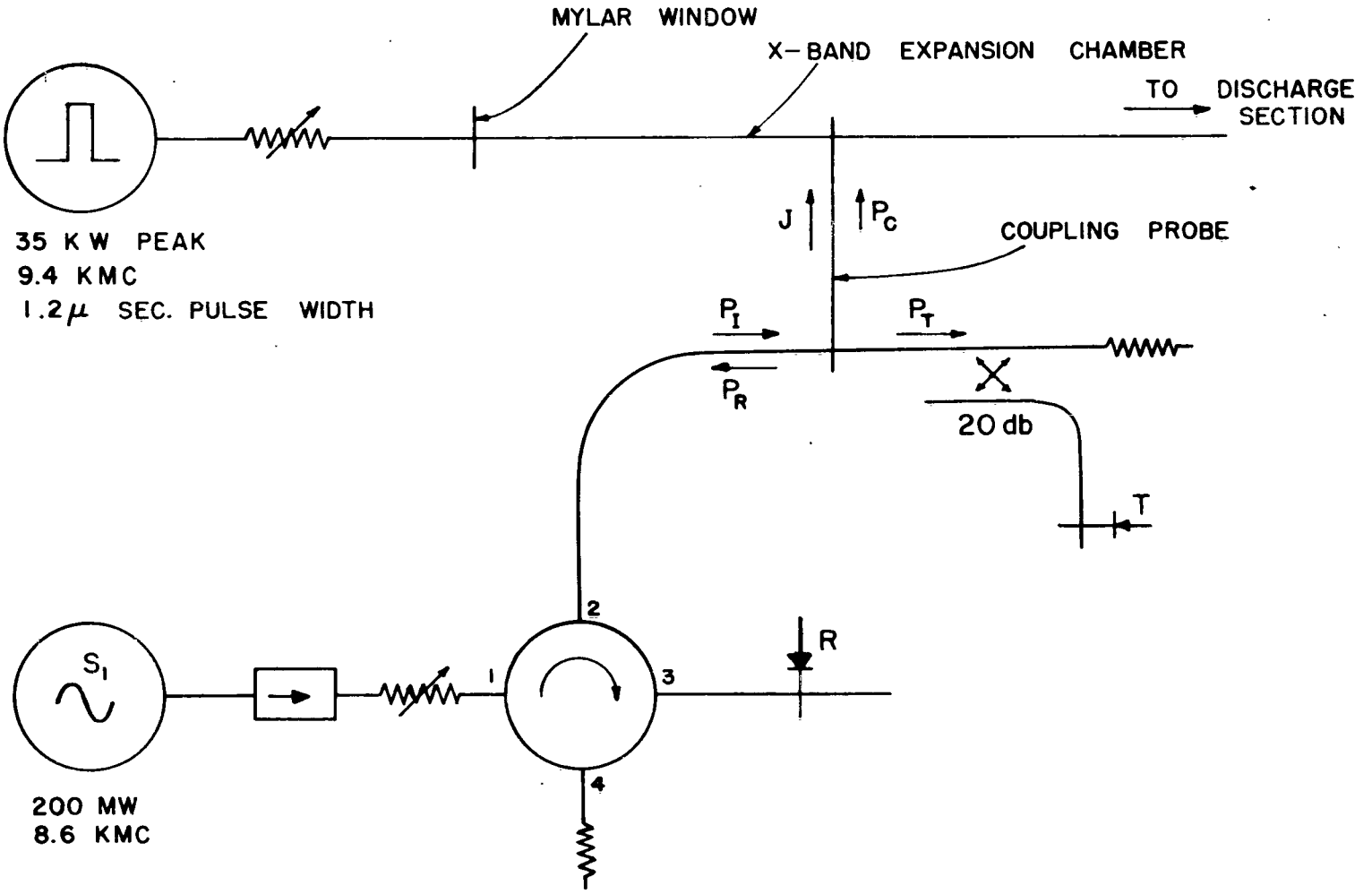

Figure 20. Microwave instrumentation used to preionize the gas filling the expansion chamber prior to the passage of the shock wave and also to measure the electrical properties of the shock wave as it passes over the probe.

radiation process and one could no longer use the dipole analogy.

Initial experimental observations showed that the radiation impedance of the probe in the expansion chamber was significantly dependent on only that portion of the medium located in the immediate vicinity of the probe. Hence it will be assumed that the functional dependence of the radiation impedance of the probe is similar to that of a dipole immersed in an identical but boundless medium. In addition, due to the intense near field dependence only the case where the probe is completely immersed in a uniform plasma need be considered. With these approximations the radiation impedance is found to be directly proportional to the characteristic impedance of the medium. In the case of a uniform plasma medium characterized by its plasma frequency ω_p and electron-molecule collision frequency for momentum transfer ν, the radiation impedance at angular frequency ω is given by

$$Z_{RAD} = K \sqrt{\mu/\epsilon_o} \left[\frac{1 - (\omega_p/\omega)^2 + (\nu/\omega)^2 + j\, \nu\omega_p^2/\omega^3}{1 - (\omega_p/\omega)^2 + (\nu/\omega)^2} \right]^{1/2} \qquad (37)$$

where K is a constant which depends on the frequency of the EM field and on geometrical factors. The power radiated by this antenna is given by the following expression

$$P_{RAD} = J_{eff}^2 \left[\mathrm{Re}\ Z_{RAD} \right] \qquad (38)$$

where: J_{eff} is the effective value of the antenna current and $\mathrm{Re}Z_{RAD}$ is the real part of the radiation impedance. In this equation the probe current (J) is uniquely determined by the EM fields in the source (secondary) waveguide and therefore is not directly dependent on the properties of the medium which surrounds the probe in the main waveguide. However, since the magnitude of the power coupled, hence the EM field in the secondary guide is dependent on the

medium surrounding the probe in the main waveguide, then the probe current (J) is also dependent on the properties of this medium. However, this dependence is of a second order and will be neglected in the following discussion.

It is seen that the power coupled from the secondary waveguide into the main waveguide is maximum when the quantity $1/\omega^2(\omega_p^2 - \nu^2)/\omega^2$ is equal to unity. If the surrounding medium is partially ionized low pressure (~ mm Hg) neon gas and if the frequency of the EM wave is in the 9 Gc range, then the electron collision frequency (ν) can usually be neglected in this quantity (see Chapter 9) and the power coupled is a maximum when the plasma frequency is equal to the angular signal frequency. With this approximation it is seen that if the electron density, hence plasma frequency, of the medium which surrounds the probe in the waveguide increases with time from a sufficient low initial value (i.e., $\omega_p \ll \omega$), then the power radiated increases monotonically as the magnitude of the plasma frequency approaches that of the signal frequency. The magnitude of the power radiated reaches a maximum value when the plasma frequency is equal to the signal frequency, the value attained being determined by the value of the collision frequency. With further increase of plasma frequency (i.e., $\omega_p > \omega$) the radiation impedance rapidly approaches pure reactance and the power radiated decreases to a low value.

The variation in the magnitude of the power radiated from the probe during the passage of the cloud of ionized gas associated with a shock over the probe is illustrated in Figure 21. The upper trace represents the variation in amplitude of the EM wave reflected by the coupling probe (P_R). This signal was detected by detector R (see Figure 20). On this trace downward deflection corresponds to an increase in the amplitude of the measured EM wave. The lower trace is the simultaneously detected EM wave which was transmitted past the probe and detected by detector T (see Figure 20). Downward deflection on this trace also represents an increase in amplitude of the EM wave. In the case illustrated

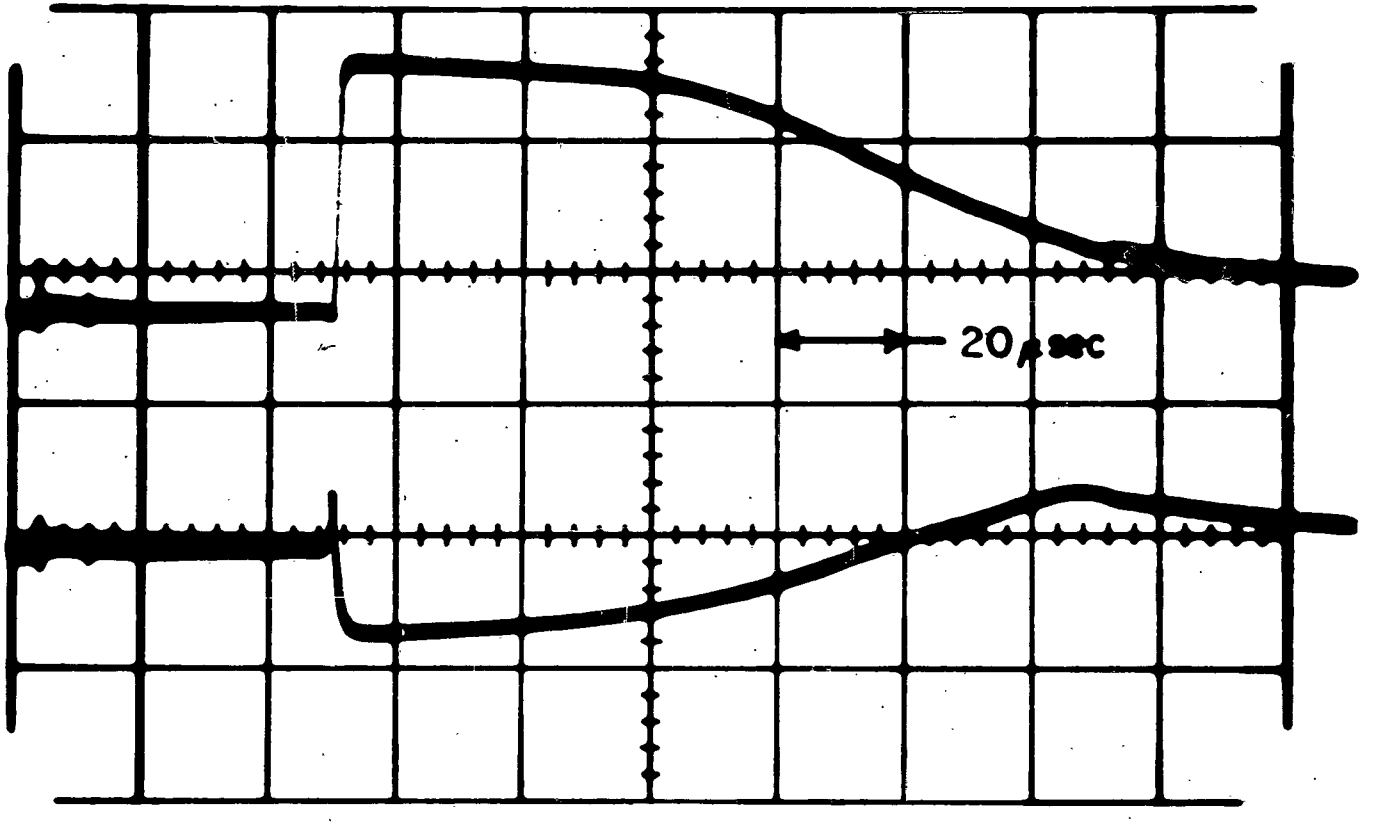

Figure 21. Represents the variation in amplitude of the power radiated from the metal probe during the passage of a shock wave over the probe. The shock front reached the probe at approximately 50 microseconds after initiation of the scope trace. The upper trace represents the amplitude of the reflected EM wave P_R and the lower trace the amplitude of the transmitted wave. Neon gas, p_1 = 2 mm Hg, f_1 = 8.6 Gc.

the shock wave was traveling at a velocity equal to about Mach 8 as it passed the coupling probe. It is clear from this recording that, from the time of the shock producing electrical discharge to the time at which the shock front reached the coupling probe, no significant variations were observed on either of the two traces. At time t_o both the reflected and the transmitted EM waves, exhibit a decrease in amplitude. After this time the amplitude of the reflected EM wave remained at this lower value for several tens of microseconds, but the amplitude of the transmitted EM wave reached its minimum value in about one microsecond and then immediately began to increase and reached a new maximum value after a delay of about one microsecond. The amplitude of the transmitted EM wave then remained at this increased value for several microseconds before it began to return to its previous value. The change in the magnitude of the power coupled by the probe from the secondary waveguide into the expansion chamber was determined from this recording by applying the principle of conservation of energy (i.e., $\Delta P_C + \Delta P_R + \Delta P_T = 0$). At the initial instant of change both ΔP_R and ΔP_T were negative which indicates that the magnitude of the coupled power was greater at that time than it was in the case when the waveguide was empty (i.e., void of plasma). Equations (37) and (38) indicate that this increase in coupled power occurred when the plasma frequency of the medium in the immediate vicinity of the probe was nearly equal to the signal frequency. The subsequent decrease in coupled EM power likewise indicates that the plasma frequency of the surrounding medium had reached a value greater than the signal frequency.

After the initial rapid variations, the amplitude of both the reflected and transmitted EM waves began to return to the value they had when the expansion chamber was empty. However, for a short time (from 140 microseconds to about 190 microseconds) the amplitudes of both of the EM waves were once again both negative with respect to the value they had when the waveguide was void of plasma. This indicates that during this time the plasma frequency of the medium surround-

ing the probe approached the value of the signal frequency from a higher value. After this time the magnitude of the coupled power once again decreased to its empty guide value which indicates that the plasma frequency of the medium in the vicinity of the probe had fallen to a negligible value (i.e., $\omega_p \ll \omega$).

The location of the shock light front with respect to the point at which the plasma frequency of the ionized gas column, associated with the shock, first reached a value equal to the signal frequency is illustrated in Figure 22. The shock in the case illustrated here was traveling at about a Mach 11 velocity as it passed the point of observation. The initial decrease in amplitude of the transmitted EM wave (upper trace), from t=0 to t=20 microseconds, was due to the presence of a plasma medium in the vicinity of the probe. This plasma was produced by photo-ionization of the background gas by high energy photons from the discharge chamber during the shock wave producing electrical discharge.

Comparison of the photograph shown in Figure 22 with Figure 18 indicates that the initial rapid change in the amplitude of the EM wave transmitted past the probe in the secondary waveguide, corresponds to the driver gas interface. However, in both Figure 21 and in Figure 22 no variations are noted which might correspond to the shock front. The reason for this is that the shock wave compressed electron gas in the vicinity of the probe was of insufficient value to appreciably affect the impedance of the probe (i.e., see Equation (22)). This phenomenon is better illustrated in the recordings shown in Figures 23 and 24. In each case the upper trace represents the microwave signal transmitted past the coupling probe in the secondary waveguide and the lower trace represents the intensity of the visible light emitted from the plasma at a position along the expansion chamber identical to the position of the coupling EM probe. In Figure 23 a small decrease in the amplitude of the transmitted EM wave is exhibited 5 microseconds before the passage of the ionization front. This decrease corresponds to the passage of the shock front. However, since the effect is only very

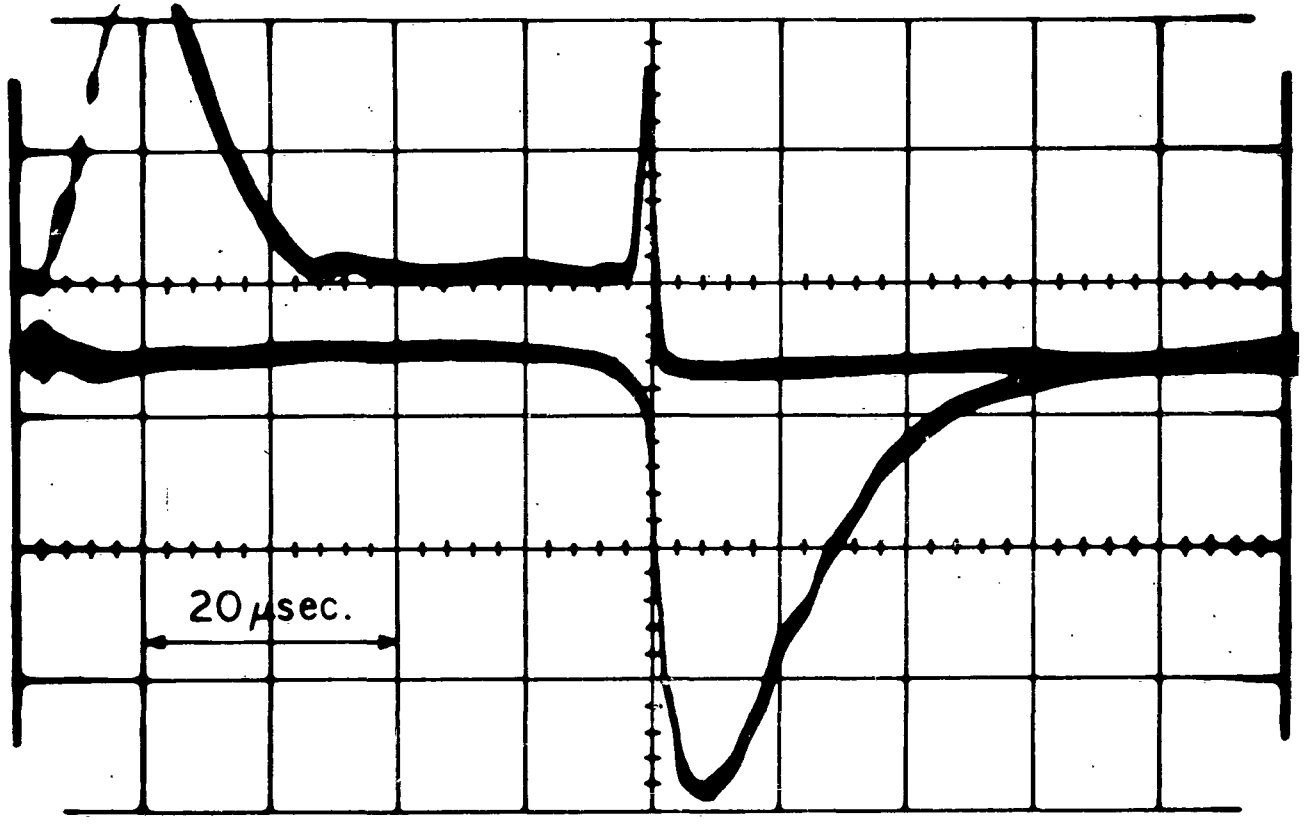

Figure 22. The upper trace represents the amplitude of the transmitted EM wave P_T and the lower trace represents the output of a photomultiplier viewing the visible light emitted from the portion of the gas in the vicinity of the coupling probe. Neon gas, p_1 = 2 mm Hg, f_1 = 8.6 Gc, M = 11.

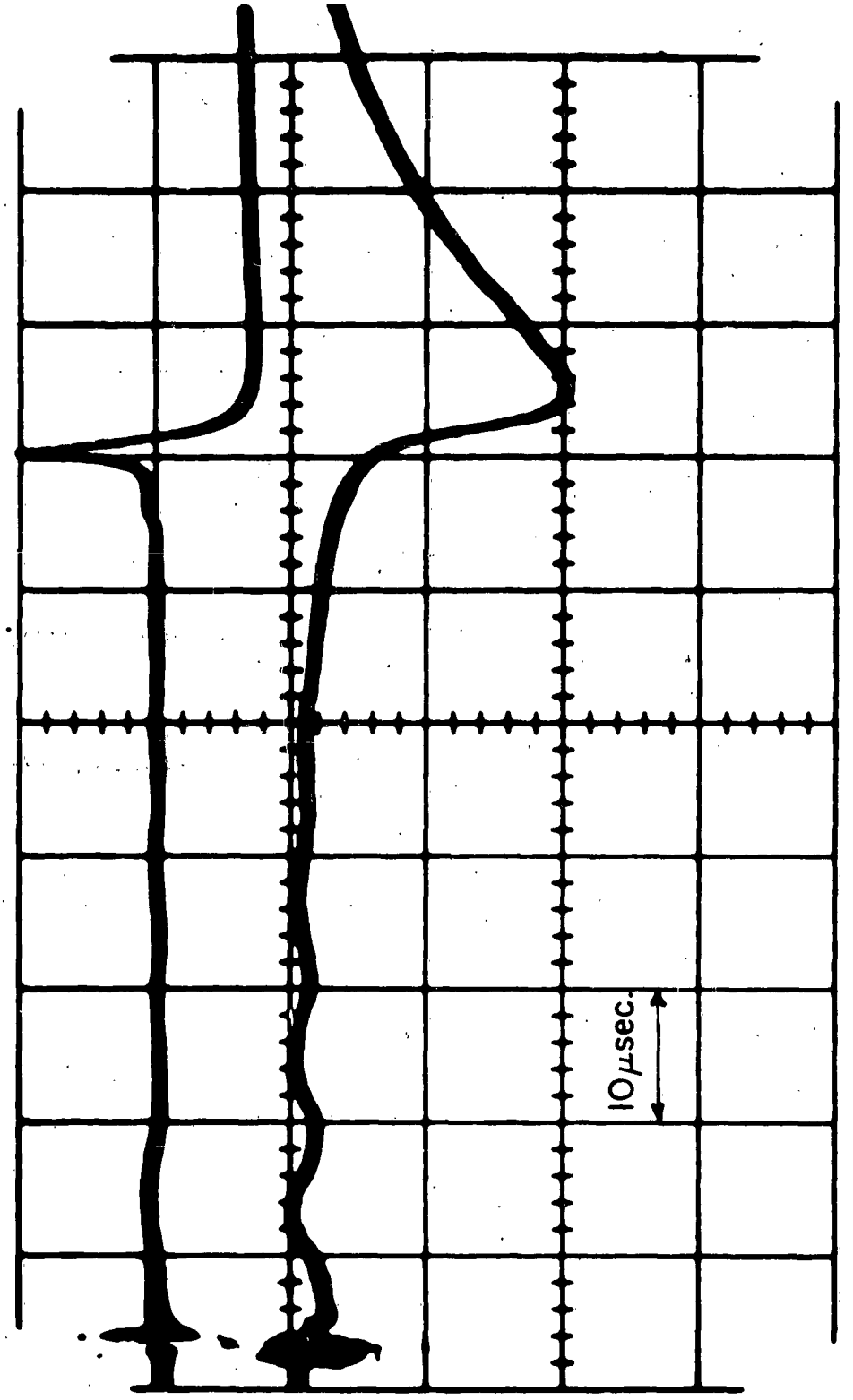

Figure 23. Same as Figure 22 except M = 6.

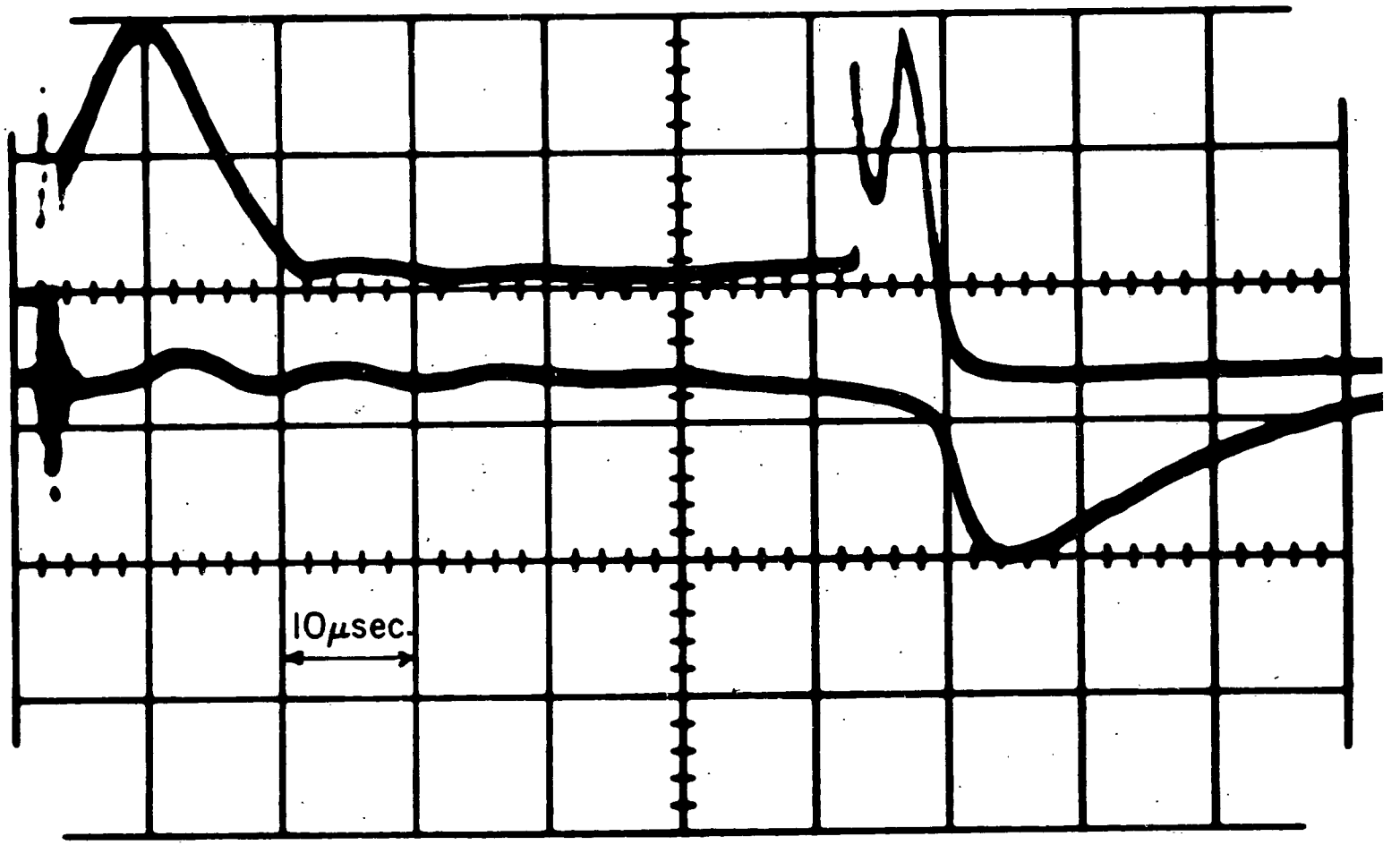

Figure 24. Same as Figure 23 except the background gas was pre-ionized by radio frequency breakdown prior to the passage of the shock wave over the probe.

slight, it indicates that the electron density of the shock compressed electron gas is less than, but nearly equal to, the density required to produce a significant effect. When the electron density of the background gas is slightly enhanced by external means, then the electron density in the shock wave compressed gas is sufficient to produce an appreciable effect on the radiation impedance of the EM coupling probe (the electron density in the shock compressed gas with respect to that in the background gas is given by Equation (22)). This phenomenon is illustrated in Figure 24. The experimental conditions for Figure 24 is the same as that for Figure 23 except in this case the background gas was preionized by means of the high power pulsed EM radio wave prior to the passage of the shock wave. Due to the enhanced electron density in the background gas the electron density in the shock wave compressed gas was also enhanced. In this case, as is clearly evident in Figure 24, the shock wave compressed electron gas produced a pronounced alteration in the amplitude of the low level EM sensing wave transmitted past the EM coupling probe in the secondary waveguide. A detailed discussion of the observed waveform would be similar to the discussion conducted above in connection with Figure 15. Hence, we will not repeat that discussion here. It is interesting to note, however, the rapid rate of electron density increase at the shock front. This is evidenced in Figure 24 by the rapid change in amplitude of the EM wave at the shock front. This very rapid increase in electron density at the shock front is also in agreement with Figure 15.

In the above discussion of experimental results, the shock front was identified, without question, with the disturbance observed in front of the shock light front (i.e., t_1 on Figure 15, S_n on Figure 16, leading pulse on Figures 18, 23, and 24). This identification is consistent with both the experimental results and expected shock wave phenomena. In spite of this, the significance of this identification deemed it desirable and worth while to verify it. This was investigated with the aid of the expansion chamber illustrated in Figure 25. The

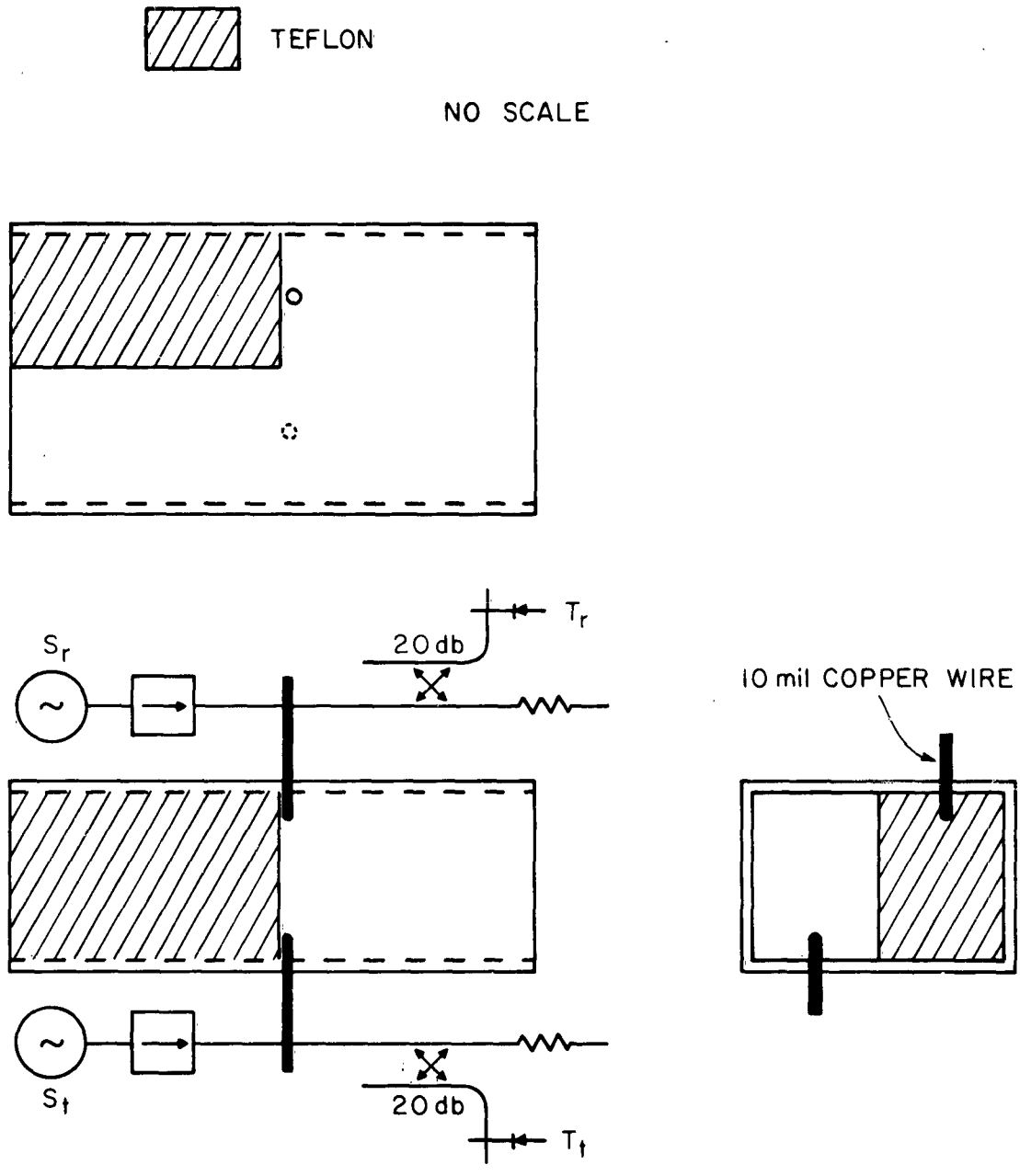

Figure 25. An expansion chamber test section employing two radio frequency antennas located in the same cross sectional plane of the expansion chamber and a teflon barrier to reflect one half of the shock wave.

construction of this chamber is similar to the construction of the chamber illustrated in Figure 7 except in this case two probe antennas were placed in the same cross sectional plane. A teflon plug filled half of the volume of the expansion chamber downstream from the two probe antennas. The microwave probing apparatus consisted of two signal sources S_r and S_t tuned to nearly the same frequency and two microwave detectors T_r and T_t. The specific microwave technique used to investigate the shock wave plasma was similar to the technique previously described in connection with Figure 20. The coupling of microwave energy from one microwave system to the other via the two coupling antennas was experimentally found to be negligible.

The experimental procedure used in this investigation was as follows. An electrically driven shock wave was made to propagate down the expansion chamber test section illustrated in Figure 25. The two microwave signals T_r and T_t were detected and each was displayed on one trace of a dual beam oscilloscope. When the shock wave reached the position of the two probes, half of the shock wave continued past the probe and down the gas filled half of the expansion chamber. The other half of the shock wave was reflected by the teflon plug filling the remaining half of the waveguide downstream from the antennas. When a shock wave is reflected, it travels back through the shock heated gas it originally passed through. Hence, if the shock wave is sufficiently intense to partially ionize a cold background gas, then the reflected shock wave will travel back through this ionized gas, compressing and further ionizing it. Therefore, at the boundary where the shock wave is reflected the electron density rapidly increases as the shock front reaches the boundary and is reflected. This technique was used to locate the position of the shock front with respect to the disturbances previously discussed. Typical observations are shown in Figure 26. These signals are similar to those illustrated in Figures 23 and 24 but differ slightly in appearance due to the teflon plug which slightly affects the impedance of the an-

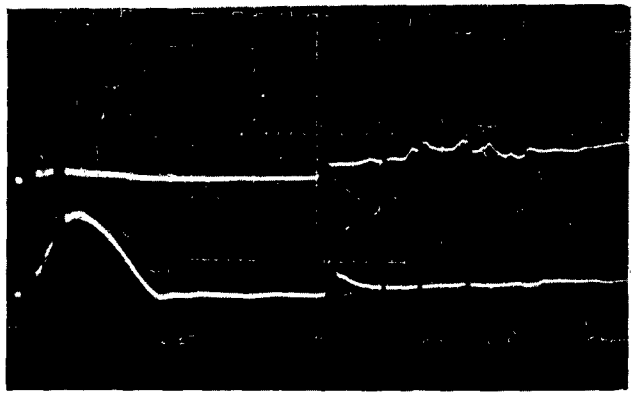

NO EXTERNAL
PREIONIZATION

(a)

2 mm Hg, NEON GAS
10 μs/division

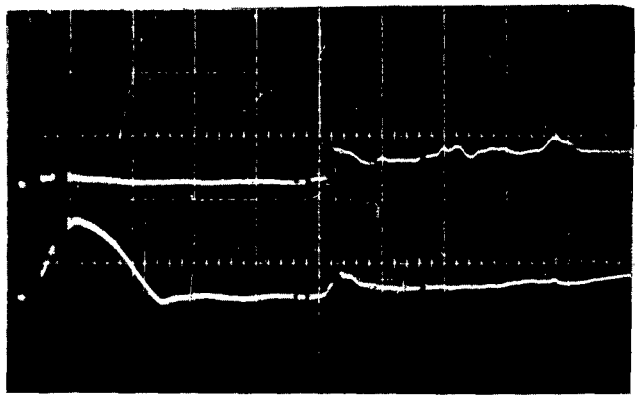

EXTERNAL
PREIONIZATION

(b)

Figure 26. Mircowave signals T_r and T_t as illustrated in Figure 25.

tennas. However, they can be interpreted in a manner identical to that discussed above. In relation to Figure 26b the background gas was preionized by a high power, pulsed, radio frequency wave. The degree of preionization was not enhanced in Figure 26a.

In both Figures 26a and 26b, the detected signal T_r attained a minimum value approximately 1 microsecond prior to the time at which T_t attained its minimum value, ($t=51\mu$ sec. and $t=52\mu$ sec. respectively). According to the above discussion, for sufficiently intense shock waves, T_r should reach its minimum value as soon as the shock front reaches the teflon plug. Hence, the shock front can be identified with the time of minimum T_r (i.e., in the case illustrated at time $t=51\mu$ sec.). In Figure 26b it is seen that T_t exhibits a rapid decrease at the same time that T_r attained its minimum value. This decrease in T_t is recognized as being due to shock wave compression of the background electron gas as was previously discussed in connection with Figures 15, 16, 18, 23, 24, etc. Hence, it can be concluded that the leading disturbance in each of the previously discussed cases was due to shock compression of the background electron gas and in addition, this disturbance can definitely be identified with the shock front.

The effect of a high peak power pulsed radio frequency wave (10^3 to 35 x 10^3 watts) on the properties of both the shock and the ionized driver gas was also investigated. It was found that the properties of the shock compressed gas could be appreciably altered by action of the high power microwave but in no case was it possible to appreciably alter the properties of the ionized driver gas. This was true even in the case of quite low shock velocities (Mach 6) which indicates that the ionized driver gas of even a low velocity electrically driven shock is very highly ionized. It also indicates that the rate of increase of electron density at the leading edge of the driver gas is sufficient to prevent appreciable penetration of the incident (3 cm.) radio wave beyond the position of the driver gas interface (this was also shown to be true in connection with

Figure 15). Specifically, it was found, by using the apparatus which is illustrated in Figure 20, that a high power microwave, if incident on the shock would breakdown the partially ionized gas which is formed by shock compression. This gas breakdown greatly increased the magnitude of the electron density in the region between the shock front and the driver gas interface and also increased the electron density at the leading edge of the column of ionized driver gas. As a result of the gas breakdown by the first few cycles of this high power wave train, succeeding cycles of the wave train are attenuated (by reflection), and hence do not reach with sufficient amplitude the driver gas interface of the shock provided plasma. These experimental observations seem to provide a satisfactory explanation to the fact that the effect of the high power EM wave on the driver gas plasma was slight.

THIS
PAGE
IS
MISSING
IN
ORIGINAL
DOCUMENT

carrying noise power

$$P_\omega = \frac{hf}{\exp(hf/kT) - 1} \tag{40}$$

where h is Planck's constant and $f = \omega/2\pi$. If the wave-guiding system propagates more than one mode, then each mode will carry uncorrelated noise waves and each of these modes will carry the noise power P_ω given by Equation (40). At typical microwave frequencies and termination temperatures $f/T \ll k/h \approx 2 \times 10^{10}$ and in this case Equation (40) reduces approximately to

$$P_\omega = kT \tag{41}$$

If the noise radiating medium is not matched to the wave-guiding structure, then only a fraction of the available power P_ω is radiated by the medium into the wave-guiding structure. In this case the actual power radiated P in each mode is related to the available power P_ω by Kirchoff's law and is given by

$$P = kTAdf \tag{42}$$

where P is the total power radiated by each propagating mode in the frequency interval f + df and A represents the absorption coefficient of the radiating medium, defined as that fraction of the total incident power absorbed by the medium from a test wave launched from the position of the noise wave detector. The power absorption coefficient A can be obtained from the field components of the incident test wave $\vec{E}_i$ and $\vec{H}_i$ and the electric field inside the radiating medium $\vec{E}$, if this information is available. In the case of a plasma medium lo-

cated in a waveguide, A is given by

$$A = \frac{\int_{\text{plasma}} R_e(\frac{1}{2}\vec{E} \cdot \vec{J}^*)dv}{\int_{\text{waveguide}} R_e(\frac{1}{2}\vec{E}_i \times \vec{H}_i^*) \cdot d\vec{a}} \tag{43}$$

where the current density J is related to the electric conductivity $\sigma = \omega_p^2 \epsilon_o \nu / (\nu^2 + \omega^2)$ by ohms law $\vec{J} = \sigma \vec{E}$. The integration in the numerator of Equation (43) is carried out over the volume of the plasma and the integration in the denominator is over the cross section of the waveguide. In general, the term in the numerator of Equation (43) cannot be evaluated because the electric field inside the plasma is not known. However, A is amenable to direct measurement and is related to the power reflection and power transmission coefficients R_p and T_p by

$$A = 1 - \left|R_p\right| - \left|T_p\right|$$

where

$$R_p = (\vec{E}_r \times \vec{H}_r^*) / (\vec{E}_i \times \vec{H}_i^*) \tag{44}$$

$$T_p = (\vec{E}_t \times \vec{H}_t^*) / (\vec{E}_i \times \vec{H}_i^*)$$

and the subscripts i,r, and t denote the incident, reflected, and transmitted fields respectively. Both R_p and T_p can be measured directly by measuring the power of the incident, reflected, and transmitted test wave. In this measurement the test wave should be a noise wave with a bandwidth equal to that of the noise wave detector. However, in most cases a monochromatic source set at a frequency equal to the center frequency of the radiometer noise detector gives sufficiently accurate results.

In the case of a plasma medium radiating noise power P, the radiation temperature T in Equation (42) is not necessarily equal to the temperature of the plasma or any one constituent of the plasma. However, if the free electron gas in the plasma has a Maxwellian velocity distribution, then comparison of Equations (39) and (42) leads to the conclusion that the radiation temperature T is equal to the temperature of the electron gas. This same conclusion can also be reached in a phenomenological manner if it is argued that the noise arises from collisions of electrons with atoms and ions. The number of collisions per unit time between an electron and the heavy particles is governed by the average velocity of the electrons. If the electrons have a Maxwellian velocity distribution, then an electron temperature can be defined in the usual manner and its value is determined by the average velocity of the electrons. Hence, if the radiation temperature corresponds to a temperature state of the plasma constituents, then this correspondence could only be with the temperature state of the electron gas. However, this has meaning only if the electrons have a Maxwellian velocity distribution. Experimentally it has been shown that the radiation temperature of a plasma is very nearly equal to the temperature of the electrons as measured by Langmuir probes if the condition of Maxwellianization of the electrons is satisifed.

The purpose of the experimental work discussed below was to measure the noise power radiated by a shocked gas through the shock front and attempt to relate the radiation temperature to the temperature of the electron gas. Such measurements have special significance because noise radiation from a shocked gas could possibly lead to a missile detection system. Also the radiation in the radio frequency spectrum from the plasma sheath of a re-entry vehicle will alter considerably the effective noise temperature of an antenna located in such a vehicle.

In this experimental investigation an electrically driven shock wave was propagated through an x-band metal waveguide. The microwave apparatus used to measure the noise power radiated by the shocked gas and associated driver gas is illustrated in Figure 27. The noise power from the shocked gas was measured with the aid of a superheterodyne receiver consisting of a balanced crystal mixer and a 8.5 Gc local oscillator. The heterodyned signal was amplified with an L.E.L. model 1F65D preamplifier which has a center frequency of 60 Mc and an 11 Mc bandwidth and an L.E.L. model 1F66D amplifier which has a center frequency of 60 Mc and an 11.2 Mc bandwidth. The over-all gain of the preamplifier and amplifier was approximately 100 db. The local oscillator power to the balanced mixer was approximately 2 m watts. The output from the i-f strip was terminated with a 0.005 μf capacitor and connected to the vertical input of an oscilloscope.

The noise power from the shocked gas was measured by comparing it with the noise radiated by a standard noise source. The excess noise ratio of the standard noise souce used in this work was 15.28 db (as of January 9, 1962; N.B.S.; Boulder, Colorado). Hence the radiation temperature of the standard noise source was

$$10 \log (T/290 - 1) = 15.28 \qquad (45)$$

or

$$T = 10{,}000^{\circ} \text{ K}$$

The experimental procedure used in the determination of the radiation temperature of the shocked gas is as follows. With the sliding short open and the expansion chamber connected to the balanced mixer, an electric discharge was ignited in the discharge chamber of the shock tube. The amplitude of the noise radiated by the shocked gas was then displayed on an oscilloscope where it was

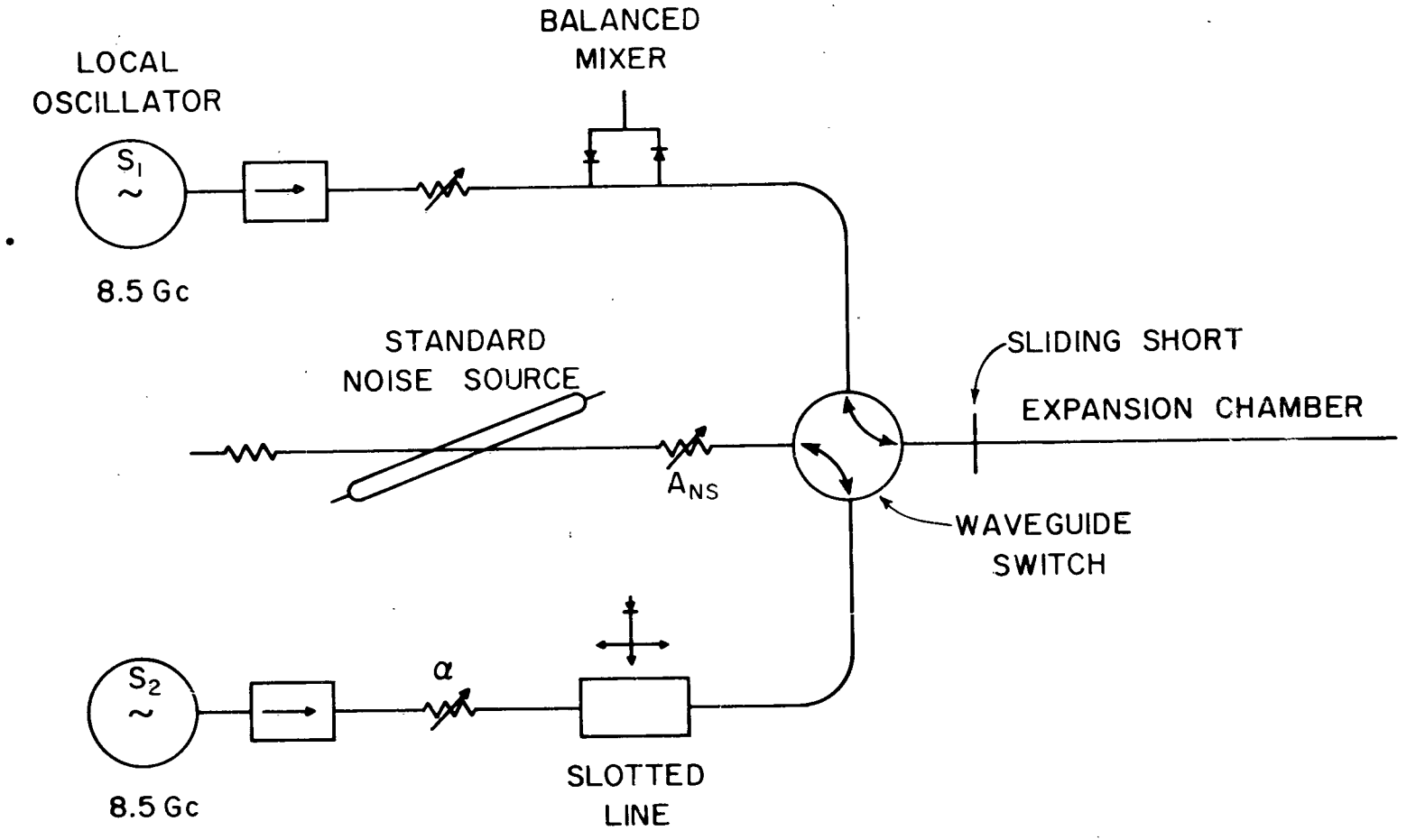

Figure 27. Microwave apparatus used to measure the radiation temperature of electrically produced shock waves.

photographed. A typical recording of the output of the balance mixer noise detector during the passage of a shock wave through the expansion chamber is illustrated in Figure 28a. The 12 k volt shock producing electric discharge was initiated simultaneously with the start of the scope trace which was swept at a 50 μ seconds per division rate. The level of the signal during the last 100 μ seconds of sweep represents zero excess noise. The detected signal during the first 50 μ seconds after the shock producing electric discharge must be disregarded. This is necessary because the balanced mixer detector is saturated during the shock producing electric discharge and does not fully recover until approximately 50 μ seconds after initiation of the discharge.

The noise power radiated from the shocked gas was determined by comparing the amplitude of the detected noise signal with the amplitude of the noise signal from the standard noise source. For example, in Figure 28a the amplitude of the noise signal at t = 150 μ seconds is equal to the amplitude of the noise signal from the standard noise source if 10 db of attenuation is inserted between the noise source and the noise detector (i.e., A_{sn} = 10 db). This is illustrated in Figure 28b which is a display of the noise signal from the standard noise source with A_{sn} = 10 db and all other setting of the noise detector the same as used in Figure 28a. Hence in Figure 28a at t = 150 μ seconds the apparent radiation temperature T_A of the shocked gas is given by

$$10 \log (T_A/290 - 1) = 15.28 - 10 \qquad (46)$$

or

$$T_A = 1265^{\circ} \text{ K}$$

The calibration for the noise detector, T_A versus division of deflection is shown in Figure 29. The apparent radiation temperature T_A is not equal to the actual radiation temperature T, given by Equation (42), because the shocked gas

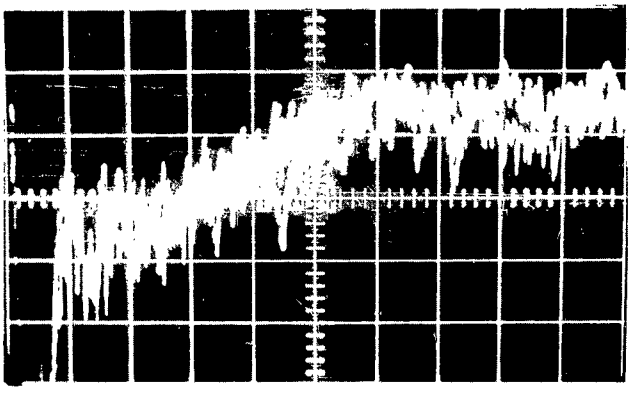

NOISE POWER FROM
SHOCK WAVE

NEON GAS
2 mm Hg
12 kvolt discharge
50 μsec./division

(a)

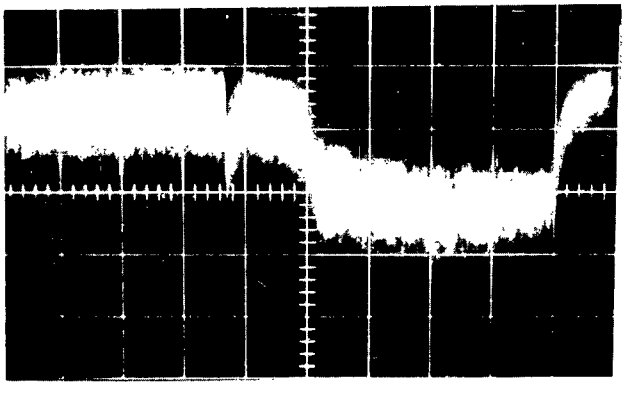

NOISE POWER FROM
STANDARD NOISE SOURCE

A_{SN} = 10 db.
50 μsec./division

(b)

Figure 28. (a) Illustrates the noise power radiated from a shock wave plasma as a function of time (b) noise power radiated from the standard noise source with 10 db attenuation.

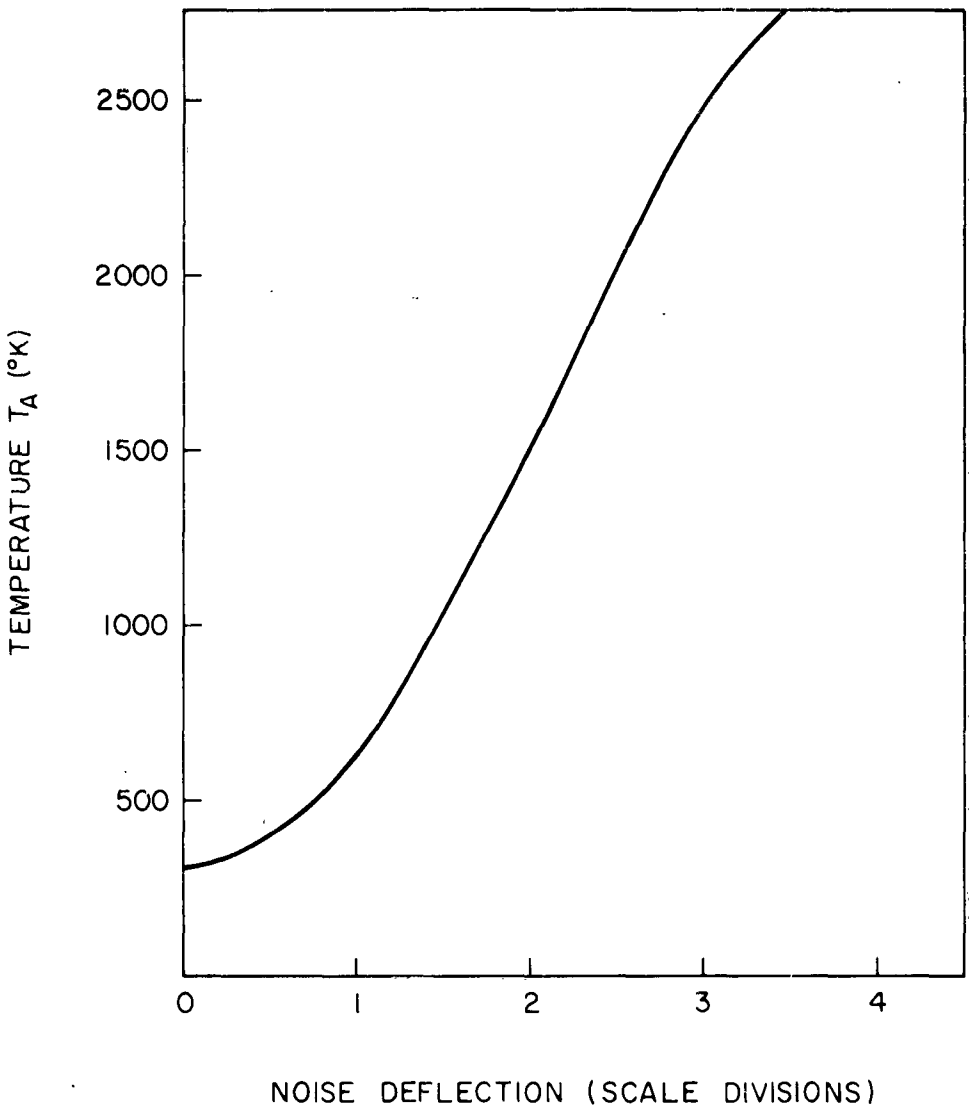

Figure 29. Radiation temperature as a function of total divisions of oscilloscope deflection of the superhetrodyned noise signal.

is not matched to the waveguide. However, if the power absorption coefficient A of the shocked gas is known then the radiation temperature T is

$$T = \frac{T_A}{A} \tag{47}$$

The coefficient A can be experimentally determined if measurements of the power reflection and transmission coefficients can be made (Equation (44)). In the case of an electrically driven shock wave with a velocity greater than about Mach 2, an 8.5 Gc wave will not propagate appreciably through the shocked and driver gas and T_p in Equation (44) can be neglected. Hence, A is equal to $1 - R_p$, where R_p is the power reflection coefficient of an 8.5 Gc test wave incident on the shocked gas. The transmission coefficient T_p may not be negligible for all electrically driven shock wave, but it is evident from Figures 10 and 15 and also from the discussion conducted in Chapter 8 that this condition is satisfied in the shock tube used in this work, and under the investigated experimental conditions.

The power reflection coefficient R_p of an 8.5 Gc EM wave reflected by the shocked and driver gas was measured with the microwave apparatus illustrated in Figure 27. In this application, the waveguide switch was set so that the expansion chamber was connected to source S_2 and its associated detection apparatus. The techniques most commonly used to measure the reflection coefficient of a microwave load are not applicable for the measurement of the reflection coefficient of the shocked gas because the microwave load (shocked gas) propagates along the waveguide. In addition, the reflection coefficient of the shocked gas is very high which increases the difficulty of obtaining accurate measurements. However, a method was devised and is discussed below by which the desired measurements could be made within the accuracy of available calibrated attenuators. Of course, for these measurements to have meaning it is necessary that the power absorbed in the shocked gas be much greater than the microwave power ab-

sorbed in the waveguide walls and associated waveguide equipment. As is discussed below this condition was not satisfied in the case of very intense shock waves ($M > 12$).

Consider a waveguide terminated in a lossy, partially reflecting load. Let the amplitude of the incident r-f electric field be represented by E_i. Assume that no power is transmitted through the load and let the magnitude of the electric field reflection coefficient be given by Γ, (i.e., $\Gamma = \sqrt{|R_p|}$). The total electric field E in the waveguide is equal to the sum of the incident and reflected waves.

$$E = E_i \left[e^{-j\beta z} + \Gamma e^{j\beta z + j\phi} \right] e^{j\omega t} \tag{48}$$

where ϕ is a phase constant which is a function of the location of the microwave load in the waveguide and this term also includes the argument of the complex reflection coefficient. The magnitude squared of the total electric field is equal to

$$E^2 = \vec{E} \cdot \vec{E}^* = E_i^2 \left[(1-\Gamma)^2 + 4\Gamma \cos^2 (\beta z + \phi/2) \right] \tag{49}$$

The reference point for the position variable z is arbitrary. If z is the distance from a point of maximum E^2, then ϕ is equal to zero. However, if z is the distance from a point of minimum E^2, then ϕ is equal to π. If we represent the value of z for these respective reference positions by z^+ and z^- respectively, then E^2 can be written in either of the following two equivalent forms.

$$E^2 = E_i^2 \left[(1 - \Gamma)^2 + 4\Gamma \cos^2 \beta z^+ \right] \tag{50a}$$

$$E^2 = E_i^2 \left[(1 + \Gamma)^2 - 4\Gamma \cos^2 \beta z^- \right] \tag{50b}$$

The reflection coefficient of the load Γ can be measured in a variety of ways. For example, if the load is stationary, then the maximum and the minimum values of E can be measured by varying z and in this case Γ is given by

$$\Gamma = \frac{r - 1}{r + 1} \tag{51}$$

where r is equal to the ratio of the maximum to the minimum value of E.

In the case of a shock wave, we can determine Γ by measuring E at a constant value of z because in this case the phase angle ϕ in Equation (49) changes as the shock moves along the waveguide. The reflection coefficient Γ is determined by applying Equation (51). Measurements of this type could be made from a recording similar to the one shown in Figure 14.

The above described method of determining Γ by measuring the standing wave ratio r is sufficiently accurate for small values of r but the accuracy of this measurement is very poor if r is large. This is especially true in the case of square law detectors such as crystal microwave detectors, where the voltage across the detector is proportional to the square of the electric field intensity (i.e., $V = K E^2$). In this case the reflection coefficient Γ in terms of the voltage across the detector is $\Gamma = (\sqrt{\rho} - 1)/(\sqrt{\rho} + 1)$ where ρ is the standing wave ratio with respect to the detector voltage (i.e., $\rho = V_{max}/V_{min}$).

If the reflection coefficient is relatively large ($\Gamma > 0.75$), then the accuracy of the measurement is better if it is determined from the measured variation of the standing wave in the immediate vicinity of either a maximum or a minimum rather than from the standing wave ratio. Such measurements are well known if the load being investigated is stationary. However, these methods are not applicable if the load is propagating along the waveguide, such as for example a shock wave. In spite of this, methods can be formulated with the aid of Equations (50) to measure large reflection coefficients of propagating loads.

In the discussion that follows, it is assumed that ϕ is a constant and that Γ is determined by measuring the electric field intensity as a function of z. However, the procedure is the same in the case of constant z and variable ϕ, hence is applicable to the case of shock waves.

Assume k power law detection and consider the microwave detector voltage when the waveguide is terminated in a load with a reflection coefficient Γ

$$V = K \left|E\right|^k = KE_i^k \left[(1-\Gamma)^2 + 4\Gamma \cos^2 \beta z^+\right]^{k/2} \tag{52}$$

In the case of $\Gamma < 1$, the maximum value of the detector voltage occurs at $z^+ = 0$ where V is equal to $KE_i^k(1 + \Gamma)^k$. If this load is replaced by a perfect EM reflector, then in this case Γ is unity and this same value of detector voltage occurs not at $z^+ = 0$ but at the point $z^+ = z_o^+$. Under this condition the reflection coefficient of the unknown load is

$$\Gamma = 2 \cos\left(\beta z_o^+\right) - 1 \tag{53}$$

where z_o^+ is measured with the microwave short in the guide and is equal to the distance along the guide measured from the point of maximum V, such that the detector voltage is equal to the maximum detector voltage when the waveguide is terminated in the load being investigated.

An equally acceptable procedure, capable of measuring large Γ consists of attenuating E_i while the microwave short is in a position such that the maximum value of V, in this case, is equal to the maximum value of V with the investigated load terminating the waveguide and zero attenuation of E_i. Under these conditions, the reflection coefficient of the load being investigated is

$$\Gamma = 2^a - 1 \tag{54}$$

where α is the percent attenuation of the incident electric field required to equalize the maximum detected voltage with the microwave short and the maximum detected voltage with the unknown load but no attenuation of E_i.

A phase type measurement of Γ relative to a minimum value of detected voltage rather than a maximum as discussed above could also be made (similar to Equation (53)). In this case if the microwave detector was linear (i.e., k = 1), then measurement relative to a standing wave minimum would be equally accurate as those relative to a standing wave maximum such as Equations (53) and (54). However, since the detection is nearly square law, the shape of standing wave voltage is more highly dependent on Γ near a maximum than it is near a minimum. Hence, measurements of large Γ relative to a maximum value of the standing wave in the waveguide are more accurate than similar measurements made relative to a minimum.

The accuracy of the above described methods of measuring large Γ is highly dependent on the magnitude of microwave power absorbed in the waveguide walls, the accuracy by which the phase of the electric field standing wave can be measured, and also on the accuracy of the calibrated attenuator used in connection with Equation (54). If it is assumed that the phase can be determined to within a value $\beta \Delta z$, where Δz is equal to the diameter of the EM sampling probe, then for the case of a 1 mm diameter probe and 8.5 Gc EM waves in x-band waveguide, the standard deviation of the measured Γ is approximately $\pm$ 0.02. In the attenuation method of measuring large Γ (i.e., Equation (54)), the value of α can be determined with a calibrated attenuation to within $\pm$ 0.15 db. Hence, in this case the standard deviation of the measured value of Γ is approximately $\pm$ 1.5 $^{o}/_{o}$. Experimental results verified that the accuracy of these two methods of measuring large Γ was comparable but it was also found that neither method was reliable if Γ was larger than about 0.97. At least part of the difficulty of measuring values of Γ greater than 0.97 is due to microwave losses in the wave-

guide walls and in the associated microwave apparatus. Hence, in the microwave system used in this work, if the reflection coefficient of the load being investigated was greater than about 0.97, then the accuracy of the measured value of Γ was limited by loss of microwave power in the waveguide walls rather than the accuracy of the measured values of α and z_o^+.

Experimental determination of the reflection coefficients of shock waves were made with the microwave apparatus illustrated in Figure 27. With the waveguide switch set so that the expansion chamber was connected to signal source S_2, the slotted line detected voltage was displayed on an oscilloscope while the shock wave propagated through the expansion chamber. Two typical recordings of the displayed waveform are shown in Figure 30. In each case the oscilloscope trace was started simultaneous with the initiation of the shock wave producing electric discharge and the oscilloscope was swept at a 50 μ second per division rate. Figure 30a was obtained under the same experimental conditions as the noise radiation waveform illustrated in Figure 28a (i.e., neon gas, 2 mm Hg pressure, 12 k volt discharge). The slotted line detected signal illustrated in Figure 30b was obtained with a 14k volt shock producing electric discharge in argon gas at 2 mm Hg pressure.

In each of these oscilloscope recordings, the straight line on the scope trace located approximately one division up from the bottom of the screen represents the value of the voltage across the slotted line crystal detector when the sliding short was set to totally reflect the incident EM wave and also with the probe set at a standing wave maximum (the voltage across the crystal detector is negative). The upper trace represents the time variations in the magnitude of the slotted line detected EM field during a shock wave traversal of the expansion chamber. The vertical deflection of the oscilloscope was set so that only the peak values of the detected voltage were displayed on the screen. The microwave probe and associated crystal detector was calibrated with the sliding

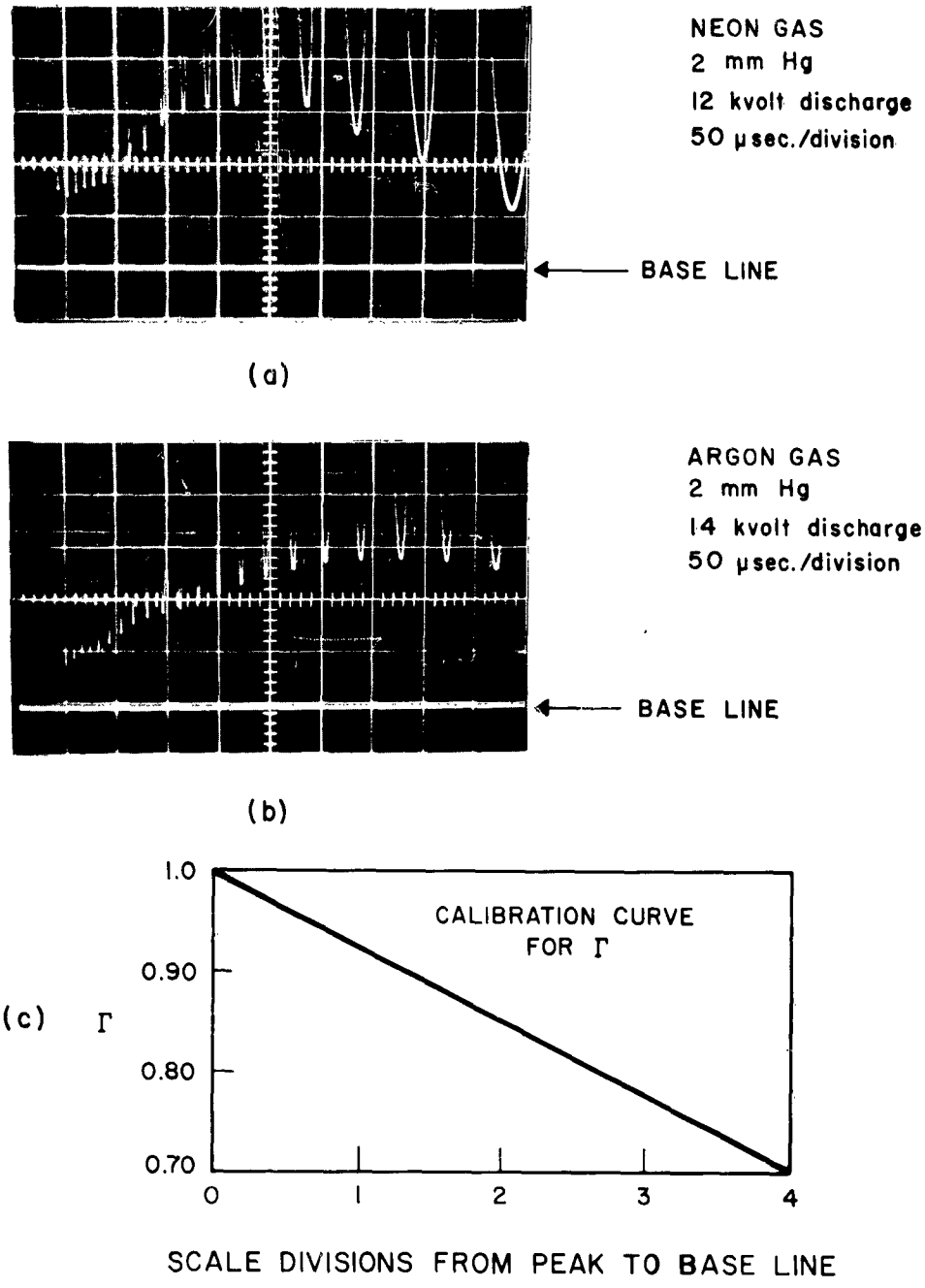

Figure 30. (a) Illustrates the time variation of the amplitude of the EM signal detected in the slotted line illustrated in Figure 27 during the passage of a shock wave through the expansion chamber. (b) Same as above except in argon gas. (c) Experimentally obtained voltage reflection coefficient Γ as a function of scope deflection from the peak of the detected EM wave to the base line.

short and the attenuator α so that the reflection coefficient of the shock wave at any specific time could be obtained according to either Equation (53) or (54) simply by measuring the difference in voltage between the peak value with the shock wave and the maximum value with the short. The calibration curve for Γ in terms of oscilloscope deflection between the peak value and the maximum value with the microwave short is shown in Figure 30c.

The oscilloscope recordings shown in Figure 30 can also be used to approximate the shock wave velocity in accordance with Equation (29) concerning Doppler frequency shift. However, as discussed in Chapter 8, these velocity measurements cannot be relied on at early times after the shock producing electric discharge.

Consider the oscilloscope recording illustrated in Figure 30b. At 50 μ seconds after the start of the scope trace the shock wave velocity is approximately Mach 12 and the EM reflection coefficient is approximately equal to 0.935. The reflection coefficient Γ rapidly decreases as the shock velocity falls below its maximum value. At 250 μ seconds the shock velocity has fallen to Mach 3.5 and Γ is approximately 0.8. Within the time interval between these two extreme values of Γ, a rather rapid time rate of change of Γ is noted at approximately 100 μ seconds after the beginning of the scope trace. This is significant because this is also the time at which the shock wave velocity fell below the value required to shock ionize the background gas (i.e., Mach 8). Of course for shock wave velocities less than about Mach 8 the measured reflection coefficient is relative to the ionized driver gas rather than the shocked gas.

The time variation of Γ for the case of neon gas (Figure 30a) is similar to that for argon although at any specific Mach number, Γ is slightly lower for neon than it is for argon. In addition, in the case of neon gas, at 2 mm Hg pressure the reflection coefficient exhibits an increase as the shock velocity falls below about Mach 2. The fact that at any specific Mach number, Γ is not the same in neon as it is in argon indicates that the profiles of electron den-

sity and/or the electron-atom/ion collision frequency for momentum transfer in front of, in, and behind the shock wave are different in the two cases. The increase in Γ at very low shock velocities is probably due to a rapid change in electron-atom/ion collision frequency for momentum transfer in the plasma medium at these low shock wave velocities. That is, consider an EM wave incident on the partially ionized shocked and/or driver gas. The power lost by the incident EM wave in the plasma medium is given by the numerator of Equation (43). This loss can be placed in the more convenient form given by

$$P_a = \frac{1}{2} \int \frac{\omega_p^2 \epsilon_o \nu}{\nu^2 \omega^2} E^2 \, dv \tag{55}$$

where the integration is carried out over the entire volume of the plasma, P_a is the power absorbed in the plasma medium, and ν is the electron collision frequency for momentum transfer with neutral atoms and ions. The electric field intensity E in the plasma is dependent on the electron density (ω_p) profile, and collision frequency ν profile and is determined by solving the appropriate boundary value problem. Calculations of this type have been made by several authors (see for example Herrman[51] or Albini et al.[52]) for various electron density gradients and various collision frequencies. In general, algebraic solutions for E cannot be obtained but numerical solutions are possible for a limited number of electron density profiles. However, as is usually the case in numerical analysis a portion of the physics of the phenomenon is lost in the calculator, hence has a limited usefulness. A short qualitative discussion of the phenomena of absorption of an EM wave incident on a plasma medium is discussed below.

Consider a partially ionized volume of neon gas in which the electron density is given by n_e and the pressure of the neutral atoms is 2 mm Hg. In this

case the electron-molecule and the electron-ion collision frequencies for momentum transfer as a function of electron temperature is illustrated in Figure 31. The effective collision frequency for momentum transfer ν, as used in Equation (55), is equal to the sum of the electron collisions frequencies with molecules and ions designated respectively by ν_{em} and ν_{ei} (i.e., $\nu = \nu_{em} + \nu_{ei}$). At high values of electron temperature $\nu_{ei} \ll \nu_{em}$ and ν is predominantly electron-molecule collisions. As the electron temperature is decreased, ν_{ei} increases and ν_{em} decreases as does ν until $\nu_{ei} = \nu_{em}$ after which ν increases with further decrease of electron temperature. Here the minimum value of ν occurs when $\nu_{em} = \nu_{ei} = \nu/2$. The electron temperature at which ν attains its minimum value and the magnitude of ν at this value of electron temperature is dependent on the electron number density.

Consider an electrically driven shock wave in neon gas at 2 mm Hg pressure (in relation to Figures 28a and 30a). Assume that the electron density monitonically increases with distance behind the shock front from a value of ω_p much less than ω immediately in front of the shock front to a value of ω_p much greater than ω in the plasma driver gas. According to Equation (55), the power of an incident EM wave of angular frequency ω which is absorbed in any particular region of the plasma is directly proportional to ω_p^2 and is also directly proportional to E^2. According to our original assumption ω_p increases monitonically with distance behind the shock front. However the electric field intensity decreases monitonically with distance behind the shock front as a result of reflections and absorption in the volume and rapidly approaches zero beyond the plane in the plasma column where ω_p is equal to ω. Hence, for any particular value of ν the absorption is predominantly in the volume between the shock front and the plane where ω_p is equal to ω. If the frequency of the test wave is 8.5 Gc, then the electron density in the volume of EM interaction in the plasma is less than about 10^{12} electrons per cm^3.

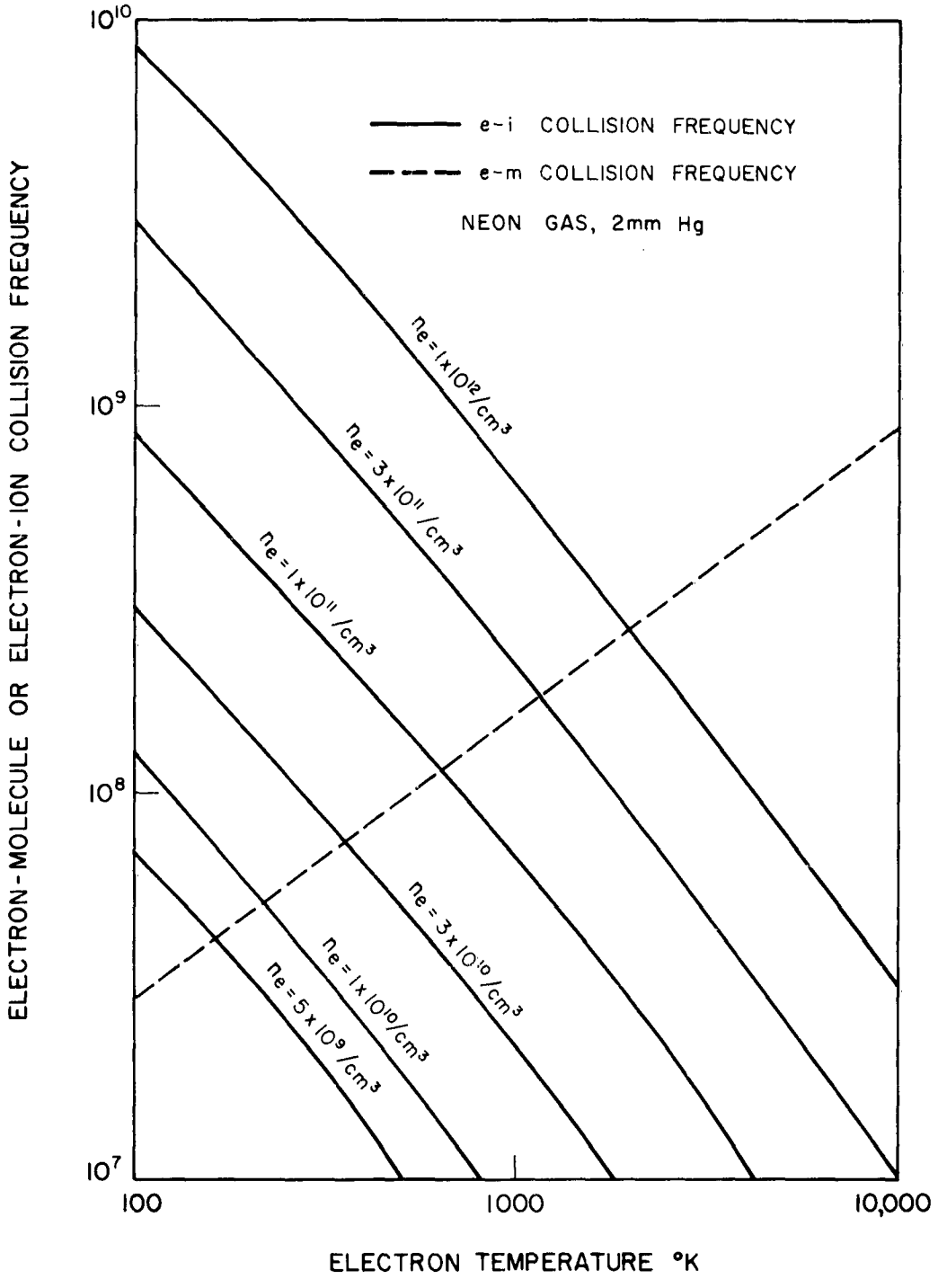

Figure 31. Electron-molecule and electron-ion collision frequency for momentum transfer as a function of the temperature of the electron gas in neon gas at 2 mm Hg pressure.

In order to consider the absorption of the incident EM wave in more detail it is convenient to follow a ray of the incident wave through the shock wave and driver plasma. Attenuation by reflection of the interacting EM wave in the leading edge of the monitonically increasing electron density plasma column is exceedingly small if the plasma frequency ω_p is less than about 0.1 ω. As the EM wave propagates beyond the plane where $\omega_p = 0.1\ \omega$ its attenuation by reflection increases rapidly. On the other hand, attenuation by absorption can be quite large even though $\omega_p \ll \omega$, if the collision frequency is sufficiently large.

Divide the plasma column in which the interaction of the EM wave occurs, into two volumes. Let ΔV_1 represent the volume of plasma between the shock front and the plane where $\omega_p = 0.1\ \omega$ and let ΔV_2 represent the volume between the plane $\omega_p = 0.1\ \omega$ and the plane where the intensity of incident wave has attenuated to a negligibly small value. The EM power absorbed in the plasma (P_a) is equal to the sum of the power absorbed in the two volumes. Each of these two volumes contribute heavily to the absorption, but the plasma in ΔV_1 does not contribute significantly to reflection. If the shock velocity is very high, then the power absorbed P_a is small as is evidenced in Figure 30. This is obviously due to the fact that the volume of interaction $\Delta V_1 + \Delta V_2$ is exceedingly small. As the shock wave velocity decreases the volume of EM interaction $\Delta V_1 + \Delta V_2$ increases and in spite of the fact that the collision frequency decreases, the power absorbed increases. Of course, the magnitude of P_a at any particular shock wave velocity is also dependent on the value of ν throughout the volume of EM interaction. The increase in P_a with decreasing shock wave velocity is evidenced in the first 250 μ seconds of Figure 30a and the first 350 μ seconds of Figure 30b. The subsequent decrease in P_a at very low shock wave velocities is most probably associated with a rapid decrease in absorption in the volume ΔV_1 due to a rapid decrease in collision frequency. That is, at very low shock wave velocities the shock heating is exceedingly small and the electron density in the volume ΔV_1 is also much smaller than it is at higher

shock wave velocities. Hence, the EM power absorbed in this volume decreases rapidly as the shock wave velocity approaches small values. This is due to decreases in both n_e and ν. On the other hand, the absorption in the volume ΔV_2 will not change drastically during this same time. By definition the electron density in ΔV_2 is greater than about 3×10^{11} electrons per $cm.^3$ From previously discussed results it is obvious that at low shock wave velocities the volume ΔV_2 is entirely in the driver gas plasma. Hence, the value of the volume ΔV_2 will not be highly dependent on the shock wave velocity and will increase with time only very slowly. It is obvious that the electron temperature in this volume will also be decreasing in time. From Figure 31 it is seen that a decrease in T_e could cause either an increase or a decrease in ν, this depending on both n_e and the temperature. It will be shown subsequently, that the measured radiation temperature from the plasma indicated that the electron temperature at these late time was usually in the range from 1000° to 2000° K. Assuming, an average electron density in the volume of interaction ΔV_2 equal to 5×10^{11} electrons per cm^3, it is seen from Figure 31 that the collision frequency in this range of electron temperatures and for the electron density cited is at its lowest possible value and is less than the signal frequency. Hence, according to Equation (55) the EM absorption in the volume ΔV_2 is also at its lowest value during this time and P_a in ΔV_2 should not vary rapidly with time since T_e does not vary rapidly. Therefore, the total absorption P_a in the volume $\Delta V_1 + \Delta V_2$ should exhibit a decrease with time at very low shock wave velocities as is experimentally observed in Figures 30a and 30b.

The experimentally measured radiation temperature T as a function of shock wave Mach number is given in Figure 32. The solid line represents the theoretical temperature of the shocked gas as predicted by Equation (5d). The experimental points were picked at random from a multitude of measured radiation temperature for the case of shock waves in neon at 2 mm Hg and at discharge voltages in the

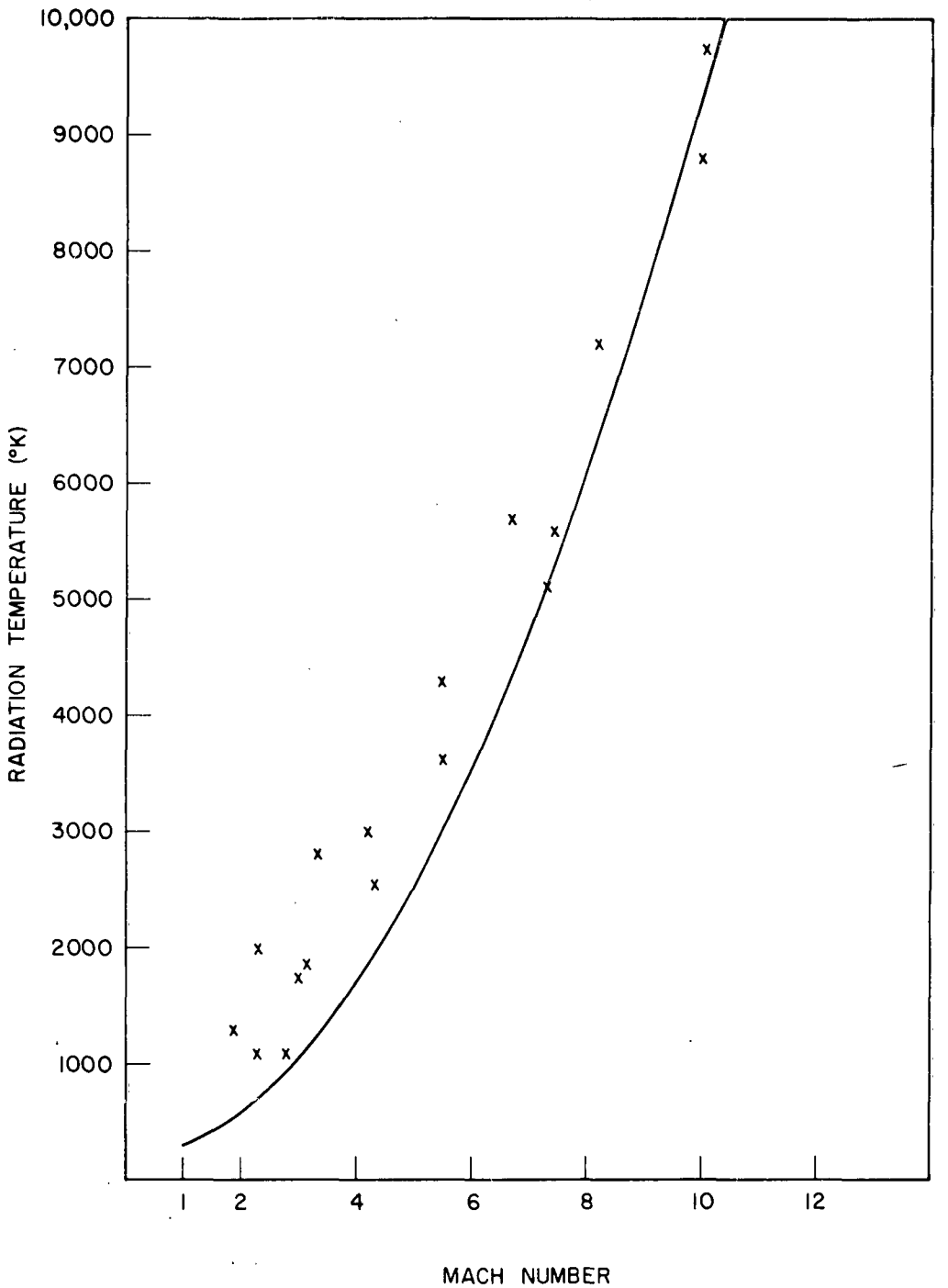

Figure 32. Solid line represents the expected temperature of the shocked gas as a function of Mach number (Figure 1). The experimental points shown are the corrected radiation temperature of the shocked and driver plasma.

range from 8 to 15 k volts. The experimental results were nonconclusive in some respects, especially since the temperature could not be accurately measured at shock velocities greater than about Mach 10. Also at velocities less than this value the temperature is relative to the plasma driver gas rather than the shocked gas. The radiation temperature could not be measured at shock velocities greater than the velocity cited above because at higher velocities the EM absorption coefficient A could not be measured with sufficient accuracy. In addition, as stated above the noise detector was saturated by the shock producing electric discharge and did not recover until about 50 μ seconds after initiation of the discharge. Hence, the apparent radiation temperature T_A could not be measured at early times after the initiation of the shock wave. Therefore under the most favorable conditions in this experiment, the apparent radiation temperature T_A of the shock wave could not be measured if the velocity of the shock wave was greater than about Mach 12.

In spite of the obvious experimental difficulties, some information on the properties of the plasma medium associated with an electrically driven shock wave can be obtained from the experimental measurements of radiation temperatures. On one hand, the experimental data indicates that the radiation temperature of the shocked gas approaches the theoretical temperature of shocked gas as the velocity of the shock wave approaches the threshold value for shock wave ionization. On the other hand, the radiation temperature at lower shock wave velocities is considerably higher than the theoretically predicted value of the temperature of the shocked gas. This indicates that either the shocked gas is hotter than the temperature predicted by theory or the measured temperature is relative to the driver gas which is at a considerably higher temperature than the shocked gas. The latter of these two possibilities seems to be the most probable.

In addition to the above inferences, the experimental data indicated that the noise power radiated from a high velocity shock wave ($M > 12$) in either neon or argon at 2 mm Hg pressure was exceedingly small. This is significant for two reasons. First of all it indicates the obvious conclusion that the noise power in the microwave frequency range radiated from a high velocity shock wave through the shock front is exceedingly small. It also indicates, in agreement with previously discussed experimental work, that the microwave reflection coefficient approaches unity as the shock velocity increases beyond about Mach 10.

10. CONCLUSION

In summary, the experimental results reported here show that the background gas in the electrically driven shock tube used in this investigation, which in many respects is similar to those used by other investigators, was preionized to a non-negligible degree during the time of the shock wave producing electric discharge. This has been attributed, in agreement with many other workers, to photoionization of the background gas by photons of adequate energy from the discharge chamber of the shock tube. In addition it was shown that this photoionization process is consistent with ionization by soft X-rays from the electron bombarded anode located in the discharge chamber. The free electron constituent of the background gas which results from this preionization was found to have a pronounced effect on the properties of the shock wave which subsequently passes through it. The direct effect of this constituent on some commonly used shock wave investigation techniques is also evident and must be considered when evaluating experimental results. In light of this it is believed that the experimental results obtained in some previous shock wave investigations might need to be re-evaluated.

It was found that the delay time between the passage of the shock front and the subsequent passage of the driver gas was exceedingly small especially at relatively high shock wave velocities. This indicates the extremely short time available to make measurements of the properties of the shocked gas in electrically driven shock tubes. If the measurements of plasma properties are completed in a time sufficiently longer than this delay time, then the measurements will be relative to the driver plasma rather than the shock wave plasma.

The radiation temperature of the combined shock wave plasma and driver gas plasma indicates that under some conditions the temperature of the driver gas is higher than the temperature of the shock wave gas. If this is the case, then

it is obvious that the driver gas will heat the shock wave gas via heat conduction and will consequently alter the properties of the shock wave gas and the structure of the shock wave. Obviously, this effect is significant only at low shock wave velocities where the temperature of the shocked gas is lower than the temperature of the driver gas and where the effective velocity of heat flow is greater than or on the order of the shock wave velocity.

BIBLIOGRAPHY

1. R. G. Fowler, J. S. Goldstein and B. E. Clotfelter, Phys. Rev., 82, 879, 1951.
2. R. G. Fowler, W. R. Atkinson and L. W. Marks, Phys. Rev., 87, 966, 1952.
3. R. Courant and K. O. Friedricks, "Supersonic Flow and Shock Waves," Interscience, 1948.
4. V. Josephson, J.A.P., 29, 30, 1958.
5. E. A. McLean, C. E. Fancuff, A. C. Kolb, and H. R. Griem, Phys. of Fluids, 3, 843, 1960.
6. V. Josephson and R. W. Hales, Phys. of Fluids, 4, 373, 1961.
7. L. Goldstein and T. Sekiguchi, Phys. Rev., 109, 625, 1958.
8. T. Sekiguchi and R. C. Herndon, Phys. Rev., 112, 1, 1958.
9. H. D. Weymann, Phys. of Fluids, 3, 545, 1960.
10. L. Goldstein, "Electrical Discharges in Gases and Modern Electronics," in "Advances in Electronics and Modern Physics," L. Marton, Ed., Academic Press, Inc., New York, N. Y., Vol. 7, 1955.
11. H. Petschek and S. Byron, Ann. Phys., 1, 270, 1957.
12. J. Bond, Phys. Rev., 105, 1683, 1957.
13. E. L. Resler, Shao-Chi Lin, and A. Kantrowitz, J.A.P., 23, 1390, 1952.
14. G. B. F. Niblet and A. Kenny, Princeton University Report NR061-020, Nbori - 105, 1957.
15. R. J. Strutt (Lord Rayleigh), Proc. Roy. Soc. (London), 183, 26, 1944.
16. Amasa S. Bishop, "Project Sherwood," Addison-Wesley, 1958.
17. A. C. Kolb, Phys. Rev., 107, 345, 1957.
18. P. J. Hart, J.A.P., 31, 436, 1960.
19. A. C. Kolb, "Magnetically Driven Shock Waves," in "Magnetohydrodynamics," Rolf K. M. Landshoff, Ed., Stanford University Press, 1957.

20. K. B. Earnshaw and C. M. Benedict, NBS report 7228, 1962.

21. H. E. Petschek, Peter H. Rose, Herbert S. Glick, Anne Kane, and A. Kantrowitz, J.A.P., 26, 83, 1955.

22. Ralph A. Alpher and Donald R. White, Phys. of Fluids, 1, 452, 1958.

23. H. T. Knight and R. E. Duff, Rev. Sci. Instr., 26, 257, 1955.

24. R. G. Jahn and F. A. Grosse, Phys. of Fluids, 2, 469, 1959.

25. D. Venable and D. E. Kaplan, J.A.P., 26, 639, 1955.

26. H. N. Ballard and D. Venable, Phys. of Fluids, 1, 225, 1958.

27. R. E. Duff, Phys. of Fluids, 2, 207, 1959.

28. J. S. Hey, J. T. Pinson and P. G. Smith, Nature, 179, 1184, 1957.

29. S. W. Kash, J. Gauger, W. Starr and V. Vali, "Velocity Measurements in Magnetically Driven Shock Tubes," in "The Plasma in a Magnetic Field," Rolf K. M. Landshoff, Ed., Stanford University Press, 1958.

30. M. Roger der Agobian, C.R., 248, 1308, 1959.

31. D. L. Schultz, Proc. of 4th International Conference on Ionization Phenomena in Gases, II, 1118, Uppsala, 1959.

32. Shao-Chi Lin, E. L. Resler and Arthur Kantrowitz, J.A.P., 26, 95, 1955.

33. G. B. Kistiakowsky, and P. H. Kydd, J. Chem. Phys., 25, 824, 1956.

34. H. T. Knight and D. Venable, Rev. Sci. Instr., 29, 92, 1958.

35. H. T. Knight, Rev. Sci. Instr., 29, 174, 1958.

36. R. J. Emrich and D. B. Wheeler, Jr., Phys. of Fluids, 1, 14, 1958.

37. G. L. Weissler, "Plasma Diagnostics with Vacuum Ultraviolet Radiation," Final Report on Grant No. DA-ORD-31-124-61-G47, U. S. Army Research Office, Durham, 1961.

38. A. Unsöld, Z. Astrophys, 24, 355, 1948.

39. C. E. Faneuff, A. D. Anderson and A. C. Kolb, U. S. Naval Research Laboratory Report NRL-5200, 1958.

40. E. B. Turner, Space Technology Laboratory Report GM-TR-0165-00460.

41. S. A. Losev, and A. I. Osipov, Soviet Phys. - Uspekhi, 74, 393, 1961.

42. S. Takeda and M. Roux, J. of Phys. Soc. Japan, 16, 1395, 1961.

43. R. G. Jahn, Phys.of Fluids, 5, 678, 1962.

44. L. Goldstein and N. Cohen, Phys. Rev., 73, 83, 1948.

45. D. Formato and A. Gilardini, "Micorwave Determination of Afterglow Temperatures and Electron Collision Frequencies in Nitrogen," Technical (Scientific) Note No. 1, Contract AF61(052)-39, 1959.

46. K. V. N. Rao, J. T. Verdeyen, and L. Goldstein, "Interaction of Microwaves in Gaseous Plasmas Immersed in Magnetic Fields," Scientific Report No. 3, Contract AF19(604)-3481, 1962.

47. P. Parzen and L. Goldstein, Phys. Rev., 82, 724, 1951.

48. G. Bekefi and S. C. Brown, American Journ. of Phys., 29, 404, 1961.

49. S. M. Rytov, (USSR Academy of Sciences, Press, Moscow, 1953) English Translation by the Air Force Cambridge Research Center, Bedford, Massachusetts, Rept. No. AFCRC-TR-59-162, 1959.

50. M. L. Levin, Doklady Akad. Nauk. S.S.S.R., 102, 53, 1955.

51. G. F. Herrmann, "The Absorption of Microwave Radiation in a Plasma Whose Electron Density Varies Linearly with Distance," Technical Report No. 2, Contract AF30(602)-2452, Rome Air Development Center, 1962.

52. F. A. Albini and R. G. Jahn, J.A.P., 32, 75, 1961.

Contract AF19(604)-7473

DISTRIBUTION LIST

Directorate of Development Planning
DCS Research & Technology
AFRDP-3 (Micheal Lorenzo)
Hq. USAF
Washington 25, D. C.

ASD(ASRNCF-2)
Propagation Section
Wright-Patterson AFB, Ohio

Commanding Officer
U. S. Army Signal R&D Laboratory
Attn: SIGRA/SL-PRT
Chief, Techniques Branch
Fort Monmouth, New Jersey

Commanding Officer
Diamond Ordnance Fuze Labs
Connecticut at Van Ness Street, N.W.
Attn: J. M. Stinchfield
Physicist, Br. 920
Washington 25, D. C.

Commanding Officer
U. S. Army Signal R&D Laboratory
Attn: SIGRA/SL-DR
Fort Monmouth, New Jersey

U. S. Army Signal Supply Agency
225 South 18th Street
Attn: G. I. Cooper
Industrial Mobilization Activity
Philadelphia 3, Pa.

Commanding Officer
Diamond Ordnance Fuze Laboratories
Attn: B. J. Udelson
ORDTL-930
Washington 25, D. C.

National Aeronautics & Space Administration
1520 H. Street, N. W.
Attn: C7-446
Washington 25, D. C. (2 copies)

Advisory Group on Electron Devices (AGED)
Office of the Director of Defense
Research and Engineering
346 Broadway, 8th Floor
New York 13, N. Y.

Sylvania Electric Products, Inc.
Electronic Defense Laboratory
Post Office Box 205
Mountain View, California
Thru: Commanding Officer
U.S. Army Signal
Electronic Research
Unit

Autonetics
A Division of North American Aviation, Inc.
9150 E. Imperial Highway
Attn: Technical Library
Dept. 3041-13-5877, Bldg. 2
Downey, California

Battelle Memorial Institute
505 King Avenue
Columbus, Ohio
Attn: Report Library

Raytheon Company
Spencer Laboratory
Attn: Glen Wade
Associate Director of
Engineering
(General Research)
Burlington, Mass.

Hughes Research Laboratories
3011 Malibu Canyon Road
Attn: Dr. Andrew V. Haeff
Vice-President and Director
Malibu, California

General Electric Company
Gaseous Electronics & Special Tube Group
Building 269, Room 209
Attn: Dr. A. O. Jensen
Schenectady 5, New York

Library
W. W. Hansen Laboratories of Physics
Stanford University
Stanford, California

Stanford Electronics Laboratory
Stanford University
Attn: Documents Library
Stanford, California

Contract
AF19(604)-7473 - Distribution List(continued)

Johns Hopkins University
1315 St. Paul Street
Attn: Mr. M. Scotto, Research Associate
Radiation Laboratory
Baltimore 2, Maryland

Yale University
Department of Electrical Engineering
Attn: Professor H. J. Reich
New Haven, Connecticut

Dr. James Brady
Oregon State College
Physics Department
Corvallis, Oregon

University of Mississippi
Attn: Mr. Thomas Tullos
University, Mississippi

Rensselaer Polytechnic Institute
School of Engineering
Attn: E. Howard Holt, Director
Plasma Research Laboratory
Troy, New York

Hq. AFCRL OAR (CRRCPG, D. Herskovitz)
L. G. Hanscom Field
Bedford, Mass. (10 copies)

Hq. ASD(ASRNET-3)
Wright-Patterson AFB, Ohio (2 copies)

RADC (RCLTP - W. C. Quinn)
Griffiss AFB, New York

RADC (RCWEC, Mr. Gerald Levy)
Griffiss AFB, New York

Commanding Officer
Diamond Ordnance Fuze Labs
Connecticut at Van Ness Street, N.W.
Attn: Martin J. Reddan
Tube Branch, 930
Washington 25, D. C.

Raytheon Company
55 Chapel Street
Attn: Mr. Paul W. Stutsman
Newton 58, Mass.

Diamond Ordnance Fuze Laboratories
Attn: R. T. Young
Consultant, Tube Branch, 930
Washington 25, D. C.

Commanding Officer
U.S. Army Signal R&D Laboratory
Attn: SIGRA/SL-PRG (M. Zinn)
Fort Monmouth, New Jersey

Commanding Officer
U.S. Army Signal R&D Laboratory
Attn: Mr. Irving Reingold, SIGRA/SL-PRM
Microwave Tubes Branch
Electron Tubes Division
Elec. Components Research Dept.
Fort Monmouth, New Jersey

Technical Library
G. E. TWT Product Section
601 California Avenue
Attn: Verna Van Velzer, Librarian
Palo Alto, California

General Electric Company
Post Office Box
Attn: R. J. Bondley
Superpower Microwave Tube Lab.
Nishayuna, New York

Sylvania Electronic Tubes
Division of Sylvania Electric Products, Inc.
Attn: R. E. Palmateer
Emporium, Pennsylvania

Varian Associates
611 Hansen Way
Attn: E. W. Herold
Vice-President, Research
Palo Alto, California

Tung-Sol Electric, Inc.
Chatham Electronics Division
630 W. Mt. Pleasant Avenue
Attn: Mr. B. F. Steiger
Livingston, New Jersey

General Electric Research Laboratory
Post Office Box
Attn: John M. Anderson
Nishayuna, New York

Contract
AF19(604)-7473 -Distribution List (continued)

Dr. W. H. Christoffers
Manager, Manufacturing
Microwave Tube Division
11105 S. LaCienega Blvd.
Los Angeles 45, California

Radio Corporation of America Laboratories
Attn: Dr. T. N. Chin
Princeton, New Jersey

Westinghouse Research Laboratories
Gaseous Electronics Research
Ardmore Boulevard
Attn: Dr. A. V. Phelps
East Pittsburg, Pennsylvania

General Electric Company
Electronic Components Division
One River Road, Schenectady, New York
Attn: Dr. N. J. Hawkins, Room 201,
Building 269
Tube Technology Engineering

Edgerton, Germeshausen & Grier, Inc.
160 Brookline Avenue
Attn: Dr. Seymour Goldberg
Boston 15, Mass.

General Telephone & Electronics
Laboratories, Inc.
Attn: Mr. S. J. Tetenbaum
1015 Corporation Way
Palo Alto, California

T. E. Hanley
Code 5241
Naval Research Laboratory
Washington 25, D. C.

Commanding Officer
Officer of Naval Research
Branch Office Chicago
86 E. Randolph Street
Chicago 1, Illinois (2 copies)

BUSHIPS, (Code 691A4, Mr. W. J. Riegger)
Department of the Navy
Washington 25, D. C.

Chief, Bureau of Naval Weapons
Attn: RRRE-3
Washington 25, D. C.

Chief, Bureau of Ships
Department of the Navy
Attn: Mr. C. C. Walker
Code 691A1
Washington 25, D. C.

Massachusetts Institute of Technology
Lincoln Laboratory
P. O. Box 73
Attn: Mary A. Granese, Librarian
Lexington 73, Massachusetts

Professor E. M. Boone
Department of Electrical Engineering
The Ohio State University
2024 Neil Avenue
Columbus 10, Ohio

Antenna Laboratory
Department of Electrical Engineering
The Ohio State University
Attn: Reports Librarian
2024 Neil Avenue
Columbus 10, Ohio

Harvard University
Technical Reports Collection
Gordon McKay Library-Attn: Librarian
303A Pierce Hall
Oxford Street
Cambridge 38, Massachusetts

Dr. N. T. Grisamore
Assistant Dean(Research)
School of Engineering and Applied Science
The George Washington University
Washington 6, D. C.

AFMTC (AFMTC Tech. Library - MU - 135)
Patrick AFB, Florida

AUL
Maxwell AFB, Alabama

ASD (ASAPRD-Dist)
Wright Patterson AFB, Ohio

RADC (RAALD)
Griffiss Air Force Base, New York
Attn: Documents Library

AF Missile Development Center (MDGRT)
Holloman AFB, New Mexico

Contract
AF19(604)-7473 (Distribution List - continued)

Aero. Res. Lab. (OAR)
AROL AFL 2292, Building 450
Wright-Patterson AFB, Ohio

Commanding General
USASRDL
Attn: Tech. Doc.Ctr.
SIGRA/SL-ADT
Fort Monmouth, New Jersey

Department of the Army
Office of the Chief Signal Officer
SIGRD-4a-2
Washington 25, D. C.

Commanding Officer
Attn: ORDTL-012
Diamond Ordnance Fuze Laboratories
Washington 25, D. C.

ASTIA (TIPAA)
Arlington Hall Station
Arlington 12, Virginia (20 copies)

Director
Langley Research Center
National Aeronautics and Space
Administration
Langley Field, Virginia

AFCRL, OAR (CRXRA - Stop 39)
L. G. Hanscom Field
Bedford, Massachusetts (20 copies)

Chief, Bureau of Naval Weapons
Department of the Navy
Attn: DLI-31
Washington 25, D. C. (2 copies)

Director (Code 2027)
U. S. Naval Research Laboratory
Washington 25, D. C. (2 copies)

Director, USAF Project RAND
The Rand Corporation
1700 Main Street
Thru: A. F. Liaison Office
Santa Monica, California

U. S. Army Aviation Human Research Unit
U. S. Continental Army Command
P.O. Box 428, Fort Rucker, Alabama
Attn: Maj. Arne H. Eliasson

Library
Boulder Laboratories
National Bureau of Standards
Boulder, Colorado (2 copies)

Institute of the Aerospace Sciences, Inc.
2 East 64th Street
Attn: Librarian
New York 21, New York

Alderman Library
University of Virginia
Charlottesville, Virginia

General Electric Company
Post Office Box
Attn: E.D. McArthur, Manager
Superpower Microwave Tube
Laboratory
Nishayuna, New York

Radio Corporation of America
Attn: Mr. E. E. Spitzer
Power Tube Operations
Lancaster, Pennsylvania

Bell Telephone Laboratories, Inc.
Attn: J. W. Fitzwilliam, Director
Electron Tube Development
Murray Hill, New Jersey

Microwave Associates
Attn: Dr. Lawrence Gould
Burlington, Massachusetts

Bomac Laboratories, Inc.
8 Salem Road
Attn: Dr. Arthur McCoubrey, Manager
Research and Development
Beverly, Massachusetts

Dr. H. W. Welch, Jr.
Director of Research and Development
Motorola, Inc.
P.O. Box 1417
Scottsdale, Arizona

Convair Astronautics Division
General Dynamics Corporation
Attn: F. L. Unmack
Applied Mfg. Research
Department 290-2
Main Zone 290-20
San Diego 12, California

Contract
AF19(604)-7473 (Distribution List - continued)

New York Naval Shipyard
Material Laboratory, Code 920
Attn: Mr. J. T. Fetsch
Brooklyn 1, New York

Massachusetts Institute of Technology
Research Laboratory of Electronics
Building 26, Room 327
Attn: Mr. John H. Hewitt
Cambridge 39, Massachusetts

Office of Naval Research
Branch Office, London
Navy 100, Box 39
F.P.O. New York, N. Y. (10 copies)

Technical Information Office
European Office, Aerospace Research
Shell Building, 47 Cantersteen
Brussels, Belgium

Hq. AFCRL, OAR (CRXR, John R. Marple)
L. G. Hanscom Field
Bedford, Massachusetts

Joyce E. Lunde
Reference Librarian
The Dodge Library
Northeastern University
Boston 15, Massachusetts

Irving Kaufman
Member Technical Staff
Physical Electronics Laboratory
Space Technology Laboratories, Inc.
One Space Park
Redondo Beach, California

OAR (RROS, Col. John R. Fowler)
Tempo D
4th and Independence Ave.
Washington 25, D. C.

AFOSR, OAR (SRYP)
Tempo D
4th and Independence Ave.
Washington 25, D. C.

Redstone Scientific Information Center
U. S. Army Missile Command
Redstone Arsenal, Alabama

Office of Scientific Intelligence
Central Intelligence Agency
2430 E Street, N. W.
Washington 25, D. C.

Scientific and Technical Information Facility
Attn: NASA Representative (S-AK/DL)
Bethesda, Maryland - P. O. Box 5700

Defense Research Member
Canadian Joint Staff
2450 Massachusetts Avenue, N. W.
Washington 8, D. C.

Advanced Techniques Branch (ASRNEA)
Electronics Technology Laboratory
Aeronautical Systems Division
Wright-Patterson AFB, Ohio

RCA Victor Research Laboratories
1001 Lenoir Street
Attn: Dr. J. R. Whitehead
Montreal 30, Quebec

Chief, Bureau of Ships
Department of the Navy
Attn: Mr. A. H. Young, Code 681A1A
Washington 25, D. C.

The Johns Hopkins University
Radiation Laboratory
1315 St. Paul Street
Attn: Librarian
Baltimore 2, Maryland

Prof. Turgut Boduroglu, Director
Turkish Technical Information Center
Istanbul Technical University
Istanbul, Turkey

Hq. OAR (RROSP, Maj. Richard W. Nelson
Washington 25, D. C.